School of Civil and Mechanical Engineering
Department of Mechanical Engineering

The Influence of Contaminant Particles and Filtration Regime on Fibrous Mist-Filter Performance

Arne Bredin

This thesis is presented for the Degree of
Doctor of Philosophy
of
Curtin University

February 2012

DECLARATION

To the best of my knowledge and belief this thesis contains no material previously published by any other person except where due acknowledgement has been made. This thesis contains no material which has been accepted for the award of any other degree or diploma in any university

Arne Bredin
Perth, 03 February 2012

It does not make any difference how beautiful your guess is. It does not make any difference how smart you are, who made the guess, or what his name is - if it disagrees with experiment it is wrong.

Richard P. Feynman

Acknowledgement

Though only my name appears on the cover of this work, many people have contributed to its production and I owe my gratitude to all those who have made this dissertation possible.

My deepest gratitude is to my supervisor A/Prof. Ben Mullins. He gave me the freedom to explore on my own and at the same time provided excellent guidance and encouraged me through the whole process of my research. Without his experience and support, this work would never have been possible. I have been amazingly fortunate to have had him as my advisor.

My co–supervisors Dr. Alfons Larcher and Dr. Andrew King who supported me countless times with their expertise in thermoanalysis and fluid dynamics also have my sincere thanks. I am deeply grateful for numerous discussions that helped me solve technical details of my work and for their assistance in carrying out and analysing my experiments.

I would also like to thank A/Prof. Michelle Rosano, Director of the *Sustainable Engineering Group (SEG)*, for her support and encouragement throughout my work. I furthermore would like to thank my colleagues and the staff of the *SEG* for their assistance and a highly enjoyable time in this group. I particularly have to thank my colleagues Mr. Ryan Mead–Hunter and Mr. Robert Ong for numerous discussions that helped me to bounce off new ideas and approaches.

The staff of the *Fuels and Energy Technology Institute* and the *Curtin Aquatic Research Laboratories* are also gratefully acknowledged, for their help during my experiments.

Dr. Rebecca A. O'Leary is also sincerely thanked for her help with statistical analysis of my data.

I also must also deeply thank my parents for supporting me all the way through my education and my partner Sandra who always supported me and encouraged me to pursue my goal.

Finally, financial support from the *Australian Research Council* (LP0883877) and *MANN+HUMMEL GmbH* is gratefully acknowledged.

Publications arising from this thesis

This thesis contains the following publications:

Journal articles

A. Bredin, A.V. Larcher, B.J. Mullins
Thermogravimetric analysis of carbon black and engine soot – Towards a more robust oil analysis method, *Tribology International*, 44 (2011) 1642-1650.

A. Bredin, B.J. Mullins
Influence of flow-interruption on filter performance during the filtration of liquid aerosols by fibrous filters, *Separation and Purification Technology*, 90 (2012) 53-63.

A. Bredin, R.A. O'Leary, B.J. Mullins
Filtration of soot–in–oil aerosols: Why do field and laboratory experiments differ?, *Separation and Purification Technology*, **in press** (2012).

A. Bredin, B.J. Mullins
Regeneration of mist filters by high velocity air and rotation – a comparison, *in preparation.*

R. Mead-Hunter, A. Bredin, A.J.C. King, A.V. Larcher, T. Becker, B.J. Mullins The influence of soot nanoparticles on the micromacro-scale behaviour of coalescing filters, *Chemical Engineering Science*, **submitted** (2012).

Refereed Conference Papers

B.J. Mullins, W. Heikamp, A. Bredin
Field Experience with the Provent CCV System
American Filtration & Separations Society Annual Conference, May 5-7, 2009, Bloomington, MN.

Abstract

The following thesis examined the filtration of liquid and colloid mists in significant detail under realistic filtration conditions. Numerous and significant gaps in literature pertaining to the filtration of liquid aerosols or mists with fibrous filters were found to exist. Specifically, these gaps include: a lack of information on the influence of contaminant (colloidal) particles on the properties of liquid aerosols and their influence on the performance of mist filters; little or no information on the influence of discontinuous filtration conditions on pressure drop, saturation and collection efficiency in fibrous mist filters; no research on practical means of reducing the liquid saturation in such filters. An experimental program was therefore devised which addressed these gaps in literature.

It was found that filters undergo a second loading step beyond the first equilibrium state if they were operated discontinuously. The filters were found to attain a second equilibrium state at a higher pressure drop and saturation level than at the first equilibrium state. This was attributed to a rearrangement of liquid in the filter during the breaks, clogging previously free passages, a process which was mainly driven by capillary forces. The ratio of shear and capillary forces was suggested as means of determining whether these passages were able to be cleaned once aerosol flow was recommenced. A simple phenomenological model based on the Lucas–Washburn equation was also developed, to describe drainage of supersaturated filter media. It was shown that capillary theory appeared to describe the process which occurs as liquid is drained from supersaturated filters, at least during the initial phase. Laboratory and field (on–engine) filtration tests were also conducted, which examined the influence of particulate (soot) contamination and oil ageing on the performance of mist filters. It was found that viscosity was the major determinant of pressure drop in such filters, together with some engine–specific parameters. The influence of soot was then further explored using an "accelerated loading" method. It was found that soot accumulates in oil–mist filters at a steady and predictable rate. Indeed, a good correlation between (liquid) filtration calculations and soot deposition rate was found. Three different filter cleaning methods were also developed, using rotation and/or a pulse of compressed air ("pulse jet"), in–situ or off–line. A novel rotating filter apparatus was also developed. It was found, that all three methods were able to remove a significant amount of oil from the filter and thus lead to a lower saturation and pressure drop. In all three cases pressure drop was found to decrease logarithmically with rotational speed or jet velocity, respectively, whereas the saturation decreased close to linearity.

This work has developed several novel methods for filter and soot analysis and testing, as well as novel filter cleaning technologies. This thesis was in addition to a detailed investigation into the physics and kinetics of mist filter systems and soot–in–oil colloids. It can therefore be no doubt that this thesis has provided a significant and novel contribution to the field of oil–mist and colloid aerosol filtration.

Nomenclature

Greek Letters	
α	filter packing density
α_i	model coefficients
γ	surface tension
η	dynamic viscosity
λ_η	second viscosity
λ	mean free path
μ_i	mean of the response variable over i observations
ν	kinematic viscosity
ρ	density
σ	standard deviation
τ	particle relaxation time
ΔP	pressure drop
ΔS	saturation decrease
θ	contact angle

Latin Letters	
a_i, b_i, c_i	model parameters
c	particle concentration
d_{cap}	capillary diameter
d_f	fibre diameter
$d_{f,wet}$	fibre diameter of a “wetted” fibre
d_o, d_i	outer and inner filter diameter, respectively
d_p	particle diameter
f	fibre surface
g	gravitational acceleration
h_{cap}	capillary rise height
k	porosity of the filter media (1-α)
l	distance of the gas–liquid interface from the tube inlet
m_{Filter}	filter mass
m_{Fibres}	fibre mass in the filter
m_L	liquid mass
m_{Inert}	inert mass in thermogravimetric analysis
m_{Oil}	oil mass
m_{Sample}	sample mass
m_{Soot}	soot mass
$\dot{m}$	mass flux
$mileage_{Filter}$	mileage since filter installation
n	rotational rate

n_{Cycle}	cycle number during discontinuous filtration
q	flow rate
t	time
u	velocity
w	filter width (perpendicular to flow and gravity)
y_i	response variable for $1..i^{th}$ observation
z	filter thickness (in flow direction)

Capital Letters

Bo	Bond number
$Bypass$	bypass centrifuge equipped (boolean)
C_C	slip correction factor
C_D	drag coefficient
Ca	capillary number
D	diffusion coefficient
Dr	Drainage number
E	filter efficiency
E_D	diffusional collection efficiency
E_G	gravitational collection efficiency
E_I	inertial collection efficiency
E_R	collection efficiency due to interception
E_Q	electrostatic collection efficiency
E_{DR}	collection efficiency due to interception of diffusive particles
E_Σ	overall single–fibre efficiency
J	empirically derived factor
Ma	Mach number
Kn	Knudsen number
Ku	Kuwabara hydrodynamic factor
F_{ext}	force
F_D	drag force
Odo_0, Odo_E	odometer reading at start and end, respectively
P	filter penetration
P_{Engine}	engine power
P_F	fluid pressure
Pe	Peclet Number
R	ratio between particle diameter and fibre diameter
Re	Reynolds number
S	filter saturation
SAE_u, SAE_i	SAE and W-SAE oil grade, respectively
Stk	Stokes number
T	stress tensor
V_{Engine}	engine volume

V_{Fibre}	fibre volume
V_{Filter}	filter volume
V_{Void}	void filter volume
V_L	liquid volume

Subscripts	
$actual$	actual value (calibration)
acc	accumulated
$captured$	captured by the filter
exp	experimentally obtained value
in, out	into and out off a system, respectively
max	maximal
$mean$	mean value of a distribution
$non-evaporated$	non–evaporated fraction
$pred$	predicted value
$reacted$	reacted fraction
$Drain$	drained, draining
$EQ1$	first equilibrium state
$EQ2$	second equilibrium state
F	fluid
L	liquid
N	normalised
0	initial condition
Reg	after regeneration

Abbreviations	
CPC	Condensation Particle Counter
DAD	"Dipping and Draining" filter preloading method
DMA	Differential Mobility Analyser
DSC	Differential Scanning Calometry
$FTIR$	Fourier Transform Infrared
$HEPA$	High Efficiency Particulate Air
LRP	Lower Reference Point (thermogravimetry)
MS	Mass Spectrometry
RAS	"Rapid Aerosol Saturation" filter preloading method
rpm	Revolutions per minute
SIM	Selected Ion Monitoring
$SMPS$	Scanning Mobility Particle Sizer
TGA	Thermogravimetric Analysis
URP	Upper Reference Point (thermogravimetry)

Table of Contents

1 Introduction

Due to increasingly stringent environmental regulations, vehicle manufacturers face increased pressure to satisfy emission requirements. Acceptable levels for exhaust emissions from new vehicles in Europe and Australia are defined by the *European Emission Standards* [1] and have been progressively lowered over time. This – amongst other factors – has required combustion gases in engine crankcases to be redirected into the air intake of the engine rather than being vented to the atmosphere. This is termed closed crankcase ventilation (CCV).

Crankcase ventilation is required to release pressure which results from blow-by gases passing gaps between the pistons and the cylinder walls, as significant pressure in the crankcase would cause oil seals to fail and leak. The vented gas contains unburned or partially unburned fuel residues, combustion products and oil droplets generated by thermal or mechanical means. These oil droplets are typically contaminated with solid carbonaceous combustion residues (typically referred to as soot) that are carried into the crankcase with the blow-by gases and over time accumulate in the oil. To prevent this potentially hazardous aerosol mixture from being released into environment, it is redirected into the air intake and eventually combusted in the engine. However, oil and soot can lead to the formation of deposits [2] which adversely impact the lifespan of engine compounds such as turbochargers. These deposits are also known to change the lubricant oil properties (e.g. viscosity) [3] which leads to an increase in engine wear and eventually may cause engine failure [4] if a permanent lubrication film can no longer be maintained. Therefore, the oil droplets and colloidal solid contaminants must be removed from the blow–by gases before the remainder is combusted. This is commonly achieved by filtering the gas using either fibrous aerosol filters, cyclones or plate separators. It was shown that the installation of CCV filtration systems could reduce PM 2.5 emission by up to 30% [5, 6].

Due to comparatively low cost coupled with high separation efficiency, filtration using fibrous filters is usually the most efficient method to remove particles from air flow. Filters are commonly used in gas cleaning to reduce emissions in order to protect health and

environment. Current filtration technologies are able to remove the complete size range of aerosol particles with up to 99.99999% efficiency (HEPA – High Efficiency Particulate Air and ULPA - Ultra Low Penetration Air), although filter efficiency is characteristically reduced for particles of the size between approximately 100 – 500 nm. The removal of particles of this size range is however especially crucial, since such particles are able to deeply penetrate the respiratory system upon inhalation and obstruct the alveoli [7]. It is well known that long-term inhalation can lead to serious cardiovascular [8] and pulmonary [9] conditions. Therefore, occupational exposure is limited by law. For example diesel engine lubricant has an exposure limit of 5 mg/m^3 [10], whereas diesel soot has a limit of 0.1 mg/m^3 (both 8 hours average).

In general, two different cases exist in the filtration of aerosols: filtration of solid particles and filtration of liquid particles (termed as "mist" or "coalescing" filtration). In addition to CCV systems, fibrous mist filters are also used in compressed gas cleaning, industrial mist eliminators, treatment of aerosols generated by lubricated machining and cutting processes, and other applications.

Whereas filtration of solid particles has extensively being studied [11–13], relatively little is known about the effects governing liquid and particularly colloidal (when the liquid is contaminated by solid particles such as in soot–in–oil mixtures) aerosol filtration. These aerosols behave differently from solid particles during filtration and the collection mechanisms are by far more complex. Whereas solid particles usually form a layer on the filter surface and thus increase collection efficiency, liquid particles coalesce on the filter fibres into much larger droplets, which are able to move within the filter and tend to decrease filter efficiency. Once the filter is saturated, liquid starts to drain. At this stage it is also likely that larger coalesced droplets are carried off from the rear of the filter by the gas flow (re-entrainment) which obviously is not advantageous with respect to the filtration efficiency. Due to the complexity of these mechanisms, modelling behaviour of mist filters is difficult and filter development is mainly based on experimental approaches.

Although it is common to regenerate (surface) filters in dust filtration in order to reduce their pressure drop and thus their flow resistance, no studies could be found which investigated the ability of mist–filters to be regenerated in a similar way. A common

technique to regenerate surface filters is to apply compressed air against the normal flow direction ("reverse pulse-jet") to remove the layer or cake of particles on the surface of the filter. Applying a similar technique to saturated mist filters would possibly allow oil to be expelled from the filter, thus decreasing saturation and pressure drop and increasing efficiency. This could significantly prolong the lifetime of filters and be beneficial both operationally and environmentally, since it would decrease downtime and the need for frequent disposal of used and contaminated filters. At the same time, a lower pressure drop would result in reduced energy consumption.

Filtration systems that collect multiphase or colloidal aerosols (such as CCV systems) are the least understood, having received very little research. The complex collection process of solid and liquid particles in CCV systems is aggravated by the fact that lubricant oil properties change due to oil deterioration and contamination which may have detrimental impacts on filter performance. Although such oil deterioration processes have been well–investigated and their mechanisms are generally known [14, 15], little is known about their impact on the filtration behaviour of mist filters and the fate of collected soot particles in the filter remained completely un–investigated to date. An understanding of accumulation and transport processes of collected solid contaminant in the filter is crucial for the development of new filters to prolong lifespan and increase efficiency and economy.

This work aims to add a significant, novel contribution to knowledge of oil–mist filter systems. It is particularly hoped that the development of more realistic filter test methods will provide a better insight into "real–world" filtration processes and ultimately improve the design and optimisation process for fibrous mist filters. For this reason, this work will include an investigation of the influence of solid contaminants, thermooxidative oil degradation and air flow breaks on performance of oil–mist filters and will investigate the "fate" of solid contaminant particles in the filter. Furthermore, different cleaning techniques to regenerate saturated oil–mist filters will be developed and the ability of filters to be cleaned and re–used will be assessed.

2 Literature Review

2.1. Filtration

Filtration is usually the most efficient method to remove solid and/or liquid particles from aerosol streams. For this reason, filters are widely used in industry, health and automotive applications. Typical examples of filter application are respiratory protection, product processing, analytical sampling or gas cleaning [16]. Although other separation methods such as cyclones, electrostatic precipitators or venturi scrubbers work more efficiently in distinct size ranges or at higher flow velocities, filters provide the highest efficiency over a very broad particle size range (typically 1 nm — 100 µm).

The most significant disadvantage of filters however, is the fact that collected particles lead to filter clogging over time which causes higher flow resistance and therefore reduced energy efficiency and higher operation costs. Thus filters require frequent replacement or cleaning which means either down–time in filtration or additional operational costs. Furthermore, most filter cleaning processes apply mechanical stress on the media which can lead to a reduced life span by inducing wear and possibly pinholes [12].

2.2. Type of Filters

Due to the a broad range of applications, a wide range of filters are commercially available. However, filters can generally be differentiated into two principle groups depending on where particle collection takes place. Depth filters collect particles through the entire filter media whereas surface filters mainly collect particles on their surface where deposited particles form a cake that again serves as a filter. Thus it is important to choose the correct filter for each application depending on aerosol properties such as aggregate phase, viscosity, particle concentration or chemical reactivity.

The most common filter types are membrane filters, granular filters and fibrous filters.

Membrane filters are a special type of surface filter which contain a complex pore structure with a relatively low porosity and comparably small pore diameter [16]. Although this structure allows such filters to reach a high efficiency, it also results in a high flow resistance and makes the filter prone to clogging and difficult to clean. Hence, such filters are rarely used in aerosol filtration but are quite common in aerosol sampling equipment and other industrial applications (e.g. desalination). Membrane filters are usually made of cellulose esters, sintered metals or plastics such as Teflon. The behaviour of this filter type has extensively been studied [17, 18]. Membrane filters are not utilised for long–term collection of liquid aerosols as they cannot retain liquid in a significant quantity.

Granular filters (or packed bed filters) consist of a packed bed of fine isometric granules often made of ceramic materials [19]. The single granules are sintered or glued together by heating the filters during manufacturing. These filters are often able to withstand high temperatures and adverse environments and are usually inert to most chemicals. Therefore, they can predominantly be found in flue gas or (salt–)water treatment applications. Granular filters usually act as depth filters, however, especially when coated, can also work as surface filters.

Fibrous filters are made from fine fibres of a broad range of materials such as stainless steel, glass, cellulose or a wide variety of plastics (PE, PP, PET, PTFE, PA). Asbestos fibres were previously used to manufacture fibrous filters for high temperature applications, however this has now discontinued due to obvious health risks. Such fibres have been replaced by ceramic and stainless steel fibres [20, 21]. These materials can also withstand high temperatures (to a certain extent) and corrosive environments, providing high filtration efficiencies in the range of HEPA (High Efficiency Particulate Air) and ULPA (Ultra Low Penetration Air). The fibres are usually of varying length and thickness ($d_f \ll 100$ µm) and are randomly arranged in the filter without intentional orientation. Most commercially available filters are either felted or needled to increase their strength and are often supported by interlaced thicker fibres. Fibrous filters initially behave as depth filters when new, however with increasing operation will eventually transition to

surface filtration, where the particles collected on the filter surface form a cake. At this stage, particles are mainly captured by the highly porous filter cake rather by the filter fibres themselves [11]. Filters designed to operate as depth filters would be replaced at or before the transition to surface filtration. For surface filters, the change from depth to surface filtration is very beneficial for filter efficiency, however pressure drop across the filter increases with increased filter clogging and cake thickness, thus requiring more power to force air through the filter. Therefore, surface filters are typically regenerated by periodically blowing air through the filter opposite the flow direction and/or are shaken to (partially) remove the filter cake. Due to the nature of this filtration mechanism, surface filters are suited for high dust concentrations and are commonly used in flue gas treatment or product collection from air streams. Surface filters often occur in the form of large filter bags ("socks") or filter candles in installations of tens to thousands of individual elements and are operated parallel in so–called filter clusters equipped with sophisticated regeneration devices.

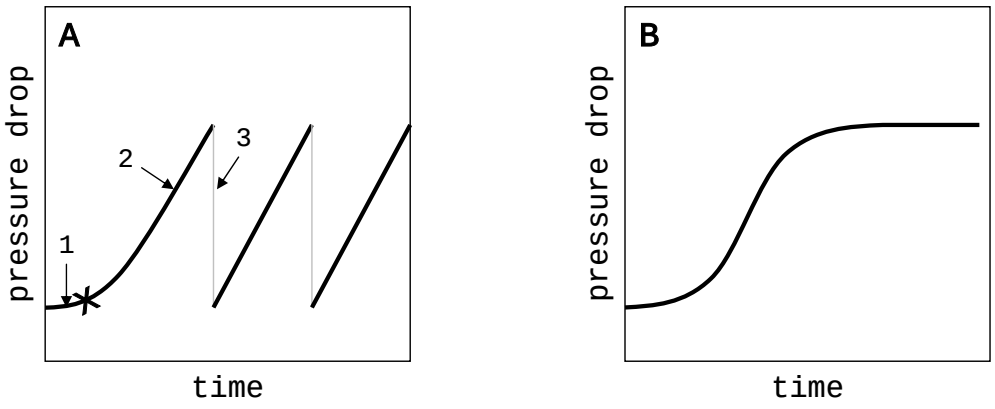

Figure 2.1.: Pressure drop behaviour of filters loaded by solid (A) and liquid (B) aerosol. The different filtration stages for filter A are marked as: depth filtration (1), surface filtration (2) and regeneration(3). X marks the transition point from depth to surface filtration. Liquid aerosol filters generally show a similar initial relationship to dust filters, however eventually attain a "steady state", where drainage of coalesced aerosol is equal to aerosol loading.

Fibrous filters can also be used for the collection of liquid aerosol particles, however filter loading shows different relationships. The collected droplets coalesce on the fibres and liquid starts to clog the filter, which increases the pressure drop. Once saturated, oil starts draining and the pressure drop levels off at a constant value (as will be discussed later). The different pressure drop behaviour of a surface (solid aerosol) and mist (liquid aerosol) filter can be seen in Figure 2.1.

2.3. Characterisation of Aerosols

Atmospheric aerosols are a mixture of liquid and solid particles from both natural and anthropogenic sources [16]. Natural aerosols are, as the name suggests, from natural sources and are also present in the absence of human activity. Typical examples for this type of aerosol are soil dust, sea salt, volcanic emissions and pollen, though many atmospheric aerosols are agglomerated from many sources. The second type of aerosols is predominant in urban regions where activities such as combustion and mechanical processes are responsible for their generation. Both kinds of aerosols however can be divided into three modes, according to their size as shown in Figure 2.2.

Primary particles (nuclei) are in the range between 1 nm and 0.1 µm and are typically derived from combustion or liquid–to–particle conversion (condensation). Particles of this size are thus often found near highways or industrial areas. Nuclei particles have a relatively short lifetime in the atmosphere since they rapidly agglomerate to form larger particles. The second mode, the accumulation mode, includes these agglomerated or coagulated particles in addition to larger primary particles. Their size typically ranges from 0.01 to 5 µm. These particles can exist a long time in the atmosphere since removal mechanisms for this particle size range are weak – they are usually removed by rainfall. Due to their low agglomeration rate they usually do not grow large enough to be counted in the coarse–particle mode. This is the third mode and usually contains large particles such as windblown sand, salt particles from sea spray and anthropogenic particles from mechanical sources like grinding, mining or agriculture. Their size is typically in the

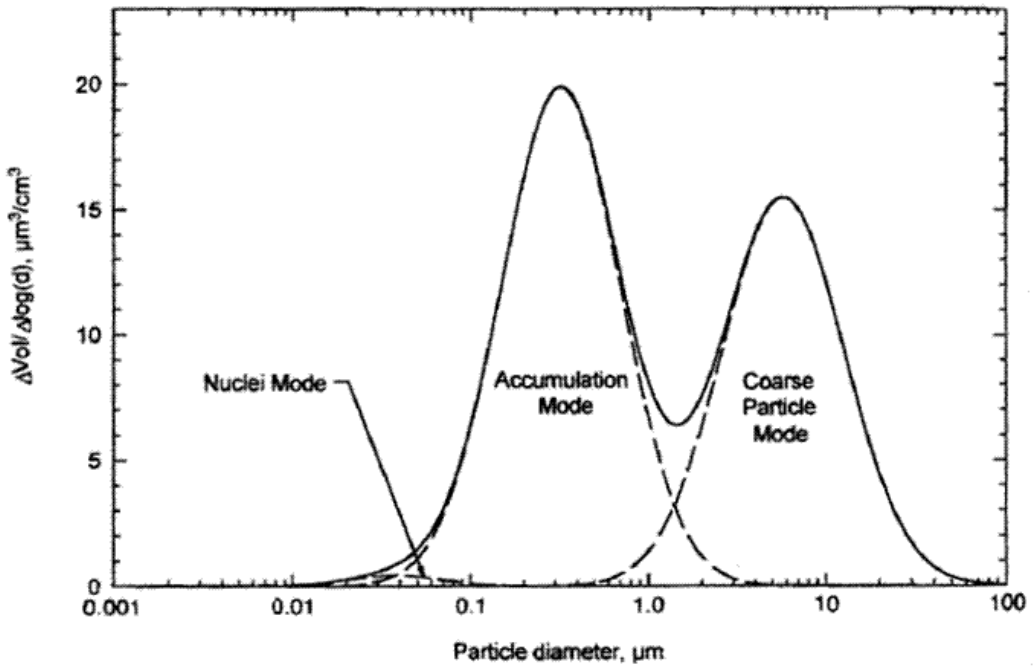

Figure 2.2.: Volume distribution of atmospheric aerosols and division into nuclei, accumulation and coarse–particle mode according to their classification and size. Source: Hinds [16].

range of 0.5 to 100 µm. Due to their size, these particles easily settle out or impact on vegetation, so their lifetime in the atmosphere is usually only a few hours or days, unless specific atmospheric conditions exist to allow them to remain longer.

Depending on their formation mechanism, industrially derived aerosols can be separated into two groups, namely disperse and condensation aerosols. Disperse aerosols are formed during mechanical processes like grinding or when atomizing liquids whereas condensation aerosols are generated by, as the name suggests, condensation of vapours. Due to their mechanism of generation disperse aerosols are usually coarser.

2.4. Filtration Theory

2.4.1. Navier–Stokes Equations

The fundamental equations for motion of a fluid through a filter are the Navier–Stokes equations, a series of nonlinear partial differential equations that derive from the basic principles of mass, momentum and energy conservation. By applying Newton's Second Law (the rate of change in momentum of a fluid particle equals the sum of forces that act upon the particle) on the motion of an arbitrary fluid particle one obtains the equation for the change of the particle's momentum of the form

$$\rho \left(\frac{\partial u}{\partial t} + u \nabla u \right) = -\nabla P_F + \nabla T + F \tag{2.1}$$

with u being the flow velocity, t the time, ρ the density of the fluid, P the pressure, T the viscous stress tensor and F the external forces on the particle, ∇ is the Nabla operator. The fluid is considered as a continuum.

For low Mach numbers ($Ma < 0.3$) it is legitimate to simplify the equation by assuming that the fluid acts as an incompressible Newtonian fluid [22]. In a Newtonian fluid, the viscous stress is linearly proportional to the rate of deformation ($T \sim du/dx$) with the constant of proportionality being the dynamic viscosity η. Thus the contribution of the stress tensor T can be written as

$$\nabla T = \eta \, \nabla^2 u \tag{2.2}$$

with ∇^2 being the vector Laplacian. For compressible Newtonian fluids, an additional term is needed which takes into account fluid compressibility, however dynamic viscosity still remains constant as it is the case for incompressible fluids. The momentum equation for a compressible Newtonian fluid is thus

$$\rho\left(\frac{\partial u}{\partial t}+u\nabla u\right) = -\nabla P_F+\eta\nabla^2 u+\left(\frac{1}{3}\eta+\lambda_\eta\right)\nabla(\nabla u)+F_{ext} \tag{2.3}$$

with λ_η being the second viscosity [23]. It is suggested [24] that $\lambda = -2/3\eta$ forms a good working approximation for gases. External forces such as gravity, Coriolis forces or pressure forces are contained in F_{ext}.

A second important equation in the Navier–Stokes series of equations is the continuity equation that describes the conservation of mass. In case of compressible fluid, the mass continuity equation is written as

$$\frac{\partial \rho}{\partial t}+\nabla(\rho u) = 0 \tag{2.4}$$

which for incompressible fluids ($\rho = const.$) simplifies to

$$\nabla u = 0 \tag{2.5}$$

Due to the complexity of a system of three dimensional flow, it has not yet been proven that a solution always exists. Indeed, relatively few solutions to a small number of special cases are known. However, solutions can be obtained using numerical methods and suitable boundary conditions [23].

Many important equations and characteristic variables can be derived from the Navier–Stokes equations, such as Reynolds number, Prandtl number and Darcy's Law.

2.4.2. Reynolds Number

Reynolds number is a dimensionless number that gives the ratio between inertial and viscous forces. It can be obtained from the incompressible form of the momentum

equation in the series of Navier–Stokes equations for a Newtonian fluid. In case of a filter which is permeated by a fluid (in this case a gas) the Reynolds number Re is defined as

$$Re = \frac{d_f \rho_G \, u}{\eta} \tag{2.6}$$

with d_f being the fibre diameter, ρ_G the gas density, u the flow velocity of the gas and η the dynamic viscosity of the gas. For macroscopic scales, Reynolds numbers $Re < 1$ are considered to characterise laminar flow whereas Reynolds numbers $Re > 2300$ characterise a turbulent flow. The switch from laminar to turbulent flow does not occur immediately, but develops slowly, forming a transition regime in which turbulent effects may begin to occur (typically at $Re > 40$), however are smothered by viscosity and thus do not fully develop [12, 25]. It has been shown [26] that at $Re \geq 250$, spheres begin to emit turbulent vertices.

2.4.3. Uniform Particle Motion in a Fluid

As the Navier–Stokes equations are difficult to solve due to their nonlinearity, some simplification is required. Most air filters operate in the laminar regime at small Reynolds numbers [12] where inertial forces on a moving particle in a fluid are negligible in comparison to viscosity forces. Stokes eliminated the higher order terms (omitting inertia effects) and thus the Navier–Stokes equations transition into a set of linear equations which can be readily solved. The resulting equations describe the forces that act on a spherical particle moving in a fluid at low Reynolds numbers ($Re < 1$). By integration, the drag force F_D can be obtained as

$$F_D = 3\pi \, \eta \, d_p \, u \tag{2.7}$$

with d_p being the particle diameter. This equation is *Stokes' Law*. Due to friction losses generated by the deformation of the layers of liquid surrounding the particle (the boundary layer), the observed drag force differs from Equation 2.7. The difference is given as 12% for $Re = 1$ and 5% for $Re = 0.3$ [16].

For high Reynolds numbers ($Re > 1000$) the drag force can be described by *Newton's Law*, which in contrast to Stokes' Law neglects viscosity as it assumes inertial forces are dominant. It is calculated by

$$F_D = C_D \frac{\pi}{8} \rho_F \, d_p^2 \, u^2 \tag{2.8}$$

with ρ_F being the fluid density and C_D the drag coefficient, which can be obtained by combining Equation 2.7 and Equation 2.8 as

$$C_D = \frac{24}{Re} \tag{2.9}$$

For small particles, a correction factor must be included which takes into account the "slip" at the surface of the particle, which means that the relative fluid velocity in proximity of the particle is not zero and thus the particle settles faster than predicted. The correction factor is known as the *slip correction factor* C_C and was experimentally derived for small oil droplets and solid particles ($d_p < 100$ nm) [27] as

$$C_C = 1 + \frac{\lambda}{d_p} \left[2.34 + 1.05 exp \left(-0.39 \frac{d_p}{\lambda} \right) \right] \tag{2.10}$$

with λ being the mean free path of the fluid. For air at 20 °C and 1.013 bar, $\lambda = 66$ nm.

With the slip correction factor included, Stokes' Law (Equation 2.7) becomes

$$F_D = \frac{3\pi \, \eta \, d_p \, u}{C_C} \tag{2.11}$$

The Knudsen number, Kn is often used to describe the ratio between particle size and the mean free path and is defined as

$$Kn = \frac{2\lambda}{d_p} \tag{2.12}$$

2.4.4. Single Fibre Efficiency Theory

Since fibrous filtration is a complex process, it is common to use a single fibre approach to examine particle collection efficiency. The fibre is considered to be perpendicular to the air flow. It is assumed that no interference with walls or other fibres occurs and that the aerosol flow is laminar. It is furthermore assumed that particles, once collected, adhere perfectly to the fibre and are permanently removed from the air stream [16].

The fraction of particles collected by the filter is termed efficiency, whereas penetration describes the fraction of particles that penetrate the filter.

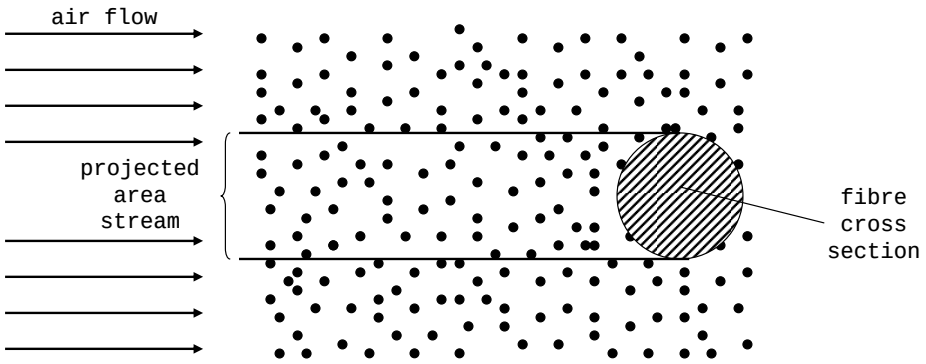

Figure 2.3.: Projected fibre collection area. After: Hinds [16].

The single fibre efficiency is defined as the number of collected particles on the complete

fibre length, divided by the number of particles geometrically incident on this length (the collection area is the projected area of the fibre as shown in Figure 2.3). Assuming that all fibres in the filter are of the same diameter, the filter can mathematically be considered as one long fibre and thus the overall filter efficiency E can be calculated as a function of the single–fibre efficiency [16] as

$$E = 1 - P = 1 - exp\left(\frac{-4\alpha E_{\Sigma} z}{\pi d_f}\right) \tag{2.13}$$

with P being the filter penetration, α the packing density of the filter, E_{Σ} the single–fibre efficiency and z the filter thickness.

The packing density of the filter describes the ratio of fibre volume V_{Fibre} to filter volume V_{Filter}

$$\alpha = \frac{V_{Fibre}}{V_{Filter}} \tag{2.14}$$

The principal difficulty in applying the single–fibre efficiency equation, is determining the value of E_{Σ} since it is the sum of a number of different mechanisms which lead to the removal of particles in a filter [16]. Practically, the overall efficiency of the filter is usually calculated as

$$E = 1 - \frac{c_{out}}{c_{in}} \tag{2.15}$$

with c_{in} and c_{out} being the particle mass or number concentration entering and leaving the filter, respectively.

Different particle collection mechanisms exist and the effectiveness of each depends on the filtration regime and filter properties. The main particle collection mechanisms are interception, inertial impaction and diffusion. These are illustrated in Figure 2.4 and are discussed in the following section. Other mechanisms (e.g. electrostatic deposition

and gravitational settling) are usually of little importance in mist filters, so will not be discussed in detail here.

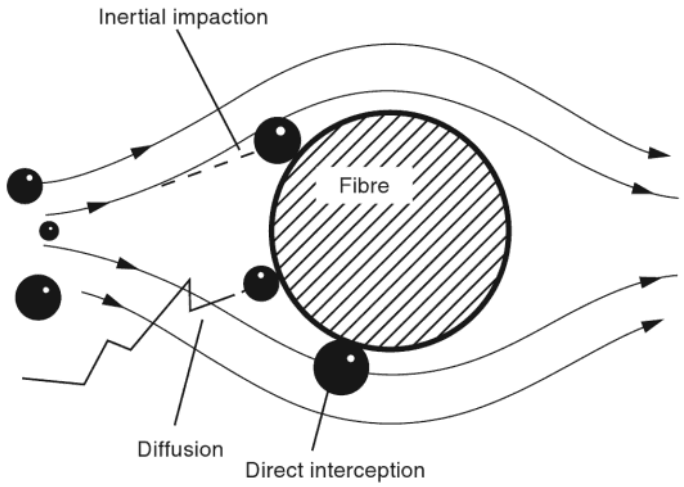

Figure 2.4.: Principal particle collection mechanisms on a single fibre: impaction, interception and diffusion. Source: Sutherland [28].

Collection by interception occurs when a particle is able to follow the flow streamline around the fibre (and therefore should not be captured), however due to its finite size, contacts the fibre on its transit and therefore is removed from the aerosol flow. It is evident that this collection mechanism can only occur when the flow streamline passes the fibre surface within one particle radius. The single–fibre efficiency for interception E_R is given as

$$E_R = \frac{(1-\alpha)R^2}{Ku(1+R)} \tag{2.16}$$

with R being the ratio between particle diameter and fibre diameter d_f and $Ku = f(\alpha)$ the Kuwabara hydrodynamic factor, which counts for the effect of distortion of the flow field around a fibre because of its proximity to other fibres [16]. The Kuwabara hydrodynamic factor is defined as

$$Ku = -\frac{1}{2} ln(\alpha) - \frac{3}{4} + \alpha - \frac{a^2}{4} \tag{2.17}$$

Inertial impaction occurs when a particle is not able to follow a flow streamline around the fibre due to its inertia and thus leaves its initial streamline and hits the fibre, where it is collected. The Stokes number Stk characterises this process by giving the ratio of the particle stopping distance to the fibre diameter, and is defined as

$$Stk = \frac{\tau u_0}{d_f} = \frac{\rho_P \, d_p^2 \, C_C \, u_0}{18 \, \eta \, d_f} \tag{2.18}$$

with τ being the relaxation time of the particle, C_C the slip correction factor (see Equation 2.10) and u_0 the velocity of the particle (identical to the fluid velocity). The single–fibre efficiency for inertial impaction E_I is a function of the Stokes number, and is given by

$$E_I = \frac{Stk \, J}{2Ku^2} \tag{2.19}$$

with the $J = f(\alpha, d_p/d_f)$, being an empirical parameter [16]. Considering the definition of the Stokes number, it becomes clear that a E_I improves with higher particle mass (i.e. density and/or diameter) and/or velocity, as well as with decreasing fibre diameter.

Collection by diffusion (Brownian motion) on the other hand, is inversely proportional to both particle diameter and flow velocity, as can be seen by the definition of the single–fibre efficiency E_D which is given by

$$E_D = 2.6 Pe^{-2/3} \tag{2.20}$$

with the Peclet Number Pe which is defined as

$$Pe = \frac{d_f u_0}{D} \tag{2.21}$$

with D being the diffusion coefficient. Brownian motion is the random movement of particles in a fluid and thus is less disturbed when particle diameter and velocity is small. An additional interaction term (E_{DR}) must be considered, especially for particle diameters near the minimum efficiency, in order to account for enhanced collection efficiency due to interception of diffusive particles [16].

Electrostatic collection E_Q occurs when the particles possess elementary charges and/or the filter a space–charge. This effect is unlikely in filters collecting aerosols or droplets long–term, and less likely when the filters are composed of metal fibres.

The fifth deposition mechanism is gravitational settling (E_G). This method is only relevant for large diameter particles and/or low velocity filtration (or horizontal filters).

For the filtration of liquid aerosol of the size distribution as used in this work (typically 20 nm $< d_p <$ 1000 nm) the dominant collection mechanisms are diffusion, interception and impaction. Combining the single–fibre efficiencies for each collection mechanism gives the overall filter collection efficiency E_Σ

$$E_\Sigma = E_R + E_I + E_D + E_Q + E_G \tag{2.22}$$

Equation 2.22 however, is technically incorrect as different mechanisms are competing for the same particle and thus efficiency is often overestimated. However, it is usually the case that one mechanism is dominant, therefore the overall collection efficiency can be assumed to depend on only this mechanism [16]. A typical filter efficiency curve is shown in Figure 2.5.

Although efficiencies may differ for different filter properties and filtration conditions, this figure is still representative for most filters. The collection of smaller particles is dominated by mechanisms that depend on the aerodynamic diameter of the particle

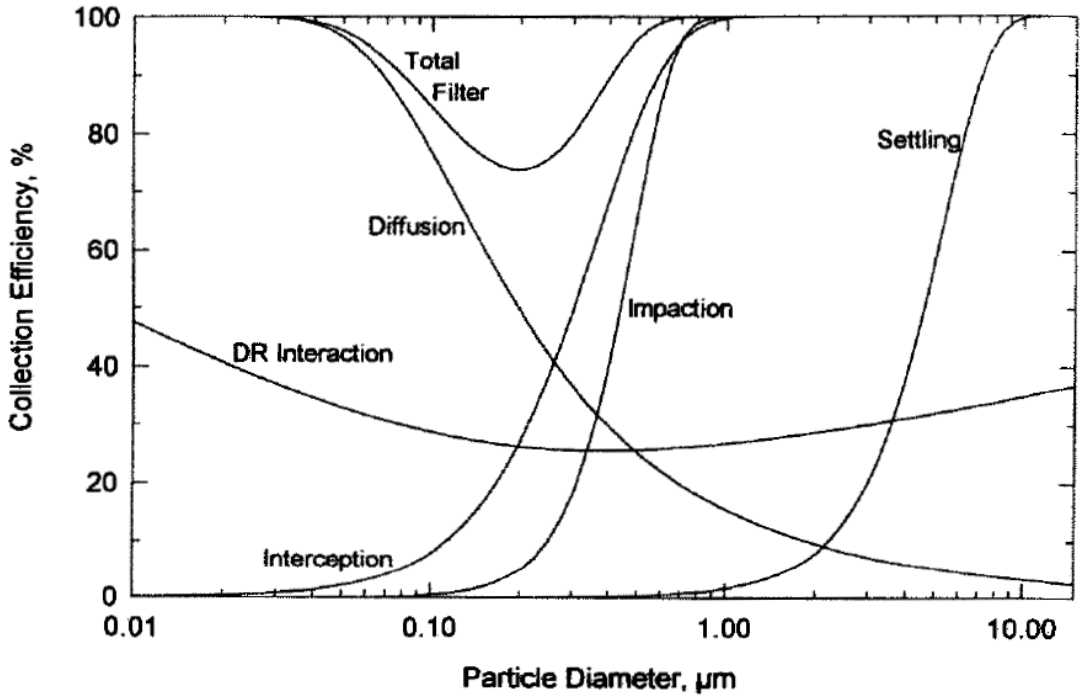

Figure 2.5.: Filter efficiency for different collection mechanisms and total filter efficiency for particles between 10 nm and 10 µm. (z = 1 mm, α = 0.05, d_f = 2 µm, u_0 = 10 cm/s). Source: Hinds [16].

(diffusion) whereas the physical diameter governs the collection of larger particles (interception, inertia) [16]. The aerodynamic diameter is an equivalent diameter that corresponds to the (physical) diameter of a spherical water droplet with the identical settling velocity. In–between the collection mechanisms, a minimum efficiency can be observed for particles which are too large to be captured by diffusion but not large enough to be effectively captured by interception and impaction. This effect is usually most pronounced between 0.1 and 0.5 µm, however this depends on flow velocity and fibre diameter.

2.5. Fluid Flow through Porous Media

Fluid flow through porous media may be described using the equations of motion and continuity (see Section 2.4.1). Darcy's Law describes the laminar flow of a single phase fluid through a porous media and was developed based on experiments of water flow through packed beds of sand. It describes the (liquid) mass transport through a porous medium, depending on the viscosity of the fluid and the pressure drop over a given distance. Although initially empirically derived, Darcy's Law can also be derived from the Navier–Stokes equations by homogenisation. It is only applicable to Newtonian fluids at low Reynolds numbers ($Re \ll 1$). It is commonly used to describe fluid flow through porous media of high packing density.

The flow rate q through the filter is given as

$$q = -\frac{k\,\Delta P}{\eta\, z} \tag{2.23}$$

with k being the porosity of the filter media, z the thickness of the filter media and ΔP the pressure drop (see Section 2.6.2). The pressure drop is the resistance to air flow across the media and represents the total drag force of all fibres.

However, most fibrous filters are of a much lower packing density and other models to describe the flow through such filter appear to be more suitable for most cases (Davies model [29] or Kuwabara model [30] - see Section 2.6.2).

2.6. Filtration of Liquid Aerosols

Since aerosols can derive from different sources, droplets can be present as liquid particles, solid particles or a mixture of both. Whereas fibrous filtration of solid aerosols has widely been studied [11, 12, 29] a rather small body of research exists in the field of liquid or

(combined liquid/solid) aerosol filtration. As a result, mechanisms are generally poorly understood.

The significant difference between solid and liquid aerosol filtration is the ability of liquids to wet the fibre, coalesce into larger droplets and drain from the filter. This means that solid particles usually remain where collected (on the surface of the fibre or filter), whereas in the case of liquid filtration, the filter reaches a state of equilibrium, the so–called "steady state" or "equilibrium state", where the amount of liquid collected by the filter equals the amount of liquid draining from the filter [31, 32].

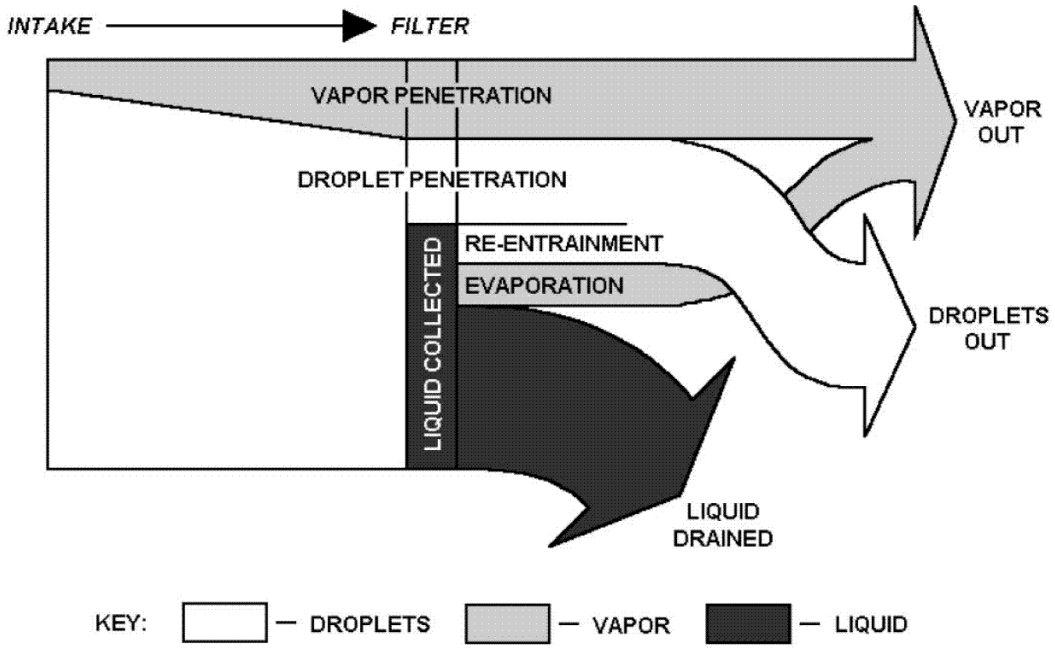

Figure 2.6.: Schematic diagram of processes which occur during fibrous filtration of (oil) mists. Source: Raynor and Leith [33].

Figure 2.6 schematically shows the macroscopic mechanisms which occur when liquid aerosols are collected by a fibrous filter system. At (or prior to) the intake droplets can coexist with volatile or semi–volatile vapour in the aerosol. Volatile compounds, together with droplets that possibly evaporate during their travel through the filter, penetrate the

filter and may later re–condense or coalesce downstream. Droplets captured by the filter can evaporate again and leave the filter with the outgoing air stream. Larger particles (typically $d_p > 1000$ µm) accumulating on the rear of the filter may be re–entrained by air flow. Due to the large size of coalesced droplets, the mass of one re–entrained droplet is often equal to the mass of many influent particles, thus re–entrainment is not trivial. Re–entrainment often occurs at high aerosol concentrations, high flow velocity and high packing densities [33].

The majority of particles however, could be expected to be captured, accumulate and finally drain from the bottom of the filter. A certain amount of liquid will be held in the filter indefinitely by capillary forces [34].

2.6.1. Filter Loading and Clogging with Liquid Particles

From the filtration of solid particles, it is well known that with time, collected particles clog the filter leading to an increase in pressure drop and filter efficiency. For liquid aerosol filtration however, several studies have examined the clogging process, with often contradictious explanations, conceptual models and even experimental results.

In early studies [35], a decrease in filter efficiency during clogging was observed, which was explained later [29] as being due to collected droplets which wet the fibres, thereby increasing the (equivalent) fibre diameter and thus reducing filtration efficiency (see Equation 2.13). This was later found [36] to only be true in the diffusional regime and only for filters with very low packing density and large fibre diameters. It was also stated [37] that filter efficiency is higher if the liquid on the fibre is present as a droplet, rather than as a liquid film surrounding the fibre, which was explained [36] by the fact that the unoccupied (and therefore still available for filtration) fibre surface has a much greater capture efficiency than a coalesced droplet on the film. However, the assumption of the existence of uniform liquid film surrounding the fibre like a tube (as was also assumed by others [32]) was proven to be incorrect in almost all cases [38].

It was shown, that fibre wettability influences the conformation of droplets on fibres, for small contact angles ($\theta < 60°$) the shape of the droplet is symmetrical in relation to the axis of the fibre (termed "barrel shaped"), for contact angles $\theta > 60°$ axisymmetric droplets will form (termed "clamshell") [39].

It was also shown, that the wettability of fibres influences droplet coalescence and movement within the filter [40]. When droplets are collected on vertical wettable fibres, they coalesce with droplets already present, thus increasing their size until gravitational forces are high enough to overcome adhesion forces, enabling them to start moving down the fibre. During this process, they are able to wet other parts of the fibre and can deposit between fibres forming liquid bridges. In contrast, on non–wettable fibres, aerosols do not drain along fibres preferentially, rather they must be detached by a combination of drag and gravitational forces. The movement of droplets was also found to be influenced by the fibre angle, with respect to air flow direction [41].

An examination of the distribution of liquid inside the filter has shown [36] that for packing densities $\alpha \geq 0.1$ the space between two fibres is small enough for droplets to form liquid bridges between different fibres, which eventually become quite large, losing their distinctive, near spherical shape. For low packing densities $\alpha < 0.004$ the space between the fibres is to large for liquid bridges to form, therefore liquid is deposited at intersections and the length of the fibres remains largely uncovered. Figure 2.7 shows the liquid distribution schematically for the two cases.

To describe wetting behaviour during filter clogging (of wettable filters) the loading process was split into different stages [31, 42]. During the first stage, the filter is wetted reasonably uniformly, however deposited droplets rarely interfere with air flow. Therefore pressure drop increases only very slowly whereas the filter penetration increases significantly. Collected liquid forms a thin layer around the fibre which once a certain thickness of the film is reached, will invariably be broken up due to Plateau–Rayleigh instability and form a series of droplets on the fibres [38, 43]. The second step is characterised by droplet coalescence and the formation of first bridges between fibres leading to an exponential increase in penetration and pressure drop starts to increase noticeably. In the third step, interstices between fibres close more and more, pools of

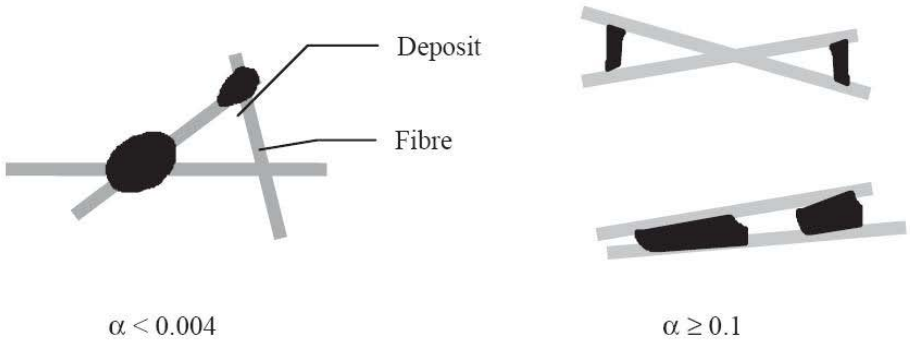

Figure 2.7.: Liquid deposits at fibre intersections for low ($\alpha < 0.004$) and and high ($\alpha \geq 0.1$) packing density filters. Source: Liew and Conder [36].

liquid form between the fibres, leading to a substantial increase in pressure drop. Due to high gas velocity in the remaining interstices, particle collection by impaction improves, thus filter penetration decreases. Once a certain threshold of oil is reached in the filter, the filter enters a stationary state ("steady state"). In this regime, pressure drop and filter penetration are constant and liquid drains from the filter at the same rate at which it is captured.

2.6.2. Pressure Drop Models

Due to variations in parameters and the complexity of the filtration process, modelling liquid aerosol filtration is difficult. Most existing models are empirically derived and therefore strongly depend on the experimental conditions (fibre diameter, packing density, face velocity) and are not broadly applicable.

Different models have been presented in literature to predict the pressure drop of fibrous filters. The common approach based either on flow past a single fibre (Davies [29]) or on flow past an array of parallel fibres (Kuwabara [30]).

The Davies model predicts the pressure drop of a clean (dry) filter as

$$\Delta P = \frac{\eta\, z\, u_0}{d_f^2} f(\alpha) \tag{2.24}$$

with $f(\alpha)$ being an empirically derived factor that includes non–ideal effects such as fibres not perpendicular to the flow direction [29]. For $0.006 < \alpha < 0.3$ it has been calculated as

$$f(\alpha) = 64\alpha^{1.5}(1 + 56\alpha)^3 \tag{2.25}$$

The Kuwabara model accounts for the distortion of the flow generated by adjacent fibres and is perhaps the most suitable model to describe air flow through a fibrous media with low packing density. Pressure drop can be calculated by this model as

$$\Delta P = \frac{\eta\, z\, u_0}{d_f^2} \frac{32\alpha}{-2Ku} \tag{2.26}$$

To be able to apply Equation 2.24 on wetted filters, modified fibre diameters and packing densities were introduced to account for the increase in effective fibre diameter due to the collection of liquid on the fibre surface [32]. This approach however, requires an even and uniform distribution of the collected liquid over all fibres in the filter and therefore is only applicable for early stages of the filter loading process.

An equation to predict the pressure drop at the "steady state" was derived empirically [36] based on correlation factors between the initial pressure drop of the filter ΔP_0 and the pressure drop at the "steady state" ΔP_{EQ1}. However, due to its empirical nature, this model is not broadly applicable. Other models [33] express the ratio between ΔP_0 and ΔP_{EQ1} as a function of the saturation S_{EQ1} by

$$ln\left(\frac{\Delta P_{EQ1}}{\Delta P_0}\right) = \frac{S_{EQ1}^{0.91\pm0.06}}{\alpha^{0.69\pm0.06}}\, exp(-1.21 \pm 0.24) \tag{2.27}$$

The coefficients of the equation were also empirically derived and thus this relationship is also not necessarily broadly applicable.

2.6.3. Efficiency and Penetration Models for Mist Filters

Most efficiency models are modified forms of the single fibre efficiency theory equation (Equation 2.22). Adapted expressions for diffusion dominated collection can be found in [44], expressions for diffusion and interception driven collection in [45] and expressions for the combined collection by impaction, interception and diffusion are presented in [33].

Several penetration models are presented in literature are derived from Equation 2.13. Adaptions have been made depending on the predominant collection mechanisms and filter properties (i.e. packing density α). From Figure 2.7, it can be seen that fibre orientation and packing density have a significant influence on the distribution of the liquid in the filter.

For low packing densities ($0.016 < \alpha < 0.054$) - where distinctive droplets on the fibres are present - a modification of $\alpha = \alpha(f)$ was suggested [33] which accounts for the decrease in available fibre surface (f) since the capture efficiency of coalesced droplets is so insignificant that it can be neglected. Thus the penetration can be expressed by

$$P = exp\left(-\frac{4E_\Sigma z\alpha(f)}{\pi(1-\alpha)(1-S_{EQ1})d_f}\right) \tag{2.28}$$

For higher packing densities ($\alpha = 0.08$) the formation of large liquid deposits between fibres was observed [46] which was accounted for by a modification of $\alpha = \alpha(S_{EQ1})$ and thus the penetration could be expressed by

$$P = exp\left(-\frac{4E_{\Sigma}z\alpha(1-S_{EQ1}(1-\alpha))}{\pi(1-\alpha(1-S_{EQ1}(1-\alpha)))d_f}\right) \tag{2.29}$$

A similar approach was presented [47] which – instead of adapting α – modified the fibre diameter $d_f = d_{f,wet}$ to account for the increase of the effective fibre diameter due to accretion of liquid on the fibre. $d_{f,wet}$ is the diameter of a wetted fibre and is defined in [29].

2.6.4. Saturation Models for Mist Filters

The filter saturation S is defined as the fraction of void volume V_{Void} replaced by collected liquid V_L [46] and can be calculated as

$$S = \frac{V_{Liquid}}{V_{Void}} = \frac{m_L}{\rho_L V_{Filter}(1-\alpha)} = \frac{m_{Filter} - m_{Filter,0}}{m_{L,max}} \tag{2.30}$$

with m_L being the mass of collected liquid, V_{Filter} the filter volume and ρ_L the density of the liquid. The maximum liquid holding capacity $m_{L,max}$ of the filter media is the theoretical maximum amount of liquid which the filter media can contain at no air flow when fully saturated, i.e. all available void space is filled with liquid. $m_{Filter,0}$ is the initial mass of the clean filter and m_{Filter} the mass of the filter and liquid together.

The mass of collected liquid can be calculated in-situ by a mass balance around the filter.

$$\frac{dm_L}{dt} = \dot{m}_{L,in} - \dot{m}_{L,out} - \dot{m}_{Drain} \tag{2.31}$$

with $\dot{m}_{L,in}$ and $\dot{m}_{L,out}$ being the mass flux of liquid into and out of, respectively, the filter. $\dot{m}_{Drain}$ is the drainage flux.

Only one model to predict filter saturation was found to be of reasonable accuracy [33].

This model is based on the relationship of saturation and three dimensionless numbers describing liquid transport, re-entrainment and drainage behaviour of the filter.

Liquid transport in fibrous filters was characterised by the Bond number Bo, which is the ratio of gravitational forces and surface tension forces. It is defined as

$$Bo = \frac{\rho_L \, g \, d_f^2}{\gamma} 10^5 \tag{2.32}$$

with g being gravitational acceleration and γ the surface tension of the liquid. Gravitational forces pull the droplets towards the bottom of the filter whereas surface tension restrains deformation of the droplets and prevents movement (drainage). The multiplier of 10^5 was included so Bo is near unity for most mist filters.

The capillary number Ca describes the ratio of drag forces to surface tension forces and is defined as

$$Ca = \frac{\eta_F \, u}{\gamma} 10^5 \tag{2.33}$$

with u being the face velocity of the filter.

The drainage rate from the filter was described by a dimensionless drainage number Dr [33] as

$$Dr = \frac{\eta_L \, \dot{m}_{Drain}}{\gamma z w} \tag{2.34}$$

with η_L being the viscosity of the draining liquid and w the filter width perpendicular to flow and gravity.

The equilibrium saturation S_{EQ1} can then be expressed by the empirically derived equation

$$S_{EQ1} = \frac{\alpha^{0.39\pm0.09}}{Bo^{[(0.47\pm0.06)+(0.24\pm0.07)ln(Bo)]}\ Ca^{0.11\pm0.04}}$$
$$exp[(-0.04 \pm 0.36) + (6.6 \pm 1.5)10^5\ Dr] \quad (2.35)$$

Due to its empirical nature, this relationship is only applicable for filters with similar conditions (α = 0.016 – 0.054, u = 5 – 25 cm/s, z = 88 mm and d_f = 2.9 – 8.5 µm).

2.7. Combined Filtration of Solid and Liquid Aerosols

In certain industrial processes, aerosols are often composed of both liquid and solid particles. Such aerosols are common in automotive (oil mixtures with soot and wear–metals), industrial (machining and drilling) and agricultural (fertilisers, pesticides) environments. Despite the prevalence of such colloidal aerosols, very little attention in literature has been given, with only a few previous studies found. A partial study on the combined filtration of oleic acid and NaCl particles [48] described the initial stages of filtration only and is therefore not overly useful. Another study investigated the capture of solid particles on wetted fibres and the behaviour of solid particles captured in liquid droplets on the fibre surface [49]. However, this work used a single fibre only and solid and liquid particles were not admitted into the system simultaneously, rather than in succession. The effect of fibre wetting on the clogging and regeneration behaviour of dust filters was investigated in [50], however the liquid aerosol was merely used as irrigation of the filter surface and therefore does not represent filtration of colloidal aerosols. The influence of solid particles on liquid filtration was investigated in an experimental study using Di–Ethyl–Hexyl–Sebacate (DEHS) and alumina particles [51]. The authors identified five different stages during filtration which were considerably different from that found for liquid–only aerosol filtration (as discussed earlier in this chapter).

During the first stage, the filter showed a moderate pressure drop increase which was

similar to the depth filtration stage for liquid and solid particle filtration. Particle collection was found to take place throughout the filter with particles preferentially deposited on other particles already present. The second stage was characterised by a sharp increase in pressure drop as also occurs for single phase filtration. The collected liquid formed large droplets, bridging fibres and hindering air flow through the filter. These phenomena explain the increase in pressure drop. During both stages, no particle deposition on the filter surface could be detected. In the third stage, the sharp increase in pressure drop ceased and the formation of a thin layer of particles on the filter surface was reported. The slow increase in pressure drop was assumed to be due to an internal rearrangement of liquid captured in the filter. This step was followed by a second sharp increase in pressure drop, albeit less distinct than the first one. It was assumed that the filter cake on the surface increased flow resistance, so that a higher energy was needed for the liquid to percolate through the cake. A second supposition was that the formation of liquid bridges in the second step, combined with filter cake formation during the third step, acted to clog preferred passageways through the filter, thus accounting for the higher flow resistance. In the final step, drainage began and the filter attained a "steady state". The authors also reported distinct passageways through the filter cake on the front surface, with no solid particles were detected in the drained liquid.

The study also investigated the influence of different solid–liquid ratios on the evolution of the pressure drop. For all mixtures containing solid particles the shape of the pressure drop curve was the same as previously and mixtures always showed a higher pressure drop than for solid–only or liquid–only aerosols. For aerosol concentrations $> 13.5\%$ (solid to liquid) up to 75% the pressure drop evolution was very similar.

Overall, little is known about the changes of oil/mixture properties caused by solid particles and their effect on aerosol filtration with fibrous filters. No literature was found describing the mechanisms of solid particle (soot) accumulation in filters during filtration of soot–in–oil colloidal aerosols.

2.8. Discontinuous Filtration of Aerosols and Filter Cleaning

All filtration models and theories discussed earlier were developed assuming a constant rate of air flow through the filter and a constant aerosol generation rate. In the vast majority of industrial and automotive applications however, filtration systems are not operated continuously, but rather with significant variation in flow rate and cessation of flow for extended periods of time (in which both air flow and aerosol generation are discontinued). Nevertheless, discontinuous operation during liquid aerosol filtration has not yet received significant research to-date, despite it being the norm in industry. Only one study was found that examined the evolution of the pressure drop and the efficiency after a single break in aerosol generation [52]. During the break, the filter was normally "flushed" with particle–free air at different velocities. It was reported that breaks during the loading stage did not affect the filtration process unless the filter had attained a "steady state". If particle generation was interrupted afters the "steady state" was reached, filter pressure drop jumped to a higher or lower level once air flow was recommenced, depending on the flow velocity of the clean air during the interruption. If the filter was "flushed" with a flow velocity greater than during filtration, then pressure drop – after particle generation was continued – reduced, whereas when being "flushed" with lower velocity air pressure drop increased. The authors supposed that a redistribution of liquid during the breaks accounted for this behaviour. At low flow velocities liquid that was about to drain from the filter was drawn back into the filter by capillary forces, whereas at high air flow rates, liquid was pushed out of the filter.

However, the above study only utilised one interruption step (again unrealistic), and due to a high degree of variability in data, the results were inconclusive. Nevertheless, it was shown that, once the filter reached a "steady state", interruptions and variations in particle generation and/or air flow velocity affected filter saturation for a long period afterwards. This study also suggested the assumption that high–flow, particle–free air might be used for cleaning the filter and thus reducing pressure drop during operation. However, this would not be possible in most "real" (industrial) cases.

2.9. Capillarity in Fibrous Filters

Chapter 2.8 and previous sections, have alluded to the influence of capillary effects in fibrous filters collecting liquid aerosols. The displacement of liquid by gas in porous media due to capillary forces is an important process that can be observed in nature and daily life. The transport of liquid in trees is a well–known example of capillarity as is water penetrating through soil or rising damp in concrete walls, masonry or wood. Liquid flow into a porous medium in the absence of significant external forces (gravity, pressure) is governed solely by capillary forces. Capillary rise is due to a potential gradient which results from a pressure difference between free liquid at the inlet of capillary tube (i.e. the porous medium) and capillary pressure inside the media. During wetting of the capillary, the flow rate of liquid into the capillary decreases due to an increase in viscous losses. The capillary number Ca represents the ratio of viscous forces to surface tension, acting across the interface between two fluid phases (see Equation 2.33).

Depending on the porosity of the wetted media, two different capillarity model approaches are commonly used. Low porosity media are commonly described by soil–type models which assume a transition area between liquid and gas rather than a sharp wetting front. Higher porosity models ($0.01 < \alpha < 0.1$) are better described by the (modified) Washburn equation, which assumes a sharp wetting front.

Fibrous filters are often considered to act in a similar way to a bundle of vertical or horizontal capillary tubes for the purpose of modelling capillary wetting [53,54]. Vertical capillary models were suggested for liquid penetration in porous media [55] and in filter paper strips [56].

2.9.1. Washburn Equation

A complete derivation of the force balance for a single vertical capillary tube was presented by Reed and Wilson [57]. This model included the acceleration terms which

were shown to be important only for the initialisation of the flow regime. Neglecting inertial effects leads to a first–order differential equation that can be solved and gives a logarithmic relationship for the capillary rise height (h_{cap}) over time (t). For $t \to \infty$ the stationary (vertical) capillary rise height ($h_{cap,\infty}$) represents a balance between capillary (i.e. surface tension) forces and gravitational force and thus can be expressed as

$$h_{cap,\infty} = \frac{4\gamma \cos\theta}{\rho_L \, g \, d_{cap}} \tag{2.36}$$

with θ being the meniscus contact angle and d_{cap} the capillary diameter.

The Washburn equation is commonly used for describing capillary rise in highly porous media such as textiles, powders or fibrous filters. It was found to be most accurate when a sharp and well defined gradient between the wetted and non–wetted media is present and where surface tension effects play a strong role in the rise of the liquid [58].

2.9.2. Soil–Type Capillarity Model

Due to its importance in the building industry, the capillarity of low porosity materials has received extensive studies [59]. Media such as concrete, brick and stone are frequently described by their hydraulic conductivity function in soil physics, since their ratio of void space to solid space is comparatively low and therefore their liquid penetration behaviour is similar to materials like clay, sand or granite.

The Washburn model assumes that the liquid/gas interface at the front is sharply defined [60], however this is not correct for media of low porosity [59]. Therefore, use of the Washburn equation would tend to overestimate saturation. Based on the approach used in soil science a capillary model was developed [61] which avoided this limiting assumption and incorporated dynamic saturation gradients in a simulation of filter media.

2.9.3. Relationship between Capillary Radius and Filter Properties

The difficulty in modelling liquid wetting of filters is the determination of the relevant parameters for the models (such as the hydraulic conductivity). Methods for determining these parameters indeed exist, however they are often not readily applicable to media of high porosity.

Thus a semi–experimental study was conducted [62] which found a relationship between the capillary diameter and readily-measurable filter properties without the requirement to conduct wetting experiments. The relationship between the capillary diameter d_{cap} and the filter properties (α/d_f) was given as

$$\frac{d_{cap}}{2} = -36.5 \ln\left(\frac{2\alpha}{d_f}\right) - 122.5 \tag{2.37}$$

with α being the filter packing density and d_f the fibre diameter in the filter. This finding also confirms the importance of surface tension effects and mean fibre spacing in capillary rise in filters. Such capillarity studies are likely to be important in predicting filter saturation.

2.10. Lubricant Oils in (Diesel) Engines

Lubricant oils are highly sophisticated blends of hydrocarbons and additives and are used for a broad range of duties in diesel and petrol engines (see Table 2.1). These duties include principally lubrication, however also wear and corrosion protection, cooling and cleaning. Thus oil is often subjected to high thermal and mechanical stresses and also contamination.

The major wear mechanisms in diesel engines are abrasion, shear, fatigue, corrosion and thermal degradation [2]. Lubricant ageing is also an important driver of wear and

Table 2.1.: Key functions of modern engine oils in combustion engines and key ingredients. After: Clague [63].

Key functions of engine oil	**Key additives**
Permit easy starting, minimise thickening induced by soot	Soot dispersants
Prevent wear, separate moving surfaces with oil film	Antiwear agents
Reduce friction, optimum viscosity of oil	Viscosity modifiers
Protect against rust and corrosion	Antioxidants
Keep engine clean	Detergents
Minimise combustion chamber deposits	Detergents
Oil must not foam (by air and contaminants entrainment)	Antifoam agents

may incorporate some of the previous mechanisms. Lubricant ageing occurs due to a deterioration in oil properties caused by contamination and thermooxidative breakdown, which is usually coupled with an increase of viscosity. A higher viscosity can lead to pumping and lubrication problems [14] which can result in excessive metal-to-metal contact and eventually in severe engine damage [3].

Incomplete combustion of diesel fuel results in the formation of soot, some of which will pass the pistons with blow-by gases or by adsorption into the thin oil film around the pistons, whereby it can eventually enter the crankcase and accumulate in the oil. Significant soot accumulation in the oil leads to an increased viscosity through thickening. Evaporation of volatiles, thermal degradation and polymerisation of the oil serve to increase oil viscosity [15, 63, 64]. During evaporation, additives such as antioxidants can also evaporate, which accelerates the thermooxidation of the oil.

Three oxidation stages were described during the thermooxidation process of engine oils [14]. In the first stage, oxidation is mainly suppressed by antioxidants in the oil and is defined by temperature and antioxidant concentration. Once the antioxidants are depleted, oil breakdown starts and occurs rapidly due to free-radical chain reactions [65]. The oil properties change and viscosity increases. The third step is the mitigation of the oxidation reactions, when most of the oil molecules are already oxidised and the increased viscosity of the oil limits the access of oxygen into the oil (by reducing the diffusion rate).

Viscosity is the resistance of a Newtonian fluid against deformation by shear or tensile stress. A Newtonian fluid behaviour can be described by

$$T = -\eta \frac{du}{dy} \tag{2.38}$$

with T being the shear stress and du/dy the velocity gradient perpendicular to the shear direction. In a Newtonian fluid, the ratio between the shear stress and the velocity gradient is constant and is known as the viscosity η.

Viscosity plays a particularly important role in engine lubrication, as it represents the lubricant's resistance against shear forces which potentially can break up the lubricant film between engine parts, typically with catastrophic consequences [66, 67]. Therefore a broad range of lubricant oils are available that suit different engine and operational conditions.

The *Society of Automotive Engineers* (*SAE*) has established a numerical code system that classifies engine oils according to their viscosity characteristics. Two different classes of oils are commonly available: Single–grade and Multi–grade oils.

Single–grade engine oils

Single–grade engine oils are – as the name proposes – only of a single oil grade and do not contain viscosity modifiers. Thus they are only suitable for a small temperature range.

Multi–grade engine oils

Multi–grade engine oils are blended with additives to maintain their lubricant ability over a broad temperature range. The SAE viscosity coding is a numerical code system to describe the lubricant's viscosity behaviour at low and at operational temperatures and is commonly of the form SAE XW–Y with X being the cold–start viscosity grade and Y the viscosity grade at operation. The additives allow the oil to cover a temperature range from –40 °C to 120 °C or higher. Typical additives are listed in Table 2.1.

2.11. Closed Crankcase Ventilation (CCV) Systems

To reduce the impact of emissions deriving from combustion engines on health and environment, regulations were introduced which limit the acceptable level of pollutants. Beside tailpipe exhaust emissions, crankcase ventilation gases are a major source of pollutants from diesel engine vehicles.

During combustion, blow–by gases from the combustion chamber pass through gaps between the cylinder wall and the piston/piston rings, into the crankcase. If the blow-by gases were not vented, the pressure in the crankcase would increase rapidly, leading to an increase in crankcase pressure, which would in turn detrimentally affect sealing and lubrication of the engine and result in engine damage.

Typical pollutants in diesel exhaust gas include nitrogen oxides, hydrocarbons and oxides. Nitrogen oxides (NO_x) and sulphur dioxide are formed during combustion and are known to cause health (mucosal irritation) and environmental (acid rain, formation of ozone) problems. Hydrocarbons result from incomplete fuel combustion or are formed during combustion. They are often a source of odour nuisance and in high concentrations are known to cause cancer (particularly polyaromatic hydrocarbons). It is obvious that these pollutants should not be released into the environment. These pollutants are also present in blow–by gases. Therefore, crankcase ventilation gases are recirculated into the air intake (closed crankcase ventilation system) of the engine and are eventually combusted as part of the fuel-air mix in the combustion chamber. However, crankcase gases do not only contain a wide range of pollutants (as mentioned above) but also lubricant oil–mist and soot particles [2]. Soot, generated by incomplete combustion, is deposited in the oil, and these depositions are the main reason for increased engine wear, particularly for turbochargers since even minor imbalances can lead to extensive damages or wear at high revolutions (turbochargers spin at speeds up to 100000 rpm) [4]. To prevent turbocharger and engine damage, the vented mixture of solid particles and oil droplets has to be removed so the filtered gas can be returned to the engine air intake. A schematic of a CCV system which utilises a fibrous filter is shown in Figure 2.8.

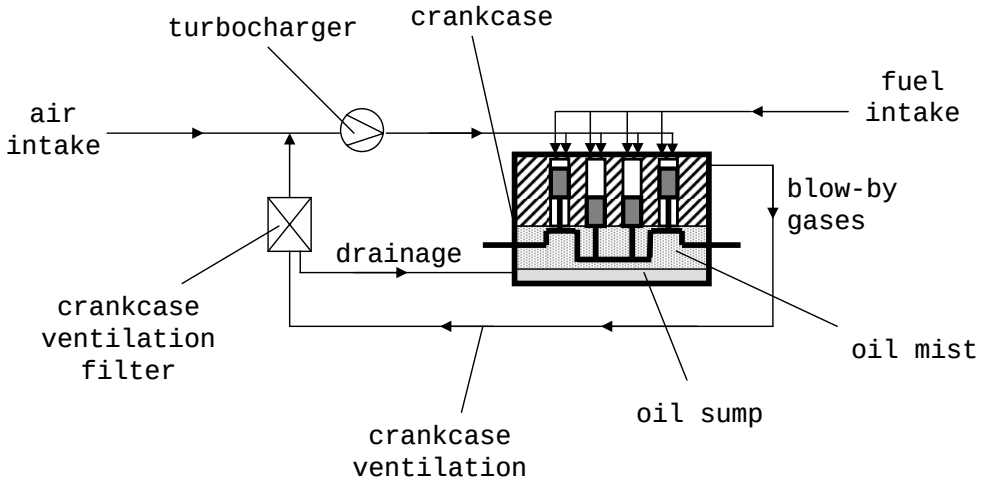

Figure 2.8.: Stylised schematic of a closed crankcase ventilation (CCV) system.

The oil–mist in the crankcase can usually be divided into three size classes (see Figure 2.2) depending on the mechanism of generation. Primary particles generated by evaporation and condensation of lubricant oil are in a size range of 10 to 100 nm (nuclei mode), particles generated by mechanical break-up of the lubricant layer by shear forces (e.g. due to blow–by gasses passing through the cylinder–piston interface) are in a size range of 100 to 500 nm (accumulation mode) and particles created by splashing from moving engine parts are approximately 1 to 20 µm in diameter. The average diameter (x_{50}) was measured as approximately 1 µm [68].

Soot particles present in the oil have approximately spherical primary particles, however rapidly agglomerate to form larger particles which are typically fractal–like agglomerates [69]. The aerodynamic diameter of soot particles inside the combustion chamber was found to vary from 150 nm to 250 nm [70]. However, soot formation is believed to be highly correlated with engine type.

2.12. Summary

It is evident, that broad gaps exist in the literature relating to the filtration of liquid aerosols. Although collection mechanisms of liquid particles on fibres and filter clogging have recently been investigated [31–33] the vast majority of these studies were conducted under filtration conditions not representative of industrial or CCV filter conditions, or only considered the loading stage, even though filters operate for the vast majority of their lifetime in a saturated state. Only one, limited study [52] was found which investigated the influence of discontinuous filtration of liquid aerosols. This study assessed the influence of breaks in the aerosol flow, however a flow of clean air (i.e. without aerosol particles) was continued in most cases. Thus this study was found not to reproduce "real" filtration applications.

Furthermore, it becomes clear that the combined filtration of liquid and solid particles has received little attention in literature to-date. A small number of studies were found, these, however, only investigated short term filter loading or were not broadly applicable due to unrealistic filtration conditions. No literature was found that investigated the "fate" of collected soot or similar particles and their ability to accumulate in the filter after being captured.

Although deterioration processes of engine lubricant oil and their impact on oil properties have received significant attention in tribology and rheology literature, nothing is known about the impact of oil deterioration processes on the performance of oil–mist filters. Particularly with respect to crankcase ventilation filters, where oil deterioration can be expected to significantly impact filter performance.

Furthermore, no studies could be found which have examined whether filters can be regenerated as per surface filters collecting solid dust particles. This would have a major impact on filter design and operation since the removal of oil from a saturated filter during operation would significantly reduce pressure drop and increase capture efficiency. This would result in increased energy efficiency, and likely, increased filter lifetime.

Therefore, the gaps in the literature include:

- the influence of longer–term discontinuous filter operation on filter performance
- the influence of oil degradation and soot contamination on filter performance
- whether CCV filters can be regenerated in a similar manner to surface (dust) filters
- whether soot accumulates in CCV filters over time

3 Research Proposal

The previous chapter identified gaps in literature which are relevant to liquid aerosol filtration, particularly of engine lubricant oils and soot–in–oil colloidal aerosols. It was found that a lack of studies existed investigating the (longer–term) influence of discontinuous filter operation and soot contamination on filter performance.

Therefore, this thesis aims to add a greater understanding to the field of both liquid and colloidal aerosol filtration, by investigating filtration under more realistic conditions. In particular, a detailed study of the influence of flow interruptions during filtration will be conducted and mechanisms occurring inside the filter during cessation and restart of the flow will be identified and assessed. The investigations will focus on the long–term behaviour of the filter (the equal of several hundred hours in real applications), long after the filter has already attained an equilibrium state ("steady state"). This stage is particularly interesting, since filters spend the vast majority of their lifetime at such conditions.

This work will also study oil ageing and its influence on filter performance and the development of a novel method to thermogravimetrically determine the soot content of filters and engine oils. The findings will be compared to filtration data collected from a field test conducted in parallel. Furthermore, methods will be developed and analysed to regenerate oil-mist filters by assisted drainage (centrifugal or high air flow cleaning).

A program of research has been developed to address these aims and objectives. This chapter gives an overview over the original research contained in this thesis, which can be divided into five categories:

- Oil analysis using thermogravimetry and mass-spectrometry
- Discontinuous filtration with interruptions in aerosol and air flow
- Influence of oil degradation on filter performance

- Soot accumulation in the filter during filtration
- Filter cleaning by assisted drainage

3.1. Thermogravimetric Analysis of Soot–in–Oil Mixtures

Chapter 4 examines the thermogravimetric behaviour of soot-in-oil mixtures and successively develops a novel method to determine the soot concentration of such mixtures. The existing soot–in–oil analysis method ASTM 5967 was proven to be inaccurate for the soot–in–oil mixtures used in this work. The problems with this method were thoroughly investigated, and an improved method is suggested. Furthermore, the ability of four different thermogravimetric analysers to imbibe oxygen and the effects of oxygen presence and pyrolysis during soot–in–oil analysis were investigated.

3.2. Discontinuous Filtration

Chapter 5 examines filter performance during long-term filtration of liquid (oil) aerosols under discontinuous operation. A novel filter testing apparatus was developed which allowed filters to be tested under discontinuous operation conditions with flow interruptions at precise intervals. Fibrous filters of different properties were tested and evolution of pressure drop, saturation and efficiency during filtration was assessed. Liquid rearrangement due to capillary forces during cessation of flow was analysed and a model developed to describe the drainage behaviour of a fully saturated filter is presented.

3.3. Influence of Oil Degradation and Contamination on Filter Performance

Chapter 6 investigates the impact of oil ageing on viscosity and on the filtration of aerosol particles with fibrous mist filters. Filtration tests with artificially aged oil (in the laboratory) helped to examine different oil ageing effects and their impact on filter performance in discontinuous operation. The findings were then compared with results from filters being used in diesel vehicles during a field test. A novel "scaled–up" thermogravimetric analysis method was developed and compared to existing thermogravimetric analysers to allow larger (filter media) samples to be analysed after filter testing experiments. The field test filters were later analysed in the (laboratory) filter testing apparatus and using this "scaled–up" thermogravimetric method. A statistical analysis using Bayesian regression was conducted and the influence of different filter and engine parameters on final filter pressure drop were identified and compared to the results of the filter tests.

3.4. Soot Accumulation in Fibrous Oil–Mist Filters

Chapter 7 investigates soot accumulation during filtration of soot–in–oil mixtures by fibrous filters. Filters were loaded using an accelerated loading method and the soot content in both filter and drained oil was determined using the large–scale thermogravimetric analysis methods presented in Chapter 6. The experimental results were compared with theoretical calculations.

3.5. Filter Regeneration Using Assisted Drainage

Chapter 8 compares different filter regeneration methods for removing oil from filters including high velocity rotation and high velocity air. This chapter also investigates the ability of filters to be re–used after being regenerated. An empirical model was developed to predict filter saturation depending on cleaning intensity (i.e. duration and rotational speed or air velocity).

4 Thermogravimetric Analysis of Diesel Engine Lubricant Oil

4.1. Introduction

As was shown in the first chapter, the duties of lubricant oils in engines are numerous and it is vital to perform regular oil analysis to ensure good oil quality and to prevent wear and damage to the engine. It is known [66, 67] that the lubricant oil changes its properties due to thermal and mechanical stress and contamination with soot and other substances during operation which restricts the lubricant's ability to perform its duties.

Several analytical techniques exist to observe the condition of engine oils [71], with Fourier Transform Infra Red (FTIR) analysis representing one of the most common methods for determining soot in routine soot-in-oil analysis. However thermogravimetric analysis (TGA) is considered to be a more accurate technique for soot content determination [72] and thus, the *American Society for Testing and Materials (ASTM)* developed a TGA procedure for soot–in–oil analysis, which has been standardised and is now part of the ASTM 5967 [73] diesel engine oil testing method and is recognised as a reference for oil testing worldwide.

In this chapter the thermal stability of both engine derived soot and "artifical" (non–engine derived) soot in inert and oxidising atmosphere is examined and the consequences for oil analysis by TGA are shown. The boundaries of the ASTM 5967 method are investigated and a modification of the method is proposed to obtain more accurate results. The impact of remaining and imbibed oxygen levels in the TGA furnace is analysed and methods to identify and reduce oxygen presence are examined. This work represents the results of several hundred TGA analyses.

4.2. Materials and Methods

4.2.1. Thermogravimetric Analysis (TGA)

Thermogravimetric analysis is a commonly used testing method to identify and quantify the composition of materials such as polymers or coal by determining their change in weight in relation to a change of temperature. Weight changes might result from thermal degradation, evaporation of volatiles or oxidation of inorganic or organic compounds. Analysis is carried out by subjecting the sample to a defined heating profile, often in conjunction with a change of the atmosphere from inert to reactive. Common inert gases used in TGA are nitrogen, helium and argon, the reactive gas is usually air, oxygen or hydrogen.

The TGA instrument consists of a high-precision balance on which the sample is placed in a heat-resistant container or crucible (ceramic or platinum) in a gas-tight environment. A small electrical furnace or infrared heating elements heat the sample following a predefined temperature profile, the temperature of the sample is monitored by thermocouples. The furnace chamber is purged during the analysis with the desired reaction gas at a known flow rate. Most TGA allow two different purge gases to be used that can be switched in-situ during the analysis. The gas flow rate is controlled by mass-flow-controllers. A schematic view of a typical thermogravimetric analyser is shown in Figure 4.1.

To gain more information about the chemical and physical reactions taking place during the heating process, the exhaust gases can be further analysed by coupling the TGA instrument to an infrared-spectrophotometer or a mass spectrometer.

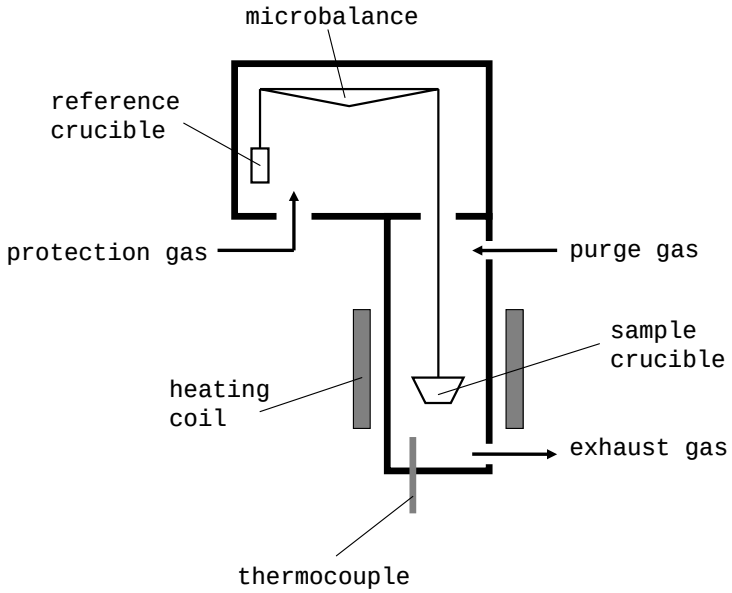

Figure 4.1.: Schematic view of a typical thermogravimetric analyser as used in this work.

4.2.2. Mass Spectrometry (MS)

Mass spectrometry is an analytical technique which allows the elemental composition of materials or the structure of molecules to be determined, by measuring the mass-to-charge-ratio (m/z ratio) of charged molecules or molecule fragments. The sample is vaporised and subjected to an electron beam generating charged molecules by removing electrons. The charged particles (ions) then pass an electric or magnetic field in the mass analyser where their direction and velocity is altered with the deflection of the particle trajectory depending on the mass and the charge of the particles according to Newton's Second Law of motion and the Lorentz Force Law. Thus the particle beam is split into different beams of ions with different mass-charge-ratio and the abundance of each ion type can then be recorded by a detector (ion trap) and can be plotted against the atomic m/z ratio receiving a mass spectrum.

The analysis of the mass spectrometry data can be complicated since a broad range of possible results can be produced which are not necessarily unique. Many mass spectrometers work in either a negative or a positive ion mode and it is crucial to know the polarity of the observed ions. Depending on the ion source, particles can be multiply charged which can significantly influence deflection in the mass analyser. The biggest difficulty is to assign the experimental mass spectrum to single compounds, therefore the first step is usually to compare the experimental result against a library of mass spectra. Due to multiply charged ions, the m/z ratio can represent a broad range of possible ion structures. It therefore is likely that several different compounds of a sample result in the same peak in the mass spectrum, particularly at higher atomic mass units (amu) when fractions of various large molecules can exist at the same time and it is usually impossible to distinguish between them.

Mass spectrometers can usually be operated in two different modes. Whereas in the total ion monitoring mode the deflecting electric or magnetic field successively changes and therefore the full range of m/z ratios is monitored, it remains constant in the single ion mode (SIM), which allows the presence/concentration of one specific m/z ratio to be monitored continuously.

4.2.3. Soot Characterisation

Two soot/carbon samples were used for the TGA experiments. Soot A was collected from the exhaust pipe section immediately after the turbocharger of a medium duty direct injection turbo diesel engine (ISUZU 4BDIT, Japan). It was collected with a plastic spatula to reduce metal particle contamination and stored in a sealed plastic container without further treatment. Soot B was a commercially produced carbon black (Printex U, Degussa Pty Ltd, Germany). Printex U has been used in several previous studies [74–76] and has been considered to be a suitable substitute for diesel soot since its thermal behaviour and particle size distribution are well characterised. The compositional analysis of the soot used is shown in Table 4.1 and was conducted using a

Thermo Finnigan EA 1112 Series Flash Elemental analyser (Finnigan, Switzerland).

Table 4.1.: Compositional analysis of engine–derived diesel soot and Printex U used in this work.

	Soot A diesel soot	**Soot B Printex U**
C (w%)	76.02	91.43
N (w%)	0.44	0.09
H (w%)	0.37	0.19
S (w%)	< 0.05	< 0.05
O (w%)	22.92	8.28

As Printex U has been proven to be a suitable surrogate for engine–derived diesel soot, it was used for most of the preliminary experiments (unless otherwise specified). Diesel engine-derived soot was used for later experiments to validate the results found using Printex U.

4.3. Preliminary Experiments

4.3.1. Copper-(II)-oxalate as a Detection Method for Oxygen in TGA

Combustion of soot due to the presence of oxygen in the furnace chamber can be disadvantageous in all TGA methods where compounds have to be evaporated under an inert atmosphere in order to separate them from the carbon containing residues such as soot. It has been shown that soot can combust at temperatures of around 450 – 500 °C and at even lower temperatures in the presence of catalytically active substances (which is possible in engine oil analysis due to metallic wear residues) [77, 78] which could have a significant impact on the result of the analysis. It is therefore vital to reduce the level of oxygen in the furnace chamber prior to the heating process if TGA is conducted in this temperature range. Unwanted oxygen traces may result from different sources, such

as impurities in the inert gas supply, leaks at seals/valves/tubing, the furnace itself or resident oxygen in the chamber after the sample is installed.

Impurities in the inert gas supply can be avoided by using ultra high purity graded purge gases where the impurity content is far less than 100 ppm. Additionally an oxygen trap can be placed inline before the TGA to remove traces of oxygen by chemical reaction on a metal catalyst. This would further reduce the oxygen level in the purge gas stream.

Leaks occurring at seals and valves can be very hard to detect and their intensity may change within the temperature range of the analysis due to thermal expansion. Although the tubing and the furnace chamber are usually held slightly above ambient pressure, oxygen can still be imbibed into the TGA due to the formation of turbulences at the gaps. A common method to detect leaks is the helium test, where helium is being sprayed around the instrument and its level in the exhaust is monitored.

In order to exclude instrument specific variations from the results, four different TGA instruments were used in this thesis. The majority of the experiments were conducted using a TA SDT Q600 instrument which also possessed DSC (Differential Scanning Calorimetry) capability (TA Instruments, Delaware, USA) using aluminium oxide crucibles. The reaction chamber was purged with nitrogen (BOC, Australia) or dry air (BOC, Australia) at a flow rate of 100 ml/min. Purge gases were a minimum of 99.99% purity. This TGA instrument's effluent gas was monitored using a Pfeiffer Thermostar TM mass spectrometer (Pfeiffer Vacuum GmbH, Asslar, Germany) via a fused silica capillary column inserted into the effluent gas stream. For comparison, selected measurements were repeated on a TA TGA Q5000 (TA Instruments, Delaware, USA), a NETZSCH STG 209F3 (Netzsch GmbH, Germany) and a NETZSCH STA 409 PC/PG (Netzsch GmbH, Germany) device. All TGA instruments were maintained and calibrated regularly, either by the manufacturer or an experienced service company.

Since it is inevitable that oxygen is present in the chamber after the installation of the sample due to the fact that the furnace has to be opened to put the sample in place, it is vital for the accuracy of the analysis to reduce the level of oxygen in the furnace chamber by pre-purging with an inert gas prior to the commencement of the analysis.

As shown in [79] the geometry of the furnace chamber and the position of the gas inlet greatly affect the expulsion of oxygen from the TGA instrument, which was assumed to be especially significant for instruments with a comparatively large furnace chamber volume as is the case for the SDT Q600 instrument.

To assess the level of oxygen traces in the furnace chamber under inert nitrogen atmosphere, a preliminary test was conducted using copper-(II)-oxalate hemihydrate since it has been shown [79] that it is a highly sensitive indicator for oxygen presence in the TGA. Copper oxalate decomposes into copper-(I)-oxide at approximately 300 °C according to Equation 4.1 with a theoretical mass of 41.9% remaining.

$$2\,Cu(COO)_2 \rightarrow Cu_2O + 3\,CO_2 + CO \tag{4.1}$$

If oxygen is present, the copper-(I)-oxide can be oxidised into copper-(II)-oxide between 300 °C and 600 °C according to Equation 4.2. This reaction results in a mass gain and thus is a simple but efficient proof of oxygen traces in the reaction chamber. Given that 100% copper-(I)-oxide was formed during the decomposition step the mass gain is 11.4% of the initial mass.

$$Cu_2O + 0.5\,O_2 \rightarrow 2\,CuO \tag{4.2}$$

In this work copper-(II)-oxalate hemihydrate (STREM Chemicals, Newburyport, USA) was used for the indication of oxygen presence in the TGA instruments.

Prior to the test the furnace chamber was purged with nitrogen for 60 minutes to expel oxygen remaining after sample insertion. During purging, the signal was monitored by MS in SIM mode and did not show any signal above background indicating oxygen was not present after purging. After the sample was heated to 600 °C at a heating rate of 20 °C/min it was held isothermal for 50 minutes. The test was conducted with three instruments (TA SDT Q600, TA TGA Q5000, Netzsch STG 209F3) as shown in Figure 4.2.

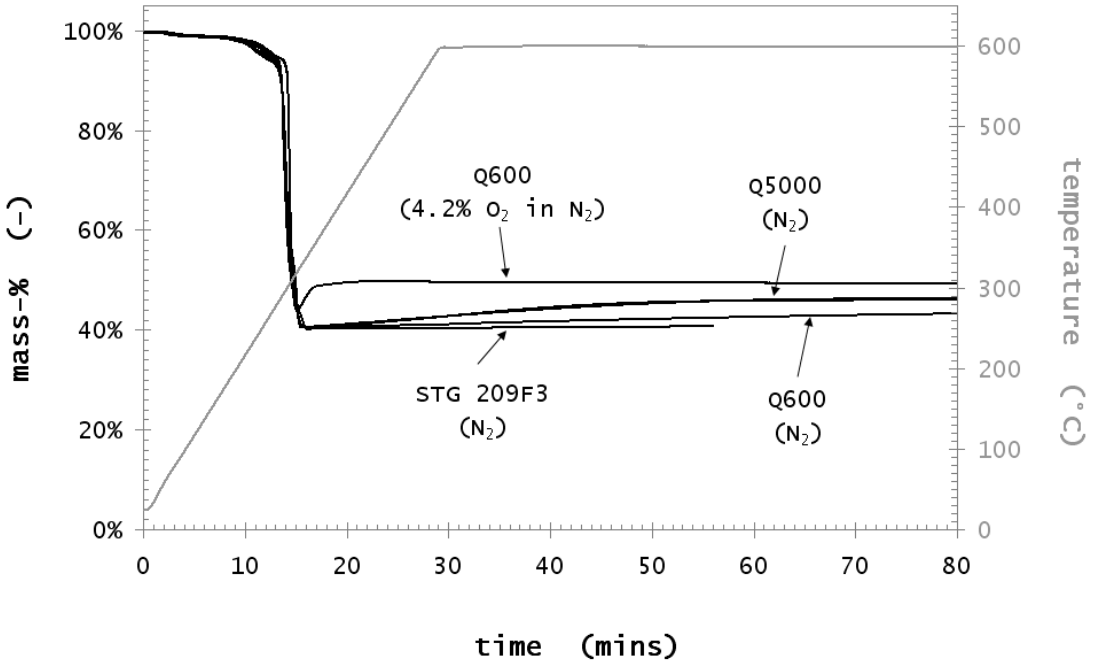

Figure 4.2.: Decomposition and mass gain of copper-(II)-oxalate in three different TGA instruments (TA SDT Q600, TA TGA Q5000, Netzsch STG 209F3) during the heating process under inert nitrogen atmosphere as an indicator for oxygen presence in the furnace chamber. For comparison purposes, the mass loss of the same experiment in a mixture of 4.2% oxygen in nitrogen was added.

All TGA instruments showed a significant decrease in mass at approximately 300 °C, as expected due to decomposition of the copper oxalate into copper-(I)-oxide. The remaining mass of 41.3% agrees precisely with the value found in literature [79]. Beyond 300 °C, both TA instruments showed a steady mass gain which indicates the presence of oxygen in the chamber and the oxidation process from copper-(I)-oxide to copper-(II)-oxide. The Netzsch instrument however showed no significant mass gain after the copper oxalate decomposed, which suggests that no/negligible oxygen was present in the chamber. Additionally, a leak test was conducted in which Helium was sprayed around the instrument. Monitoring the exhaust gas allowed the detection of Helium which would be imbibed via leaks in the apparatus. No traces of Helium were observed in the exhaust gas, therefore this instrument was considered to be leak free.

The results shown were obtained immediately after each instrument was serviced. Tests with different sample sizes (23 mg and 9 mg) showed nearly identical results, thus sample size effects could be excluded. As can be seen in Figure 4.2, reproducibility was outstanding. One test was kept isothermal for 120 minutes (instead of 50 minutes as shown in Figure 4.2) with no further mass gain being observed after approximately 90 minutes. The remaining mass was 44.5% of the initial sample mass. Conducting the same test in a nitrogen mixture containing 4.2% oxygen revealed a residual mass of 51.3% compared to 52.5% in literature [79].

This experiment shows that even after 60 minutes pre-purging of the furnace chamber, trace levels of oxygen can still be found in the two TA instruments which can react with the sample. Since both instruments have recently been serviced and tested/calibrated, these findings suggest, that it is likely that traces of oxygen remain in the furnace chamber after the experiments commenced due to TGA geometry, which can significantly affect the results of soot-in-oil analysis.

4.3.2. Oxygen Evacuation by Nitrogen Purging

To determine the purging time required for the current experiments (sufficient to expel the oxygen in the furnace chamber), the chamber was purged with nitrogen at the same flow rate as used during the experiments (100 ml/min for the TA SDT Q600 and 20 ml/min for the STG 209F3) and the exhaust gas stream was monitored using mass spectrometry (MS) in the selected ion monitoring mode (SIM, m/z = 32) (Figure 4.3). A reference nitrogen sample was also taken directly from the cylinder at the same flow rate. As shown in Figure 4.3, the oxygen concentration after the commencement of purging decreased rapidly for both instruments, reaching a constant value after approximately 40 minutes for the TA SDT Q600 and 30 minutes for the STG 209F3. Although both instruments have major differences in furnace chamber size and different flow rates, this experiment shows that more than 30 minutes is required for the oxygen concentration in both instruments to reduce to a constant limit - which is believed to be the detection limit of the MS

device. The final concentration was identical to the oxygen concentration obtained by a direct sample taken from the gas cylinder, and could be considered as less than 10 ppm as given by the manufacturer's gas specifications. All experiments in this work therefore underwent 60 minutes purging at room temperature or instrument default temperature prior to the analysis if not otherwise stated.

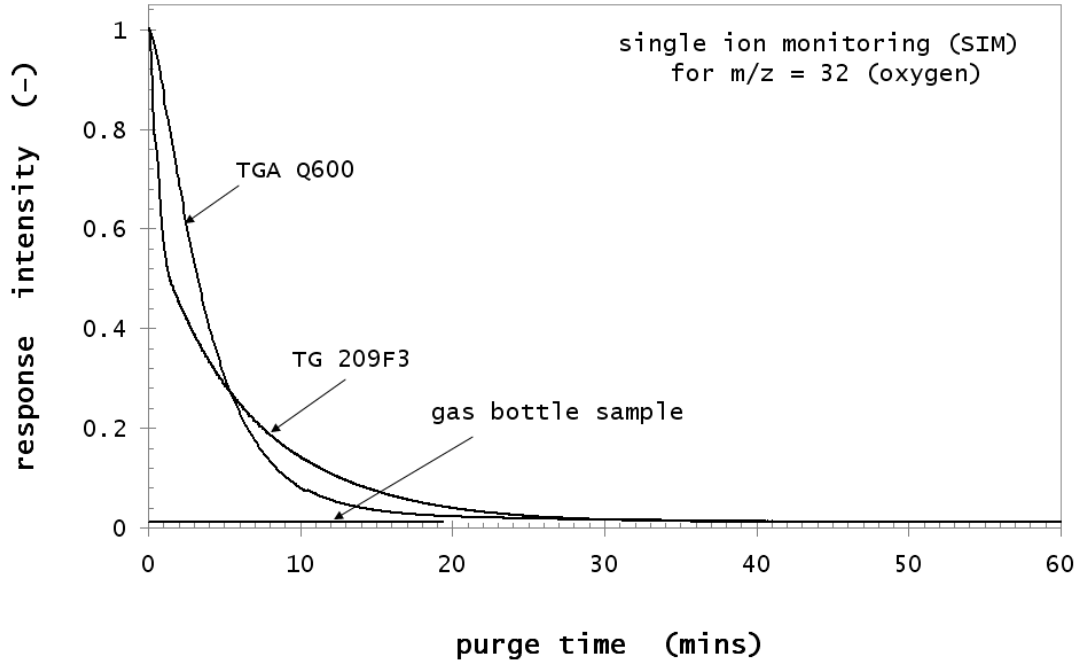

Figure 4.3.: MS signal in SIM mode for m/z = 32 (oxygen) for the TGA Q600 and the STG 209F3 instrument exhaust during a preliminary experiment to determine the necessary pre-purge time of the furnace chamber with nitrogen at a flow rate of 100 ml/min and 25 ml/min respectively. The third curve shows a reference sample taken directly from the nitrogen cylinder.

4.3.3. Thermal Degradation of Soot at High Temperatures

Elemental analysis of typical diesel engine derived soot has shown that it is primarily composed of carbon with small traces of sulphur, oxygen, hydrogen and wear metals [63]. It is known that carbon matrices can be broken down at high temperatures under the absence of oxygen, a process which is known as pyrolysis. Important examples for this process are the production of charcoal from wood, the coking of coal or the production of activated carbon.

It was shown that materials containing a large level of carbon (such as diesel engine soot) can degrade at temperatures around 500 °C to 700 °C with a mass loss of up to over 90% of the initial mass [71]. A range of different pyrolysis products could be detected [72] during this process, which were found to be mainly aromatic in nature (poly-aromatic hydrocarbons). The remaining organic residue possessed an increased carbon content as the volatile pyrolysis products had a comparatively high hydrogen-carbon ratio. Other studies [80] reported devolatilisation over a broad temperature range (between 250 °C and 750 °C) during the thermal analysis of a carbon black, which was attributed to the scission of carboxylic, sulfonic acid and other oxygen containing groups [80] which possibly are artefacts from the manufacturing process of the carbon black. Since diesel engine soot has a highly porous structure, it is likely that some of these groups (which are formed during the combustion of the fuel) are adsorbed in the exhaust pipe, and therefore can also be found in diesel soot.

To closely examine the thermal characteristics of both Printex U and the diesel soot sample used, a 7 mg sample of each was analysed using the TA SDT Q600 and the STG 209F3 with a low heating rate of 1 °C/min from ambient temperature to 750 °C (800 °C respectively) in a nitrogen atmosphere after 60 minutes of pre-purging with nitrogen. The TGA trace obtained is shown in Figure 4.4. The Printex U sample used in the STG 209F3 instrument was dried prior to the experiment.

The initial isothermal step (Region I) after heating up to 110 °C shows a mass loss of approximately 3.5% for the TA SDT Q600 instrument. This loss is most likely due to evaporation of water present [80] for both Printex U and diesel soot. Beyond 110 °C,

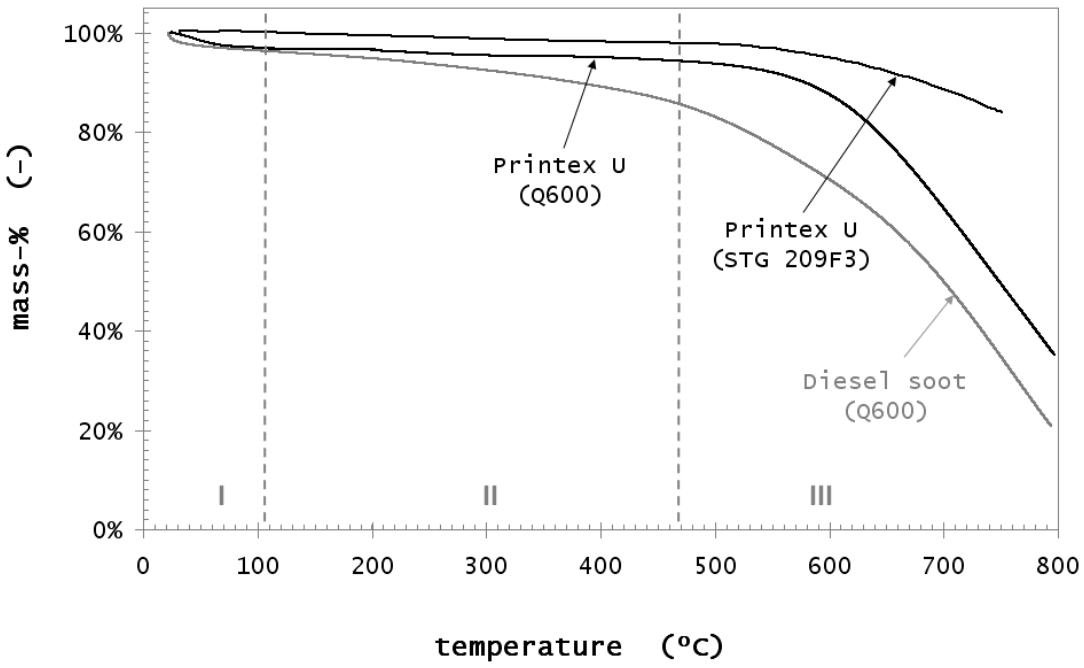

Figure 4.4.: Mass loss during the TGA of Printex U and diesel soot in a nitrogen atmosphere. Three characteristic regions where mass loss occurs can be distinguished: I (highly volatiles evaporation), II (medium volatiles evaporation) and III (combustion and/or pyrolysis of the soot).

Printex U shows a slow decay of the order of 1.5% until approximately 470 °C (Region II) for both instruments. In contrast, the equivalent mass loss for soot is significantly higher, measured at 8% to 470 °C. This mass loss for Printex U is most likely due to the volatilization of adsorbed hydrocarbon compounds [81]. The mass loss for diesel soot is greater due to the greater proportion of unburned hydrocarbons. Beyond 450 °C (Region III) an increasing rate of mass loss could be observed for all samples, leading to a near identical decay of approximately 25% (of the initial weight) per 100 °C beyond 650 °C for the TA SDT Q600 instrument. The mass loss for the STG 209F3 was significantly lower (approximately 7% per 100 °C). At 650 °C, the mass loss for Printex U was 22% for the TA SDT Q600, while for soot it was 38%. Further measurements showed that when a sample was maintained at 750 °C for 240 min only a residue of approximately 1% of the initial mass remained. The residue was non combustible in oxygen at temperatures of up to 1300 °C and was thus believed to be ash.

Hence, it appears that the mass loss observed in the TA SDT Q600 instrument beyond 450 °C was most likely attributable to combustion of carbon in the soot due to traces of oxygen. However, decomposition of the carbon matrix due to pyrolysis processes cannot be excluded at this temperature [72] and Figure 4.2 suggests that, in the case of the STG 209F3 instrument, where no significant oxygen content was left in the furnace chamber, the mass loss for this instrument is mainly due to pyrolysis since impurities in the purge gas would not provide enough oxygen to account for the magnitude of mass loss observed. Therefore the difference in residual mass between the STG 209F3 and the other instruments is assumed due to combustion. Conclusively it can be said that both combustion and pyrolysis can occur at this temperature range, depending on the condition/geometry of the TGA instrument and the oxygen content in the reaction chamber either due to residual oxygen or due to leaks. It is however evident that mass loss through either mechanism could affect the determination of soot content in lubricant oils.

4.4. Oil Analysis Using the ASTM 5967 Standard Method

Derived from techniques used in the proximate analysis of coke and coal samples (ASTM 1372 [82]) and the compound analysis of plastics (ASTM 1603 [83]) a method to analyse the soot content in used engine oils was developed in the early 1980s by a group of representatives from the coal, plastic, and petroleum diesel engine industries, as well as of thermal analysis appliances manufacturers [81]. This method was later standardised by the *ASTM* and included into the standard test method for diesel engine oils in T-8 diesel engines ASTM 5967 [73]. Since then it has been used extensively for commercial diesel engine oil analysis and is recognised as a reference for oil testing worldwide.

The analysis could be divided into two major steps. In the first step oil is evaporated under inert gas flow, commonly nitrogen or argon, with these steps being essentially completed by 525 °C [75]. In the second step, the carbon–containing components of the sample are then combusted in an oxygen atmosphere.

A characteristic mass–over–temperature plot as typically obtained from the TGA of used diesel engine oil is shown in Figure 4.5. Four distinctive stages could be observed [81] due to the different thermal stability of the compounds present. Mass loss due to the evaporation of highly volatiles (A), mass loss due to the evaporation of medium volatiles (B), mass loss due to combustible matter after switching to an oxidising atmosphere (C) and remaining mass due to ash (D).

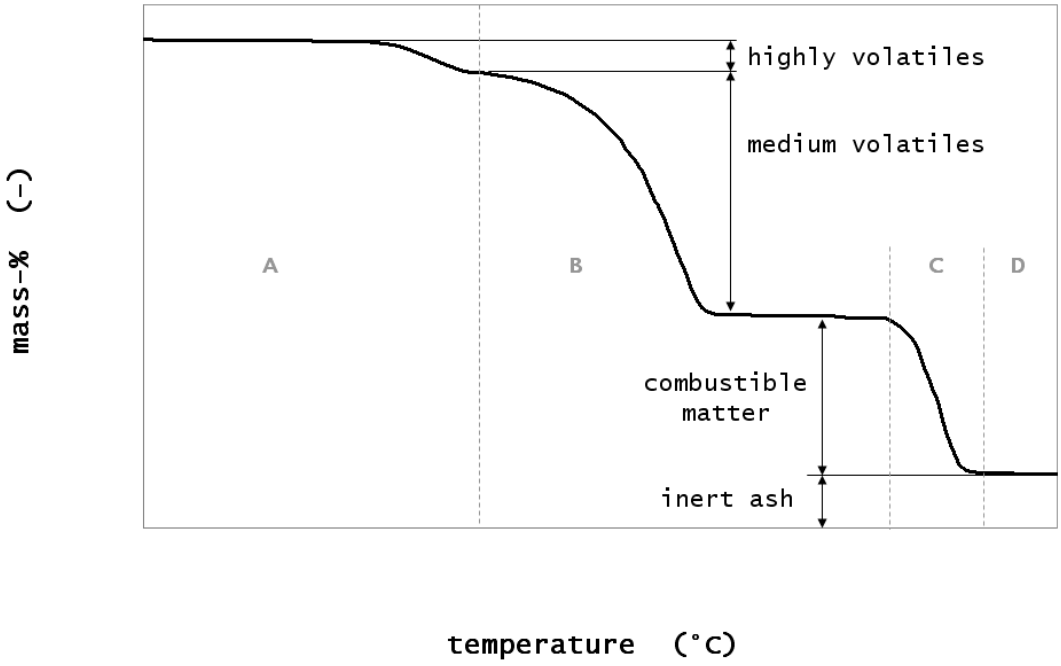

Figure 4.5.: Typical mass loss profile of a carbon containing sample during thermogravimetric analysis. The purge gas is switched from inert to oxidising atmosphere to combust the soot content after the highly (A) and medium (B) volatiles have been evaporated so as to oxidise combustible matter (C). The remaining material is defined as ash (D). After: Larkin [81].

Although there is no standardised definition of these components, it is generally agreed that they are defined as indicated in Figure 4.5 and referred to as follows:

- Highly volatile components are classified as those which result in a reduction of mass as measured by the TGA trace at less than 200 °C (Section A) typically due

to the evaporation of moisture or highly volatile compounds such as short–chain hydrocarbons.

- Medium volatile components such as oil and polymer degradation products are responsible for the mass loss in the range from 200 °C to 700 °C (Section B).

- Combustible matter (Section C) refers to non volatile but oxidisable material in its yet unoxidised form and is, according to the ASTM 5967 definition, termed as soot. Carbon is the main constituent of this material.

- The remaining material which is neither volatile nor oxidisable under the given conditions (Section D) is referred to as ash.

The evaporation of A and B usually occurs in an inert atmosphere, as it allows the highly and medium volatile fractions to evaporate without affecting the soot with which it is mixed. Once evaporation is complete, the reaction chamber atmosphere is switched to an oxidative gas (air or oxygen) to combust the soot. If the soot is combusted completely, the mass loss during this step is referred to as the soot content of the sample. The remaining ash is composed of traces of wear metals, non reactive oil additives or crustal matter which has contaminated the oil (for example dust).

Usually, the quantity of highly volatile components is negligible in used diesel engine lubricant oil, since they have already been evaporated due to the high temperatures during engine operation. Therefore the first step (Section A) is not necessarily visible for all lubricant oil samples. However, in cases where the oil was contaminated significantly with coolant or fuel, this stage would still be present in the TGA.

The ASTM 5967 method, was developed to evaluate the viscometric performance of engine oils in turbocharged and intercooled four–cycle diesel engines [73]. It covers an engine test procedure for evaluating diesel engine oils for performance characteristics including viscosity increase and soot concentrations. To detect changes in oil properties and composition, oil samples are taken in regular intervals during the test and are then analysed by thermogravimetric analyses as being suggested in Annex 4 of the ASTM method [73] and as being listed in Table 4.2 and can be seen in Figure 4.6. Prior to

analysis the oil sample is rigorously shaken for 5 minutes to assure an even distribution of the solid compounds in the mixture.

Table 4.2.: Schematic temperature profile for soot–in–oil analysis as proposed by the ASTM 5967 standard method.

Purge gas: nitrogen	
Step I	Isothermal at 50 °C for 1 min
Step II	Heat to 550 °C at 100 °C/min
Step III	Isothermal at 550 °C for 1 min
Step IV	Heat to 650 °C at 20 °C/min (URP)
Purge gas: oxygen	
Step V	Heat to 750 °C at 20 °C/min and keep isothermal until weight remains constant (LRP)

A sample is kept isothermal for one minute at 50 °C under nitrogen atmosphere followed by a quick heating step up to 550 °C. The sample is then held at this temperature for one minute allowing the evaporation of highly volatiles components and the engine oil. A further heating step to 650 °C at a lower heating rate ensures that all oil is evaporated. The atmosphere is then switched to oxygen and the sample is heated up to 750 °C to combust all soot in the sample. The program is considered to be complete once the weight of the residue remains unchanged for 5 minutes. The soot content is defined as the difference in mass between the purge gas switching point (Upper Reference Point, URP) and the Lower Reference Point (LRP), at which mass remains unchanged. The mass remaining at the LRP is calculated as the ash content.

To investigate the influence of the observed mass loss of soot during the oil analysis process, calibration mixtures of oil with differing soot content were prepared. All experiments conducted in this work that refer to the ASTM 5967 method were strictly prepared and conducted following the $ASTM$ guidelines. The samples were first stirred with a spatula to mix the particulate material with the oil and then shaken upright and inverted until the oil was of homogenous appearance and drained uniformly from a spatula. The sample mass used for the experiments was 20 mg, as suggested. Two

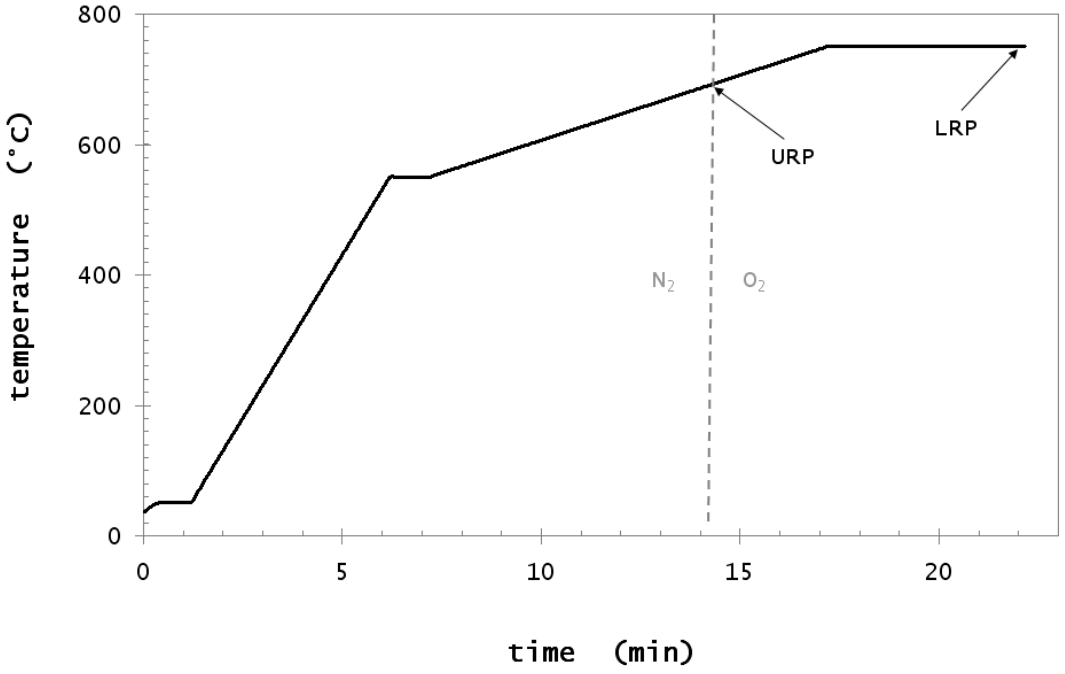

Figure 4.6.: Temperature profile for soot–in–oil analysis as proposed by the ASTM 5967 standard method. After: ASTM [73], Annex 4.

different mixtures of Castrol RX Super lurbicant oil (for specifications see Table 5.1) containing 2%, 4.6%, 5%, 7.5% and 10% (w/w) Printex U or 1%, 2%, 5% and 7% Diesel soot respectively were analysed by TGA using the ASTM 5967 standard. The instrument was not purged with nitrogen prior to the experiment to conform to the suggested method. The thermal analyser used (TA SDT Q600) was not designed to be operated with oxygen as stipulated in the ASTM 5967 method, therefore air was used as a replacement oxidising gas. It is expected that this would have no influence on the quantity of soot oxidised but only on the combustion rate. To ensure complete combustion of the soot present, a final weight reading for this step was only taken after the weight remained stable for 5 minutes. The results are shown in Figure 4.7. Each data point was gathered from at least two tests with a standard deviation of less than 0.2% throughout (therefore error bars were omitted in this graph).

All samples showed a significantly lower soot content as determined by ASTM 5967

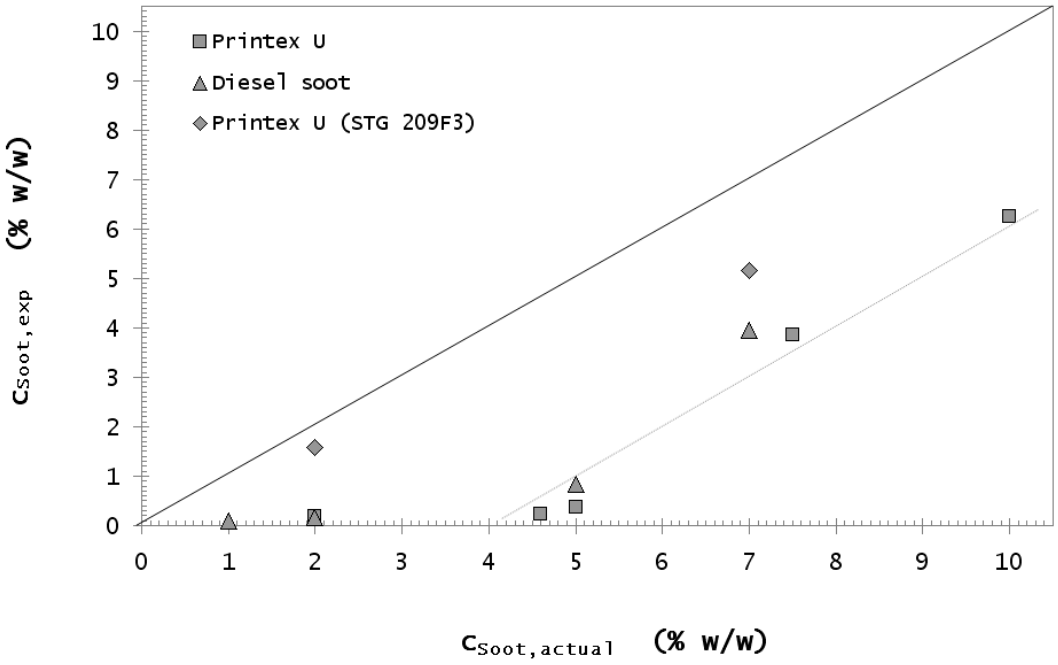

Figure 4.7.: Soot content of prepared soot–oil mixtures (2%, 4.6%, 5%, 7%, 7.5% and 10% Printex U and 1%, 2%, 5% and 7% Diesel soot in Castrol RX Super) as determined by ASTM 5967. Due to the small standard deviation of less than 0.2% for each datapoint error bars were omitted in this graph.

compared to their actual values, with the determined soot content for the 10% and 7.5% soot samples being 43% lower than their actual value in the case of Printex U and 33% lower for Diesel soot. Additionally, the soot value determined for samples with a known value of 5% soot was underestimated by more than 92%. For the samples of Printex U or Diesel soot in Castrol RX Super with a known soot content of $< 5\%$, no soot could be detected using this method. The results obtained using the STG 209F3 instrument showed slightly higher soot contents, however these values remained approximately 35% lower than the actual content.

The above results can be interpreted in terms of the soot combustion and mass loss observed in Figure 4.4. For each ASTM 5967 analysis, the results suggest that a constant amount (in relative % weight terms) of soot is combusted. If the amount of soot in the sample is higher than the amount of soot combusted, the results will be merely shifted

by the constant percentage of soot combusted towards lower values as can be seen in Figure 4.7. This threshold value is the intersection of the regression line with the abscissa and could be calculated as approximately 4.6% for Printex U and the Diesel soot used. It should be noted that the threshold would be expected to vary from this value for differing soot/oil combinations. The results determined for the 1%, 2% and 4.6% mixtures lay away from this trend as the mass of soot remaining is below the detection limit of the technique.

According to Figure 4.6, a significant portion of the ASTM 5967 method occurred in the temperature range between 550 °C and 650 °C. As has been demonstrated in this work, combustion of soot with minimal traces of oxygen has been found to occur even in well maintained TGA instruments and even after extensive pre–purging. The ASTM 5967 method suggests a short purging time of 1 minute which, according to Figure 4.3, implies more than 50% of the initial amount of oxygen remaining in the chamber for the TA SDT Q600 instrument. For the STG 209F3 instrument, the percentage was even higher (88%). This fact suggests that combustion is responsible for the majority of the mass loss of soot. Furthermore, other effects such as pyrolysis cannot be excluded at this temperature. Therefore it is very likely that most commercial TGA instruments using the ASTM 5967 method will underestimate the soot content of oil samples, since a portion of the soot has already been combusted or pyrolysed before the purge gas is switched to an oxidising atmosphere to combust the remaining soot. This is demonstrated in Figure 4.8, which shows the mass loss during heating of different soot–in–oil samples using the ASTM 5967 method.

The mass loss due to combustion and/or pyrolysis of the soot in the temperature range between 550 °C and 650 °C is clearly visible. This mass loss results in a significantly lower mass remaining at 650 °C, reducing the mass of soot present in the sample at the Upper Reference Point by approximately 4.6% for Printex U and 3.8% for soot. It is expected that the mass loss for other soot samples will occur at a similar rate. For samples with a soot content less than 5%, all soot was already decomposed before reaching the URP at 650 °C.

The results obtained by the STG 209F3 instrument show an average soot content of

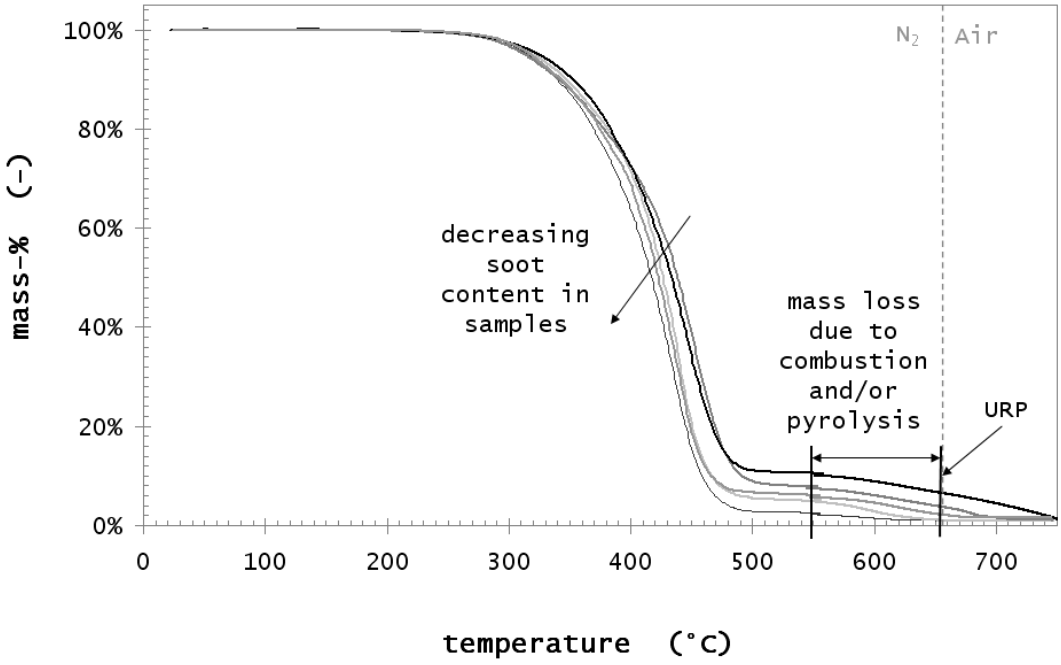

Figure 4.8.: TGA of 2%, 4.6%, 5%, 7.5% and 10% soot–oil standard sample using the ASTM 5967 method. The mass at the Upper Reference Point (URP) is reduced due to prior loss by reactions of the soot. The anomaly at 550 °C is caused by a temperature overshoot of the TGA device.

5.2% for the 7% sample and 1.5% for the 2% sample and therefore lie above the results obtained by the other two instruments. As was seen in Figure 4.4, a significantly lower mass loss during the heating of the carbon sample was again observed for the STG 209F3 (in comparison to the other two instruments) and is considered to be the loss due to pyrolysis only – hence it was expected that the soot mass loss was also lower during the analysis of a soot–in–oil mixture for the STG 209F3 instrument and therefore the measured contents were closer to the actual content.

4.5. Oil Analysis with a Modified Temperature Profile

As has been shown, combustion and/or pyrolysis of soot is responsible for inaccuracy in soot determination when using the ASTM 5967 TGA method. Especially at temperatures beyond 500 °C these effects become significant, leading to a much lower mass remaining at the Upper Reference Point. As an improvement to the method, it is therefore desirable to commence the determination of combustible matter as soon as possible after the removal of the medium volatiles. The selection of the URP at this point should reduce the amount of soot lost due to combustion and give a more accurate result. However, care must be taken that the URP temperature is not selected too low, as it is essential for the accuracy of the analysis that all oil is evaporated by the time the Upper Reference Point is reached. Any remaining oil in the mixture at the URP would be included in the soot weight and shift the analytical result towards higher–than–actual values.

Another consideration which must be taken into account when choosing the minimum URP temperature is that carbon combustion as completed in the second part of the oil analysis requires a certain temperature to overcome the activation energy for the process. Hence, to determine the combustion characteristics of Printex U, it was heated in a TGA from ambient to 650 °C at 10 °C/min in dry air. The results are shown in Figure 4.9.

After an initial mass loss in the region below 110 °C due to evaporation of moisture and highly volatiles, a slight decrease of approximately 1.5% could be observed until 400 °C. This decrease is due to evaporation of volatiles or to activation of oxygen in the soot (adsorbed / incorporated), as discussed previously and is independent from the purge gas (for comparison the mass loss of Printex U in nitrogen is added to the graph). At approximately 400 °C, combustion commences and proceeds with an increasing combustion rate towards higher temperatures, achieving a maximum at approximately 500 °C. The same peak temperature was also observed in other work [84]. At approximately 580°C, all soot had burnt off and combustion could be considered as being completed. According to these results, a minimum combustion temperature between 430 °C and 450 °C would be ideal in order to provide a fast combustion rate and minimise analysis time.

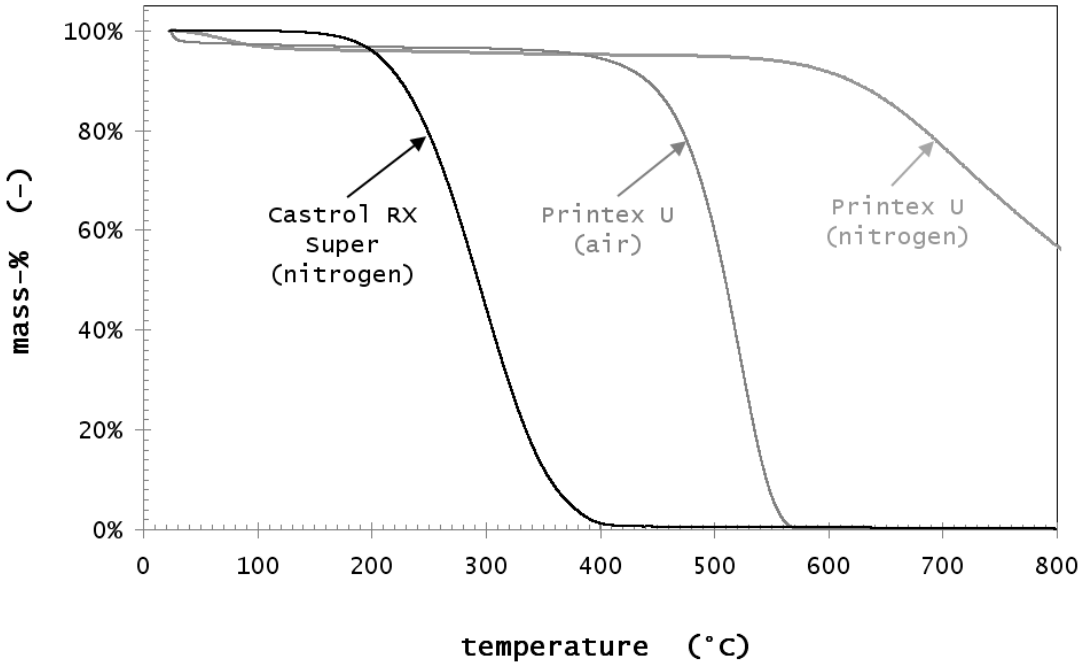

Figure 4.9.: Mass loss of Printex U and clean engine oil (Castrol RX Super) in nitrogen and dry air in a TGA using a heating rate of 1 °C/min.

Additionally, the evaporation curve of the Castrol RX Super diesel oil used in this work is also shown in Figure 4.9. The experiment was conducted in a nitrogen atmosphere until all oil was evaporated at approximately 400 °C, as evident by a constant mass. In order to check for the presence of oxidisable material, which could affect soot analysis, the purge gas was switched to dry air. However, no further mass loss was found beyond 410 °C in air. Although the boiling point of lubricant oils differs depending on the operational conditions of the oil and its properties, other studies have observed evaporation temperatures of commonly used diesel engine oil in the same temperature range [75].

Combustion and/or pyrolysis of soot has been found to be moderate up to 500 °C as can be seen in Figure 4.9. Despite the initial mass loss due to evaporation of moisture, a mass loss of less than 2% was observed within this temperature range.

It is therefore evident that a temperature of 430 °C for the URP would be ideal for

this sample with an isothermal step included at this temperature to ensure that oil evaporation was complete. After switching the purge gas to dry air, the sample is heated up to 700 °C to combust the soot contained in the sample. At this temperature, another isothermal step is provided to ensure that all soot has been combusted. Once no further mass loss can be observed, this step can be considered complete. The remaining sample mass is then classed as ash and therefore constitutes the Lower Reference Point for the calculation.

The analytical parameters for the improved oil analysis method are shown in Figure 4.10 and detailed below in Table 4.3.

Table 4.3.: Schematic temperature profile for soot–in–oil analysis suggested by the improved method.

Purge gas: nitrogen	
Step I	Heat to 120 °C at 100 °C/min
Step II	Isothermal for 8 min
Step III	Heat to 430 °C at 100 °C/min
Step IV	Isothermal for 8 min (URP)
Purge gas: dry air (or oxygen)	
Step V	Heat to 700 °C at 100 °C/min
Step VI	Keep isothermal until weight remains constant (LRP)

The initial isothermal step at 120 °C is to purge the reaction chamber to remove oxygen from the chamber (as far as possible) and to evaporate moisture in the sample. It is, as pointed out earlier, advisable to purge the instrument with nitrogen to reduce the amount of oxygen left in the furnace chamber. The purging time depends significantly on the geometry of the chamber and the gas inlet position as shown previously and is therefore instrument specific. In order to reduce the experiment time and keep conditions similar to ASTM 5967, an extended pre–purge step was removed for these experiments since this method should be less prone to oxygen traces present during the analysis and therefore was suspected to be able to perform well even with significantly shorter purging.

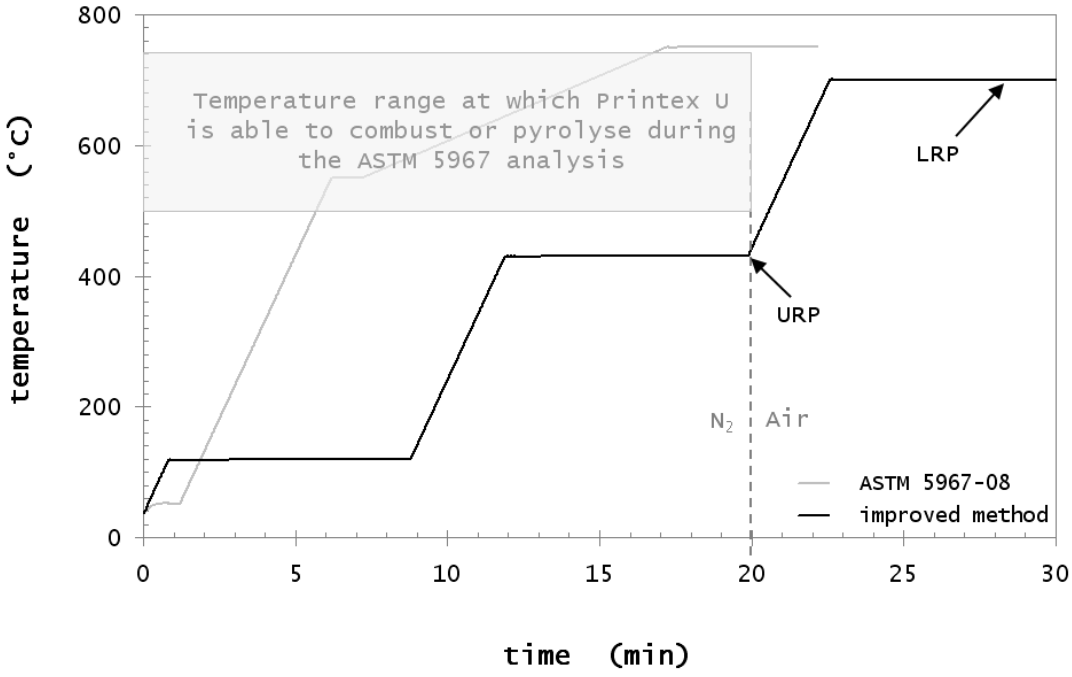

Figure 4.10.: Improved temperature profile with the Upper (URP) and Lower (LRP) Reference Points. The soot oxidising range with which the ASTM 5967 method conflicts is avoided with this improved method. Reaction chamber purge gas changes from nitrogen to air at around 19 mins 55 secs.

The improved method was tested for accuracy using a set of prepared soot–in–oil samples. Using Castrol RX Super diesel engine oil and Printex U or Diesel soot, the following samples were made (w/w): 1%, 2%, 5%, 7.5% and 10% for Printex U mixtures and 1%, 2%, 5% and 7% for Diesel soot mixtures. Sample size, preparation, purge gases and instrument parameters were used as previously. The results are shown in Figure 4.11. Each data point was gathered from at least two experiments. The standard deviation was less than 0.25% for each data point, therefore error bars were omitted.

The results gained with the improved method as shown in Figure 4.10 agree well with the actual values of the prepared standards, with determined values all being within 0.5% of the actual values. The linear fit (improved method) reveals a slope of near unity with a correlation coefficient $R^2 = 0.998$.

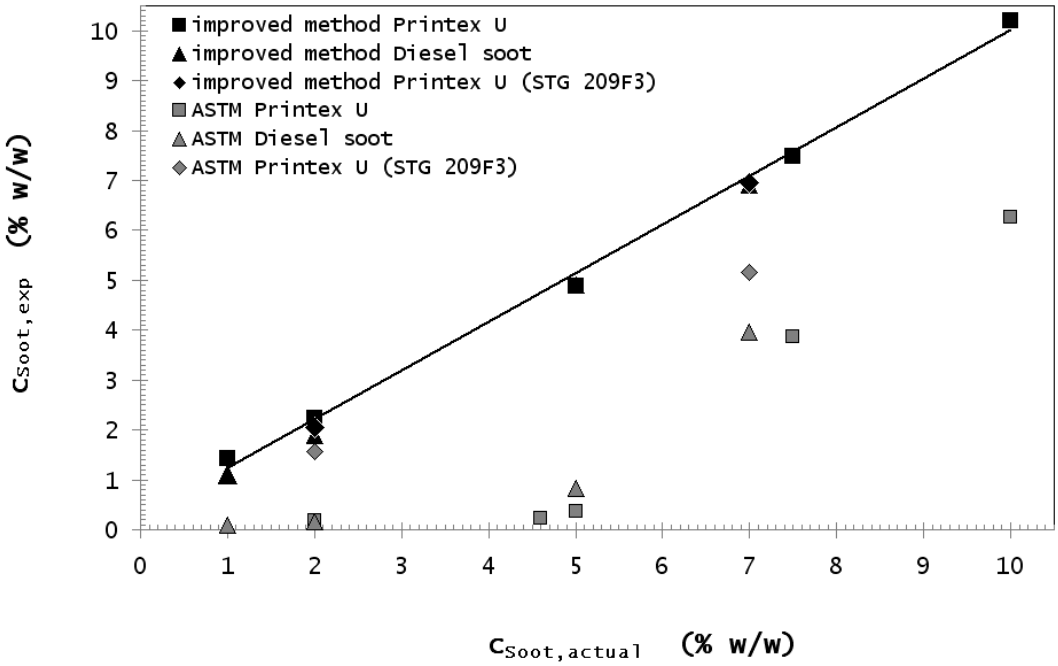

Figure 4.11.: Soot content of calibration soot–oil mixtures (1%, 2%, 5%, 7.5% and 10% Printex U and 1%, 2%, 5% and 7% Diesel soot in Castrol RX Super) analysed using the improved method in comparison to the ASTM 5967 method.

The duration of the isothermal steps was chosen at 8 minutes in order to provide a high resolution for the experimental work and the development of the method. However, it would be possible to shorten the isothermal steps to 5 or less minutes for routine oil analysis use, which would ensure that this method requires an equivalent analysis duration to the ASTM 5967 method. Measurements using a 2 minute isothermal step were conducted, with no loss in accuracy found. The high heating rate was chosen to further shorten analysis time, however to make this method applicable to a broad range of different TGA instruments which may experience problems with temperature control (overshooting), the heating rate can be reduced. Measurements with a heating rate of 50 °C/min were conducted and were found not to influence the result. The results obtained by the STG 209F3 instrument were very similar to those obtained by the other two TGA instruments. This strongly suggest that the impact of combustion, which is believed to account for the different results obtained by the STG 209F3 and the other

instruments using the ASTM 5967 method, is significantly reduced using the improved method.

Furthermore, it was found that the duration of pre–purging the TGA instrument prior to the analysis did not affect the accuracy of the improved method. For the ASTM 5967 method however, the affect was found to be significant. This is due to a the fact, that once the critical reaction temperature is reached (approximately 500 °C according to Figure 4.9) the soot combustion rate is obviously higher if conducted in an atmosphere with a higher oxygen concentration as is the case when the furnace chamber is not pre–purged. As can be seen in Figure 4.10, residence time above the critical temperature is higher for the ASTM 5967 method, which promotes mass loss due to soot combustion and/or pyrolysis and therefore produces erroneous results.

4.6. TGA of Higher SAE Graded Oils

A commercial 15W–40 oil, which is assumed to be representative of typical diesel lubricant oil for engines operation in tropical environments (and therefore of higher SAE grade and lower volatility than a typical engine oil for temperate or cold climate conditions), was used in this work. This oil, however, may not be as heavy as some fractions which can be found in–service in diesel vehicles due to polymerization, which could possibly occur at high temperatures. Since the final evaporation temperature is vital for soot content calculation (URP) in the improved oil analysis method, it is important to determine the effect of less volatile oils on the result. If the oil could not evaporate completely, the remaining oil will shift the URP to a higher value, leading to an overestimation of the soot content.

For this reason, the heaviest engine oil which is readily available commercially (Penrite HPR50, graded as SAE 40W–70) was also tested. Although this is a petrol/gasoline engine oil and a higher SAE grade than commercial diesel oils, it should nevertheless be representative of the heaviest fractions found in used diesel oil. In–service diesel engine

oil samples taken were also analysed by TGA as can be seen in a later part of this work. The oils were obtained at various service intervals (600 – 20000 km) from a range of direct injection and commonrail turbo diesel engines. Even the oil with the highest mileage and therefore the highest grade of thermal degradation was suspected to evaporate completely below 450 °C. This suggests that for engine oils subjected to typical service conditions, the URP could be chosen below 450 °C degrees and therefore still lies in the boundaries between the two oils used in the current experiment.

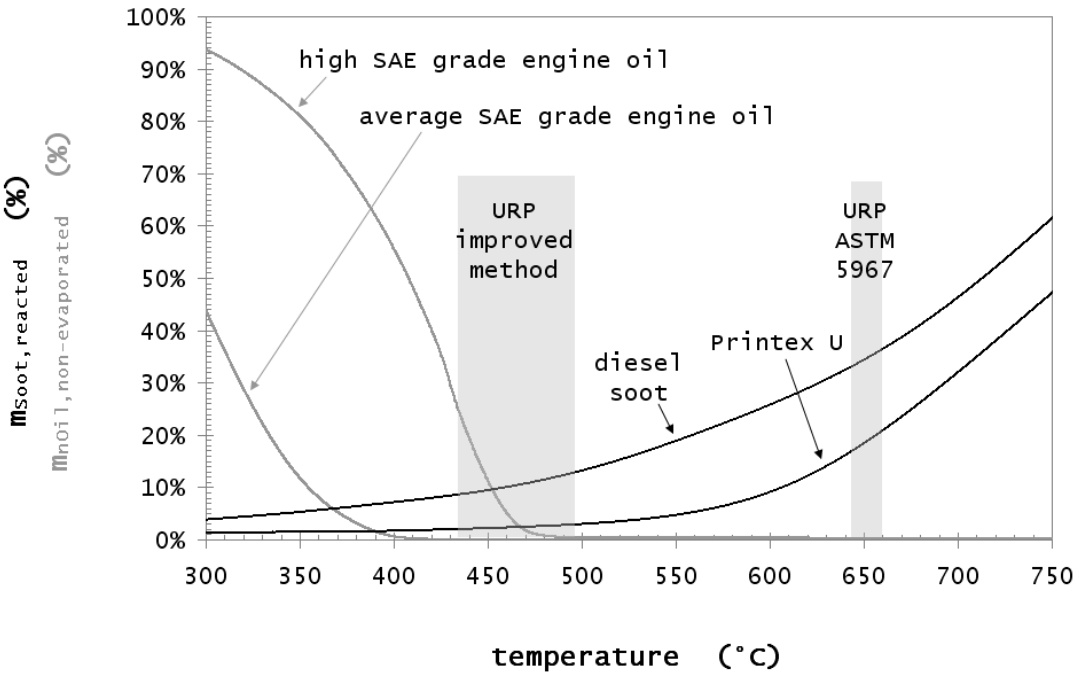

Figure 4.12.: Proportion of non evaporated oil $m_{Oil,non-evaporated}$ and reacted (combusted/pyrolysed) soot $m_{Soot,reacted}$ as a function of temperature. Different oils and soots have been used to span a representative range for each curve.

The evaporation curve in nitrogen for higher SAE grade engine oil (Penrite HPR50) to mark the expected upper boundary of oil evaporation is shown in Figure 4.12. Evaporation can be considered to be completed at approximately 500 °C for this oil. The area under the curve marks the range of possible evaporation curves of lighter engine oils

with that of an average diesel engine oil (Castrol RX Super) also included. The shift towards higher temperatures for the higher SAE graded oil is clearly visible.

Furthermore, the soot loss due to combustion in nitrogen is also shown in this graph for the two types of soot. As already shown (Figure 4.9) Printex U showed a lower mass loss rate. The area between both curves symbolises possible mass loss rate curves for common carbon blacks and soot types.

Figure 4.12 shows the difficulty of choosing the correct temperature for switching the purge gas. A compromise must be made, especially for higher SAE graded oils between complete oil evaporation and a reasonably low soot combustion/pyrolysis prior to gas change. The higher the temperature needed for complete oil evaporation, the more pronounced the issue of soot mass loss becomes, as can be seen in Figure 4.12. It may be desirable to choose an individual temperature for the URP for each oil which can be found by conducting a TG analysing of a sample of clean oil first to determine the temperature of complete oil evaporation. Such a method would however mean that some variability in accuracy of soot determination would exist when comparing results from different oils. Additionally, it is possible that some oil polymerisation during engine operation may occur [84]. The occurrence of such would imply that the "used" oil would require a higher temperature than the new oil for complete evaporation. This would lead to an overestimation of soot in the oil as some oil will be combusted along with the soot. However, such an effect may not be completely un–advantageous in practice ("false positive"), since the oil's ability to perform its lubrication and cooling duties is negatively influenced by polymerisation.

The suggestions above may not be suitable as a standard method if comparison between engine oils of different SAE grades is to be conducted. This is due to the fact that a variable quantity of soot would react prior to gas change during analysis for each oil type/SAE grade. If a universal standard for all oils was to be desired, the evaporation temperature of the higher graded oil can be used as URP temperature for all oils. This leads to an underestimation of soot as shown before, however the mass percentage of combusted soot is the same for all samples.

Depending on the application, one of, or a combination of both methods can be chosen. If only oils with a similar SAE grade are used, it is advantageous to choose one temperature for the URP which is, for accuracy reasons, close to the evaporation temperature of the clean oils to prevent unnecessary soot mass loss. This temperature is assumed to be similar for oils of a similar SAE grade. If oils with different SAE grades are to be compared, the evaporation temperature of the highest graded oil should be used as URP temperature. Some soot mass loss due to reactions will, in this case, occur for all samples, however since the temperature profile is the same for all samples, the mass percentage of reacted soot will be similar and therefore results comparable.

The difference in the quantity of combusted soot between the ASTM 5967 standard method and the improved method is clearly visible. The improved method shows at least 70% lower soot mass loss for the same soot–oil configuration than ASTM 5967. The difference becomes more significant for low SAE graded oils as it is possible to evaporate them at relatively lower temperatures, in order to further reduce soot combustion/decomposition. During this work, it was not possible to find an engine oil which requires a temperature of 650 °C for the Upper Reference Point as proposed by the ASTM 5967 method.

4.7. Conclusion

It has been found in this chapter that significant combustion and/or pyrolysis occur at temperatures above 450 °C and that the lower end of this temperature range conflicts with the temperature specified by the ASTM 5967 engine oil analysis standard. Thus carbon mass loss can significantly affect the results of soot–in–oil determination by TGA. It was shown that a constant relative amount of soot is lost during analysis which leads to an underestimation of the soot content by approximately 30 – 40% for samples with more than 5% (w/w) for the soot–in–oil mixtures examined. For samples containing significantly less than 5% (initially) the remaining soot amount is close to the detection limit of this technique [85].

An improved oil analysis method was proposed which was able to provide increased accuracy of soot determination compared to the ASTM 5967 method. The method has been proven to be significantly more robust and therefore far less sensitive to mass loss induced by combustion with oxygen traces in the instrument and pyrolysis effects [85].

Since the modified temperature profile showed a much more accurate result, this method was used for the determination of the soot content in the engine oil used for the experiments. Since the oil properties of Castrol RX Super were known, an exact adaption of the URP to 450 °C was possible which, as was shown earlier, is high enough to evaporate the oil, but at the same time minimises the loss of soot due to premature combustion or pyrolysis effects. Additionally, a pre–purging time of 60 minutes was conducted for all tests [85].

It is clear that accurate soot–in–oil analysis is essential for studying CCV filter performance. This work was not initially intended, however was made necessary due to errors found when using ASTM 5967 and the FTIR method for soot–in–oil analysis. This work also permitted the development of a "scaled–up" method for the analysis of CCV filters, which is detailed in Chapter 6.

5 Discontinuous Filtration

5.1. Introduction

Chapter 4 examined the analysis of soot–in–oil mixtures as a prelude to CCV filter testing with sooty or colloidal (oil) aerosols. However, before the influence of soot is examined, a baseline test method using clean oil must be developed and fully evaluated.

As was shown in Chapter 2, most studies investigating filter loading behaviour have been conducted using constant aerosol flow and loading rates. However, typical filtration systems such as those used in compressed gas or automotive applications are mainly operated discontinuously (cessation of flow for extended periods of time in which both air flow and aerosol generation are discontinued), or with significant variations in flow. It has been shown [31], that after a break in aerosol flow, the pressure drop of a HEPA filter collecting oil aerosol increased when the aerosol flow was re–engaged. This phenomenon however was only examined with one start–and–stop cycle and in most of the cases aerosol generation was indeed stopped however clean air was still flowing through the filter, which is quite different to the scenario in real world applications.

The current chapter aims to examine the filtration behaviour of aerosol filters during long–term and discontinuous operation as occurs in "real world" applications. Approximately 60 filters of two different filter types (both types were industrial oil–mist filters as are used in automotive crankcase ventilation systems) were tested in continuous and discontinuous operation. The filters were each operated for between 100 and 250 hours. To accelerate the attainment of the first equilibrium state, filters were preloaded using one of two additional loading methods and once an equilibrium state was reached aerosol flow was stopped at regular intervals (discontinuous operation). The behaviour of the filters during discontinuous operation was investigated and the influence of different filtration and break interval durations was evaluated.

A phenomenological model was developed to show the relationship between pressure drop

and saturation during the initial cleaning of a fully saturated filter and to investigate the effect of different "effective" capillary diameters (see Section 2.9) in a filter on the cleaning of clogged capillaries in the first seconds after air flow is continued.

5.2. Materials and Methods

5.2.1. Filter Testing Apparatus

The filtration experiments were conducted using a specially developed filter testing apparatus as shown in Figure 5.1. The test aerosol was generated by a 3–jet Collison nebuliser and was passed through a settling chamber to reduce the concentration of large droplets in the aerosol stream. After dilution with clean (HEPA filtered) air the aerosol was passed through the test filter chamber using a DVP SB10 vacuum pump (D.V.P. Vacuum Technology, Italy) at a flow rate of 55 LPM controlled by a critical orifice. A safety filter was installed before the critical orifice and the pump to capture oil droplets that passed the test filter.

The pressure drop of the filter was measured using a differential pressure sensor (SenSym SDX01D4, SensorTechnics, Germany). Iso–kinetic sample points before and after the filter allowed filtration efficiency monitoring using a condensation particle counter (CPC) (TSI 3775, TSI Inc., WN, USA) or a scanning mobility particle sizer (SMPS), consisting of the same CPC and a differential mobility analyser (DMA) (TSI 3081, TSI Inc., WN, USA). These sample points were also used for gravimetric measurements. The oil draining from the bottom of the filter chamber was collected in a vessel mounted on an analytical balance (GX400, A&D Engineering Inc., CA, USA). The entire balance was housed in a pressurised vessel at the same pressure as the filter chamber and the drainage hose from the filter chamber was not in contact with the collection can.

The compressed air supply valve for the nebuliser and the vacuum pump were controlled

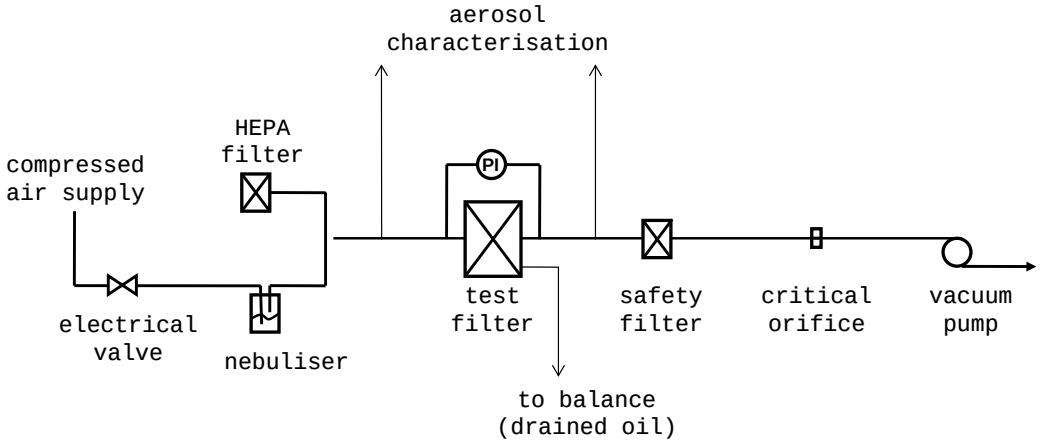

Figure 5.1.: Experimental apparatus for filter testing. The solenoid valve on the compressed air supply allowed the nebuliser to be switched on and off.

by a timer which allowed air flow and aerosol generation to be stopped simultaneously during discontinuous operation.

All filter tests were conducted at room temperature.

5.2.2. Engine Oil

Castrol RX Super (Castrol Ltd., UK) was chosen as test oil for laboratory filtration experiments since it was considered to be a representative diesel engine lubricant for subtropical conditions and is widely used in light trucks in Australia. Its properties — as provided from the manufacturer – are shown in Table 5.1.

The particle size distribution of the oil aerosol used to challenge the filter can be seen in Figure 5.2 (as measured by SMPS). The volume–mean diameter was calculated as 510 $\pm$1.5 nm from SMPS measurements.

Table 5.1.: Properties of Castrol RX Super diesel engine oil (values given by manufacturer).

SAE grade	15W–40
API grade	CI–4/SL
$\text{Viscosity}_{\text{kin},40°C}$ (cSt)	114.9
$\text{Viscosity}_{\text{kin},100°C}$ (cSt)	15.7
Flash point (°C)	230
Sulfated Ash content (–)	1.20%
Density (kg/l)	0.873

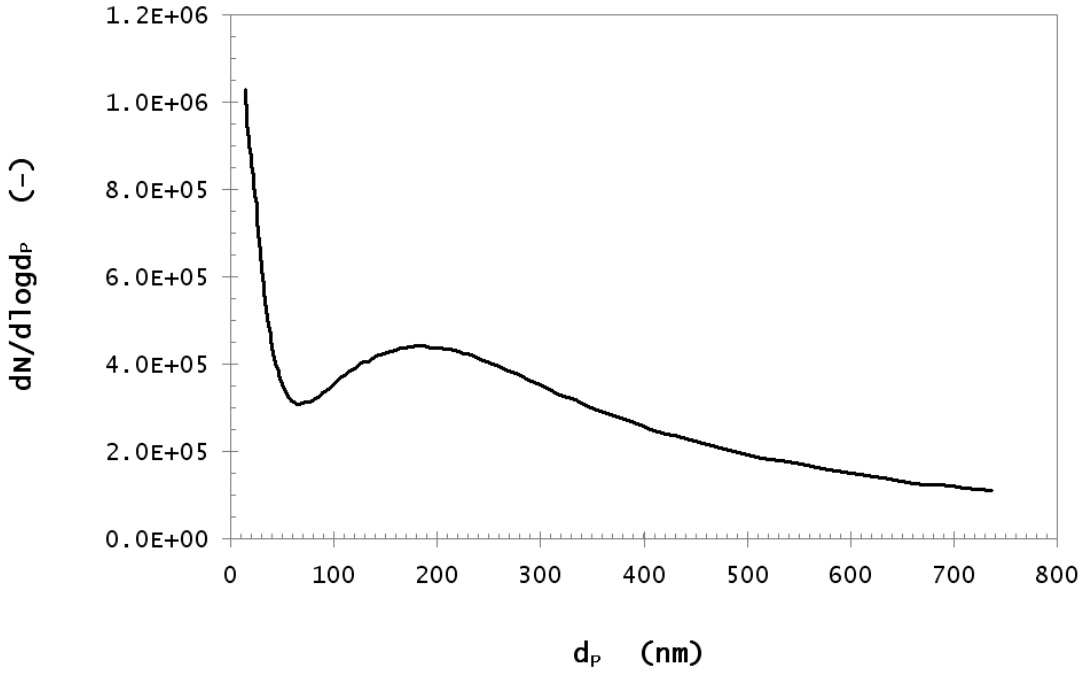

Figure 5.2.: Particle size distribution of the aerosol used to challenge the filters (measured by SMPS).

However, 850 ±17 nm was calculated from gravimetric measurements divided by CPC counts, which is likely more accurate, as the large particles which cannot be counted by SMPS would possess nontrivial mass. Gravimetric measurements showed a mass loading

rate of approximately 182 ±3.3 mg/m^3 which was in close agreement to measurements (175 ±4.3 mg/m^3) using a DUSTTRAK aerosol monitor (TSI, TSI Inc., WN, USA).

5.2.3. Filter Characterisation

Two different commercially available filters (MANN + HUMMEL GmbH, Germany) were used in this work. The filters were of cylindrical construction with the air flowing from the inside to the outside of the element. The filter element consisted of an inner support mesh, which was wrapped with layers of nonwoven stainless steel fibrous media. Each layer consisted of fibres of only one (mean) diameter d_f. SEM images of the three media are shown in Figure 5.3. The two different filter elements used in this work were designated Filter A and Filter B, their properties are shown in Table 5.2.

Table 5.2.: Properties of the oil–mist filters (filter media only) used in this work. All values determined by the author.

	Filter A	**Filter B**
Fibre material	Stainless Steel 316	Stainless Steel 316
Number of layers	4	3
d_f (µm)	4.2	2.3 and 7.8
α (–)	0.024	0.019
$m_{Oil,max}$ (g)	56.61 ±0.7	50.01 ±0.4
Total mass of filter media (g)	12.1 ±0.15	13.3 ±0.2
Filter face velocity (cm/s)	6.8	6.8
Height (mm)	91 ±0.5	91 ±0.6
Outside diameter (mm)	56 ±1.4	55 ±1.3
Thickness (mm)	9 ±0.6	8 ±0.7

The maximum oil holding capacity $m_{Oil,max}$ of the filter media can be defined as the theoretical amount of oil m_{Oil} which the filter media can contain when fully saturated, i.e. all available void space is filled with oil. This value was obtained by calculation and experimental measurement and it was found that both methods showed a good agreement (less than 1.5% difference for each filter type).

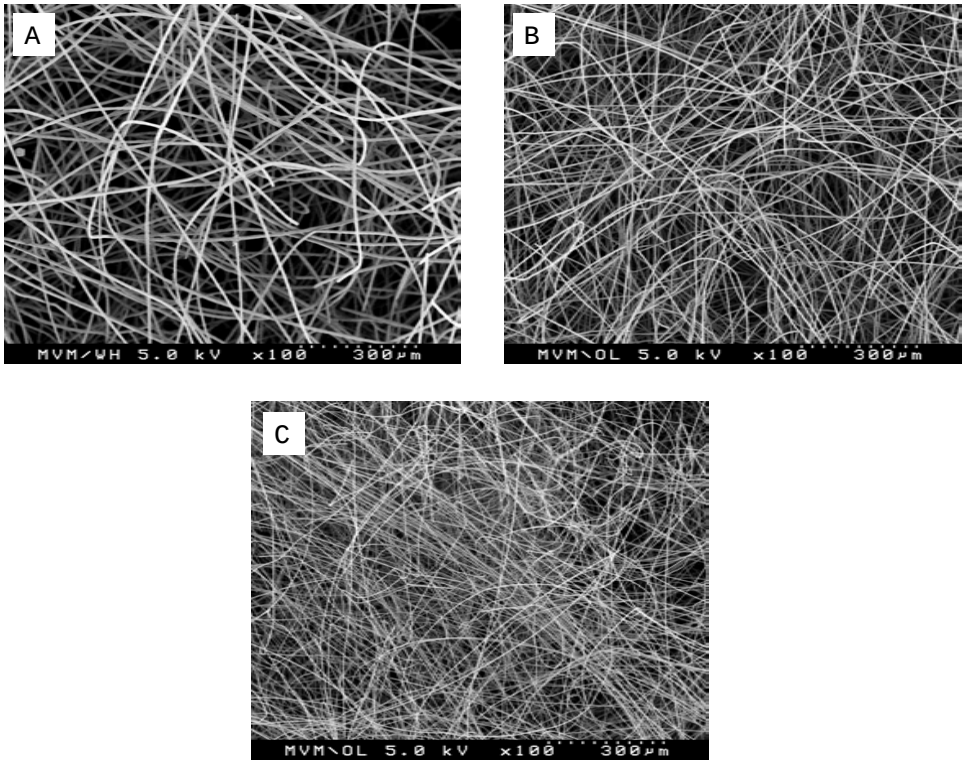

Figure 5.3.: SEM images of the three filter media from which the filters were constructed. A: $d_f = 7.8$ µm, B: $d_f = 4.2$ µm, C: $d_f = 2.3$ µm. (Courtesy of the *Institute for Mechanical Process Engineering and Mechanics, Karlsruher Institut für Technologie*).

5.2.4. Saturation and Efficiency Measurement

The filter (and oil) mass was determined by carefully removing the filter from the filter chamber and weighing it on an analytical balance (A&D GX400, A&D Engineering Inc., CA, USA).

The fractional (number based) filtration efficiency E was determined by alternately monitoring the upstream (c_{in}) and downstream (c_{out}) particle concentration in the aerosol stream with a scanning mobility particle sizer (SMPS). Sampling continued for

120 seconds which was found to be sufficient to obtain a stable concentration reading. The filtration efficiency is defined as the ratio of captured particles to particles entering the filter. If the upstream and downstream particle concentration is known, the efficiency can be calculated using Equation 2.15.

Gravimetric filtration efficiency was measured using a sampling probe before and after the filter. The probe had a diameter of 2.5 mm and a sample flow rate of 1.5 LPM was used to ensure isokinetic sampling. The sample was taken alternately upstream and downstream of the filter for a period of 60 minutes for each position. The particles were collected on a HEPA filter (Nalgene, Thermo Fisher Scientific, MA, USA) and the sample filter media was weighed on a high–precision balance (AW220, Shimadzu, Kyoto, Japan) before and after sampling.

5.3. Preliminary Experiments

5.3.1. Wall Flow Suppression

Aerosol particles which diffuse, impact or settle onto the walls of the tubes between the nebuliser and the filter chamber can accumulate and form a constant liquid stream in the tubes. This liquid slowly drains in the tubes and eventually enters the filter chamber and into the filter – a process termed "wall flow". It is obvious that additional oil draining into the filter can significantly distort the pressure drop, drainage and saturation behaviour of the test filter and therefore must be branched off before the filter chamber.

The wall flow trap was installed in–line 30 cm before the sampling points for pressure drop and concentration monitoring. It consisted of a T–shaped brass fitting that allowed the wall flow to be drained into a collection vessel. The whole assembly was installed below the level of the filter chamber at the lowest point of the tubing to make sure that wall flow always flowed towards the collection vessel rather than into the filter chamber.

A comparison between with and without the wall flow trap assembly was conducted. Both the aerosol flow rate and particle loading rate were identical for both experiments. The experiment with the wall flow trap installed were conducted first to allow wall flow to build up before the trap was removed. The results can be seen in Figure 5.4.

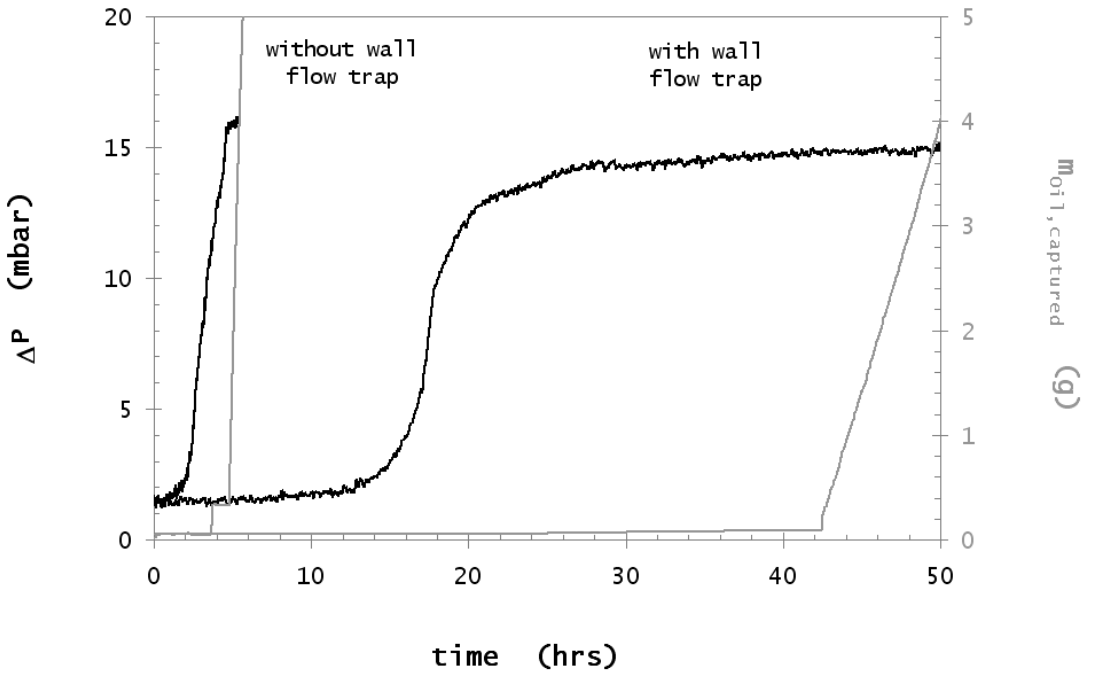

Figure 5.4.: Filter loading with and without the wall flow trap installed. Both filters were challenged with the standard aerosol loading concentration at a flow rate of 55 LPM. With $m_{Oil,captured}$ being the amount of oil being drained and ΔP the pressure drop of the filter.

It is clearly visible that the additional yield of oil from the wall flow accelerated filter loading significantly. In the experiment without the wall flow trap the filter reached the first equilibrium state EQ_1 (see 2.6) after approximately 4.5 hours – significantly faster than the other filter, which reached EQ_1 after nearly 43 hours. A similar influence on the drainage rate could be observed once drainage commenced. The drainage rate was approximately 0.48 g/hr for the filter loaded with the flow trap installed and 4.9 g/hr for the filter loaded without the flow trap installed. Visual inspection of the filters after

the experiment showed a large amount of oil on top of the filter if the flow trap was omitted. No oil was found on top of the filter which was loaded with the trap installed. The pressure drop was approximately 10% higher for the filter loaded without the trap and its saturation (the top of the filter was cleaned of excessive oil prior to weighing) was 0.68 in comparison to 0.61 for the filter with a wall flow trap fitted.

These experiments clearly demonstrated the importance of the wall flow trap to divert oil which collects on the walls in order to prevent it from draining into the filter. All further experiments in this work were conducted with the trap installed.

5.4. Filter Preloading and the First Equilibrium State (EQ_1)

To accelerate the attainment of the first equilibriums state EQ_1, filters were preloaded and then subsequently challenged with the standard particle concentration. Two preloading methods were used as described below. The preloading step was omitted for some filters, in order to ensure that preloading did not influence results. These filters were challenged with the standard aerosol concentration from the start. After the preloading process, the filters were inserted into the filter chamber, where they were challenged with the standard aerosol concentration. The filter was considered to have reached EQ_1 when pressure drop and drainage rate did not change significantly over time.

Method I: Preloading by Dipping And Draining ("DAD") The filter was preloaded by submerging it into oil (the same oil as used in the experiment) for 18 hours and then withdrawn and held upright for 6 hours to allow excessive oil to drain.

Method II: Preloading by Rapid Aerosol Saturation ("RAS") The filter was exposed to a higher aerosol concentration (two times higher than that used in the experiments) for approximately 24 hours.

Although the method of dipping the filter to accelerate the loading process is commonly

in use in industry, there exists no literature on this topic. Therefore, preliminary experiments were conducted to ensure that both preloading methods led to the same equilibrium state EQ_1 that the filter attained without preloading. Figure 5.5 shows a comparison of the 3 different (pre)loading methods ("DAD", "RAS" and no preloading).

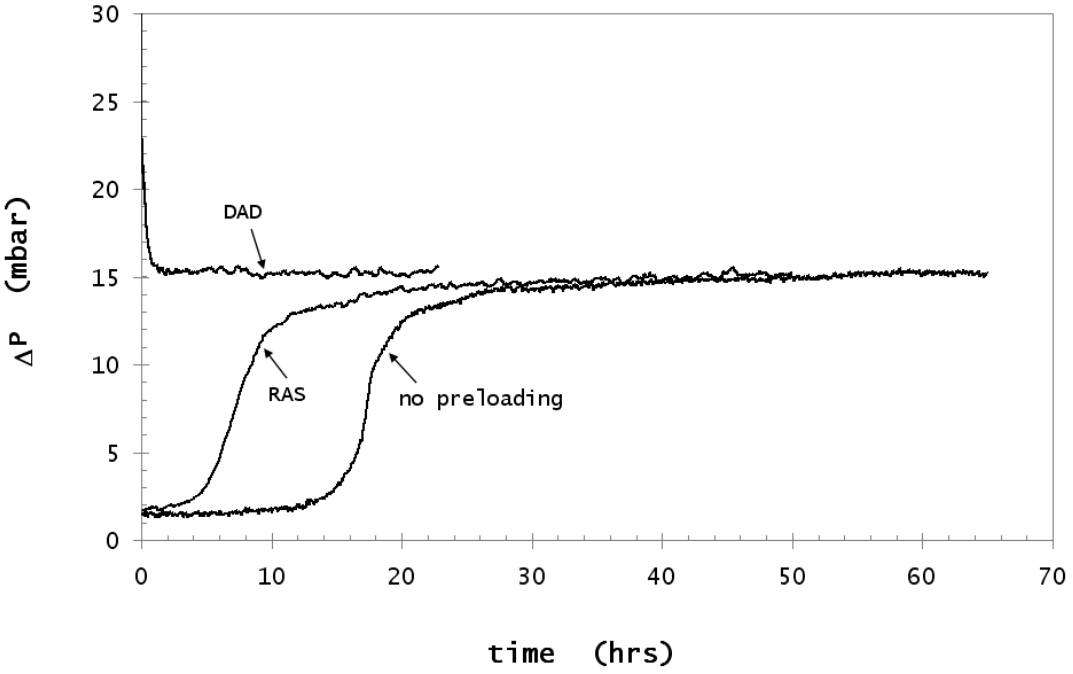

Figure 5.5.: Validation of the "RAS" and "DAD" preloading method against an experiment without preloading (*Type A*). The pressure drop axis is set at 30 mbar maximum, however the initial reading for "DAD" filters was > 70 mbar. No significant difference in ΔP_{EQ1} was observed between the different loading methods.

It can clearly be seen that after a sufficient period of time both preloaded filters attained a similar pressure drop ΔP_{EQ1} as the non preloaded filter: $\Delta P_{EQ1} = 15.2$ mbar for the "RAS" method, 15.4 mbar for the "DAD" method and 15.2 mbar for the filter without preloading. Drainage rates and filter saturation were nearly identical for all preloading methods with $\dot{m}_{Drain,EQ1} = 142 \pm 5.2$ mg/m^3 and $S_{EQ1} = 0.61 \pm 0.04$.

Filters preloaded using the "DAD" method were considered to initially be fully saturated ($S = 1$) with all void space between fibres filled with liquid. Hence, there were no free passages in the filter through which the air could flow, resulting in an extremely high pressure drop of the filter immediately after air flow was applied (in this case > 70 mbar). The extremely elevated pressure drop and high shear forces occurring during the first seconds of filtration expel the oil out of the filter, creating initial passages through the filter. The high interstitial velocities (and thus high shear forces) are due to all air flow being forced through a small number of narrow free passages in the filter. As oil is expelled from the filter, the number of passages increases and local interstitial velocities decrease – which continues until the filter reaches an equilibrium state.

These experimental data were compared against an empirically derived saturation and pressure drop model [33] using Equations 2.27 and 2.35 since packing density, particle size and filter fibre diameter were similar in both works. The predicted (see [33]) and measured values for ΔP_{EQ1} and S_{EQ1} are shown in Table 5.3.

Table 5.3.: Measured and predicted values for ΔP_{EQ1} and S_{EQ1} using Equations 2.27 and 2.35.

	experimentally	**predicted**
Type A		
ΔP_{EQ1} (mbar)	15.2 ±0.11	15.3
S_{EQ1} (-)	0.61 ±0.04	0.12
Type B		
ΔP_{EQ1} (mbar)	35.5 ±0.34	35.2
S_{EQ1} (-)	0.65 ±0.04	0.10

As can be seen the experimental pressure drop agreed well with the predicted value. However, in terms of saturation, a huge discrepancy exists between experimental and predicted values. Whereas the prediction of the pressure drop is merely a function of S_{EQ1} (for which the experimental value was used), the prediction of the saturation depends on a range of oil and filter properties (incorporated in the dimensionless numbers Bo, Ca and Dr). Although the fibre diameter, particle size and packing density used to

develop this equation [33] were within the same order of magnitude as those used in the current work, the fibre type (steel vs glass) and oil type (engine oil vs DEHS) are completely different. Therefore, it is believed, that a significant discrepancy between some properties in both works exists (which the model does not account for), which results in the difference between experimental and predicted values.

5.5. Discontinuous Filter Operation and the Second Equilibrium State (EQ_2)

Once equilibrium saturation (S_{EQ1}) and pressure drop (ΔP_{EQ1}) were reached, the filters were subjected to discontinuous operation. Air and aerosol flow were stopped for 120 minute intervals and recommenced for 120 minute intervals (120/120). To simplify the presentation of results from experiments with several dozen cycles, the "on" pressure drop values of each cycle were averaged and divided by the average pressure drop ΔP_{EQ1} at the first equilibrium state, thus giving the normalised pressure drop ΔP_N for each cycle. The determination of the normalised drainage mass $\dot{m}_{Drain,N}$ was calculated using the same method.

The evolution of the normalised pressure drop ΔP_N and drainage rate for all cycles of the experiment is shown in Figure 5.6. The curves are averaged from four experiments and the variation is represented by error bars. It can be seen that the reproducibility of the curves was excellent. The pressure drop increased during the first 5 cycles beyond ΔP_{EQ1}, reaching a second stationary level ΔP_{EQ2} in cycle #6. This new level was approximately 38% greater than the pressure drop during the first equilibrium state and once reached was found to be stable (i.e. the filter would not go back to ΔP_{EQ1}). During this period, the drainage rate decreased from its equilibrium value to nearly zero and – after the second equilibrium state (EQ_2) was reached – returned to a similar rate as before.

According to Equation 2.31 it is evident that — assuming a constant mass loading

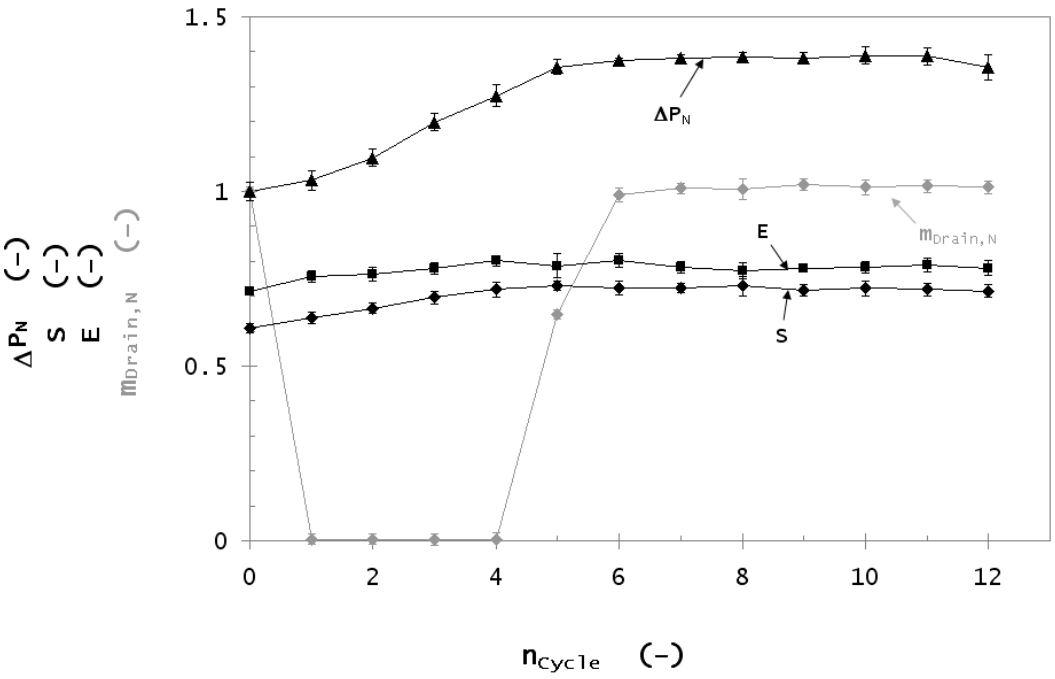

Figure 5.6.: Normalised pressure drop ΔP_N, normalised drainage rate $\dot{m}_{Drain,N}$ filter efficiency E and saturation S per cycle of the *Type A* filters, during discontinuous operation. $n_{Cycle} = \#0$ represents the filter conditions during the first equilibrium state EQ_1 before the flow was initially discontinued.

rate and capture efficiency – a change in drainage rate must produce a change in filter saturation. Since the aerosol mass entering and exiting the filter remained constant, this assumption was considered correct. The filter saturation S is displayed in Figure 5.6. Once discontinuous operation commenced, the saturation increased simultaneously with an increase in pressure drop and a cessation of drainage. These findings suggest that the filter underwent a second loading stage after discontinuous operation commenced and was capable of storing further oil inside until reaching a second equilibrium state with a saturation S_{EQ2} of 0.72 in comparison to a saturation S_{EQ1} of 0.61 during the first equilibrium state.

The gravimetric overall collection efficiency E is also shown in Figure 5.6 with Figure 5.7 showing the fractional efficiencies. E was found to increase from an average of approximately 70% at EQ_1 to approximately 78% at EQ_2. The slight increase in

efficiency was found only in the larger (interception and inertia dominated) size ranges, so is therefore likely due to the higher saturation of the filter as was found by some authors [33]. However, since the efficiency of the new filter is higher overall (compared to EQ_1 or EQ_2), this is counter–intuitive. A more likely explanation is that the re–arrangement of the oil has made the air flow paths through the filter more tortuous, thereby increasing particle capture.

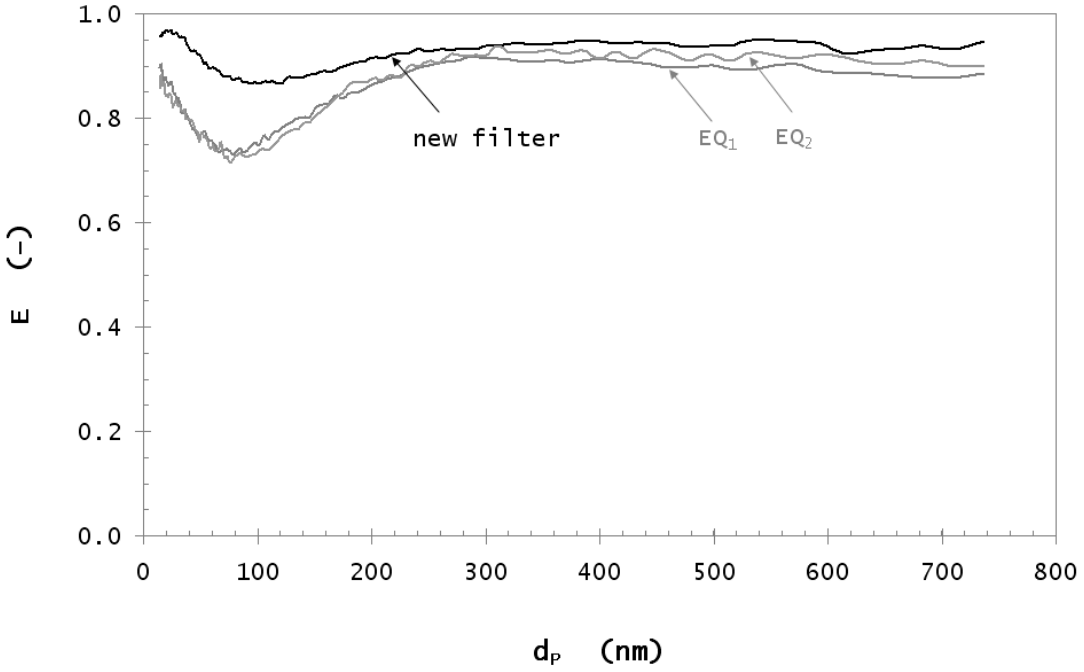

Figure 5.7.: Number–based filtration efficiency of a new filter and at the first and second equilibrium state EQ_1 and EQ_2.

The secondary loading phase and second steady state found is believed to be due to the rearrangement of oil in the filter after air flow was discontinued. The lack of shear forces allows capillary and gravitational forces to move oil into locations where it previously was not present (i.e. air flow channels). Furthermore, oil that has already been expelled from the filter, yet remains on the surface, can be drawn back into the filter through capillarity, where it can block passages, causing an additional flow resistance. If shear

forces from the recommencing air flow are too weak to clean these passages, the oil will remain in the filter, leading to a higher saturation and a higher pressure drop. If more oil is stored in the filter and hence more passages are blocked during each break, then higher local velocities will be induced through the remaining free passages in the filter. Thus shear forces will increase locally and are now able to overcome capillary forces and clean passages of smaller diameters than before. The ability to locally clean the filter and therefore the ratio between capillary forces (i.e. the number of clogged passages) and shear forces (i.e. the number of cleaned passages) is believed to be the predominant reason for the observed filter behaviour. If both forces are equal after each break in air flow, then the second equilibrium state EQ_2 is reached.

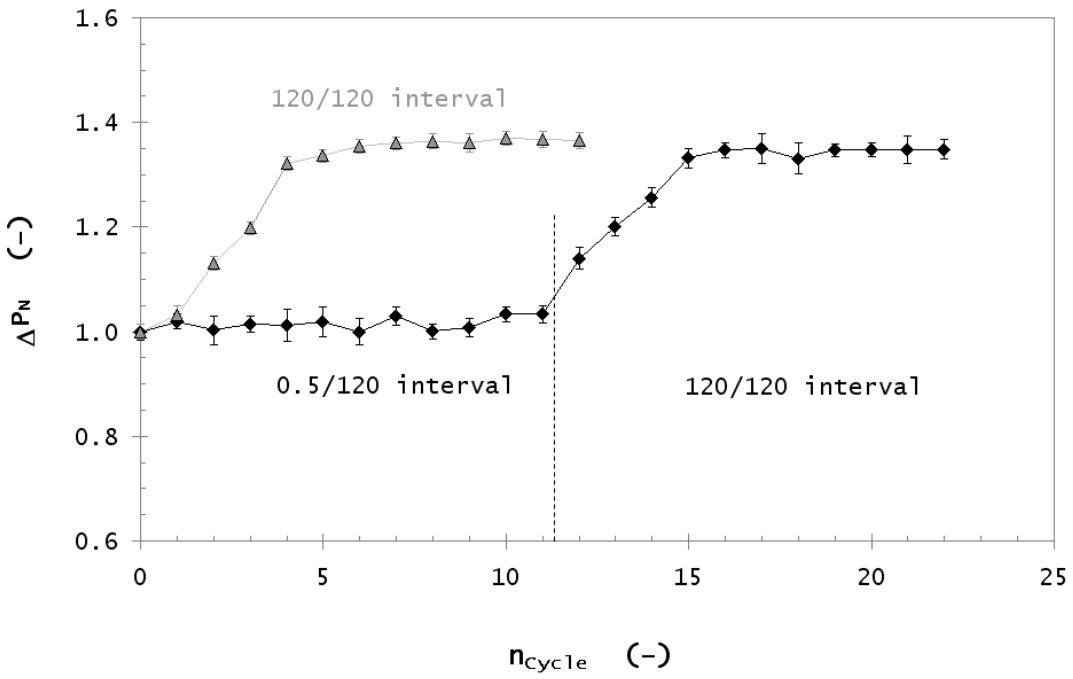

Figure 5.8.: Pressure drop behaviour of a filter (*Type A*) during discontinuous operation. The stop–and–go interval was set to 0.5 minute break and 120 minutes air–flow (0.5/120 interval) during the first 10 cycles before it was set back to the normal interval of 120/120. Also shown for comparison are the 120/120 experimental results.

The rearrangement of oil in the filter is believed not to be an instantaneous process, but rather requires some time for the relatively viscous oil droplets to flow (due to the slow nature of capillary flow). Figure 5.8 shows the result of an experiment conducted with two different stop–and–go intervals.

The first stage of the experiment was conducted using a short break of 30 seconds between the "on" periods which were kept at 2 hours (0.5/120 interval) as per the previous experiments. After 10 cycles the experiment was then changed to the usual 2–hours stop–and–go interval (120/120 interval). The curves are averaged from three (for the black curve) and five (for the grey curve) repetitions and the error bars indicate that the variation between the repetitions was minimal.

The pressure drop during the first stage remained the same as the ΔP_{EQ1} level, until the interval was changed to 120 min breaks. Once the interval was set to 120/120, the pressure drop increased each cycle until ΔP_{EQ2} was reached, which lay approximately 35% higher than ΔP_{EQ1}. The Saturation S_{EQ2} at this point was 0.73 compared to S_{EQ1} of 0.61. Both values correspond well with the results observed during experiments with a 120/120 interval from the end of the steady–filtration period.

This experiment supports the concept that the observed increase in pressure drop and saturation is induced by a rearrangement of liquid in the filter during breaks in air flow. If the air flow is recommenced before the oil has been displaced significantly, then no measurable changes in pressure drop will occur.

Type A filters consisted of 4 layers of fibres of the same diameter. Experiments were also conducted with *Type B* filters (which consisted of media containing 2 different fibre diameters). *Type B* results showed the same general relationship as the *Type A* filters.

The average values for the normalised pressure drop ΔP_N and the saturation S at the first (EQ_1) and the second (EQ_2) equilibrium state for filters of both *Type A* and *Type B* are shown in Figure 5.9. All filters were preloaded prior to discontinuous operation using either the "DAD" or the "RAS" method, data are based on approximately 60 filters.

Again it can be observed that the preloading method did not influence the results, as the

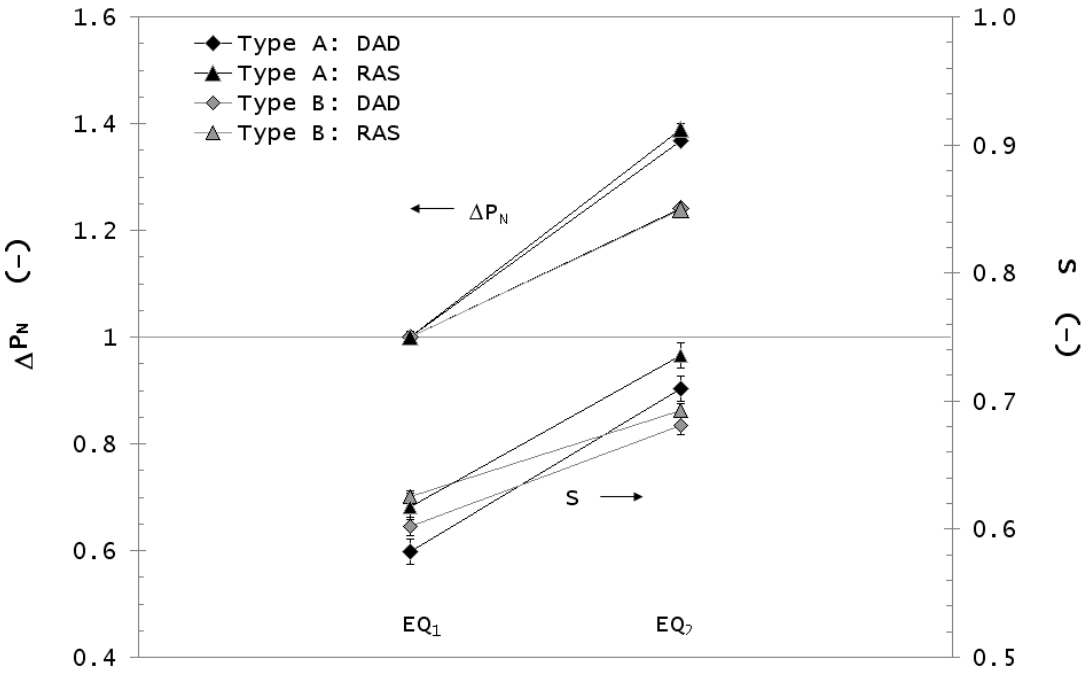

Figure 5.9.: Normalised pressure drop ΔP_N and saturation S at EQ_1 and EQ_2 for filters of *Type A* and *Type B*. The filters were preloaded using either the "DAD" or the "RAS" method.

differences between both methods are generally within the range of the error bars. For filters of *Type A*, an average increase in pressure drop of 38% ±1% could be observed, whereas filters of *Type B* showed only 24% ±0.6%. Both filters showed a marginally higher saturation if the filter was preloaded using the "RAS" method. An increase in saturation from 0.61 ±0.02 to 0.72 ±0.02 could be observed between the two equilibrium states for filters of *Type A* and from 0.61 ±0.01 to 0.69 ±0.01 for filters of *Type B* respectively.

As can be observed in Table 5.2, *Type B* filters possess a lower packing density (0.019) than *Type A* filters (0.023) – a difference of approximately 20%. This would mean that the *Type B* filters would on average have larger interstices between the fibres, and a greater equivalent capillary diameter. This is the most likely explanation of the approximately 40% difference in pressure drop and saturation increase between EQ_1 and EQ_2 in the filters.

5.6. Phenomenological Filter Drainage Model

5.6.1. Derivation of the Model

Earlier experiments showed that fully saturated (i.e. preloaded using the "DAD" method) filters lost significant amounts of oil during the initial seconds of filtration. The high pressure drop and high interstitial air velocity likely provided sufficient force to drive the oil to the rear of the filter where it was able to drain. In order to model the flow of fluid in fibrous filters, they can be approximated as a bundle of vertical or horizontal capillary tubes [53, 86] (see Chapter 2.9).

An analytical solution for capillary displacement in circular, horizontal tubes was derived by Washburn [60] using the Hagen–Poiseuille equation for laminar flow, neglecting inertial effects.

$$\frac{32\eta}{d_{cap}^2}\dot{l}(t) = \frac{P_{Oil,0} - P_{Oil,m}}{l(t)} \tag{5.1}$$

with η being the dynamic viscosity of the liquid, d_{cap} the capillary tube diameter, $l(t)$ the distance of the gas–liquid interface – also called the meniscus – from the tube inlet (depending on the time t) and $\dot{l}(t)$ its derivation (i.e. $dl(t)/dt$). $P_{Oil,0}$ and $P_{Oil,m}$ is the liquid pressure at the start of the capillary and at the gas–liquid interface respectively. For vertical capillary systems, an additional term is needed to include gravitational forces. Figure 5.10 shows the geometry of a horizontal (single) capillary system.

The capillary pressure, which is the pressure difference between the gas pressure P_g and the liquid pressure $P_{Oil,m}$ is given by the Young–Laplace equation as follows

$$P_g - P_{Oil,m} = \frac{4\gamma}{d_{cap}}\cos\theta \tag{5.2}$$

with γ being the interfacial tension between the gas and the liquid and θ the contact

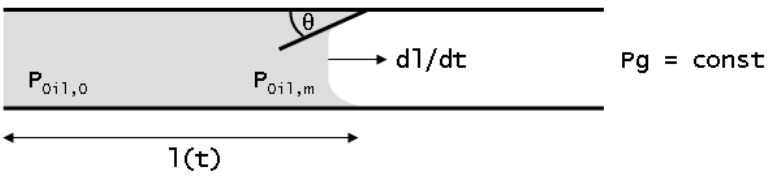

Figure 5.10.: Geometry of a gas-liquid interface advancing in a horizontal capillary tube. After: Hilpert [87].

angle of the liquid–solid interface (which was determined as 79° in previous work [62]).

Combining these two equations leads to an ordinary differential equation for the distance of the meniscus from the start of the capillary and the resulting pressure drop ΔP

$$\Delta P = P_g - P_{Oil,0} = \frac{4\gamma}{d_{cap}} \cos\theta - \frac{32\eta}{d_{cap}^2} \dot{l}(t) l(t) \tag{5.3}$$

By assuming that the contact angle θ is constant over time (as assumed by Washburn) this equation can be solved and an expression for the distance of the meniscus from the capillary inlet dependant on pressure drop, time and capillary diameter can be obtained as follows

$$l(t) = \left(\sqrt{\frac{\gamma \cos\theta}{4\eta} d_{cap} - \frac{\Delta P}{16\eta} d_{cap}^2} \right) \sqrt{t} \tag{5.4}$$

Although this equation was developed for liquid penetration into a capillary, it seems reasonable to use the same equation for the displacement of liquid from a capillary [87].

It is assumed that the horizontal capillary in this case is initially filled and is then acted on by a pressure differential. With Equation 5.4, the ratio of the emptied length of a capillary of a certain diameter can be calculated if the pressure drop behaviour over time is known (as is the case in this work). Since the filter can be represented by a bundle of horizontal capillary tubes of known diameter distribution and length, it is possible to

calculate the ratio of the emptied capillary space in the whole filter and thus the filter saturation as a function of the pressure drop during the capillary draining process.

5.6.2. Modelling

To be able to calculate the filter "cleaning" behaviour, the following assumptions were made:

- All capillaries are of the same length (the filter thickness)
- The capillary diameter distribution is a normal distribution
- The filter is fully saturated at the commencement of filtration (i.e. all capillaries are fully filled)

The filter saturation for every time step (100 ms) during cleaning of the fully saturated filter was calculated (S_{pred}) as the amount of remaining liquid in each capillary in relation to the capillary length weighted by the abundance of every capillary diameter as given by the normal distribution. The amount of liquid in each capillary was calculated using Equation 5.4 and by multiplying the distance of the meniscus from the capillary inlet by the cross sectional area of the capillary. Additionally, the experimental saturation (S_{exp}) was calculated based on the mass of collected liquid draining from the filter.

Previously published work [62] investigated capillary rise height using (stainless steel) fibrous filters of a type almost identical to those used in the current work. Thus it seems reasonable to utilise the empirical equations for the determination of the capillary diameter developed in the work mentioned above to the current filter media. If the fibre diameter and the packing density of the filter are known, the average capillary diameter could be estimated using Equation 2.37.

Using this diameter as the mean diameter d_{mean} = 80 µm of the capillary distribution with a standard deviation of σ = 20 µm (from [62]) a normal distribution was obtained

which was used as basis for model determination.

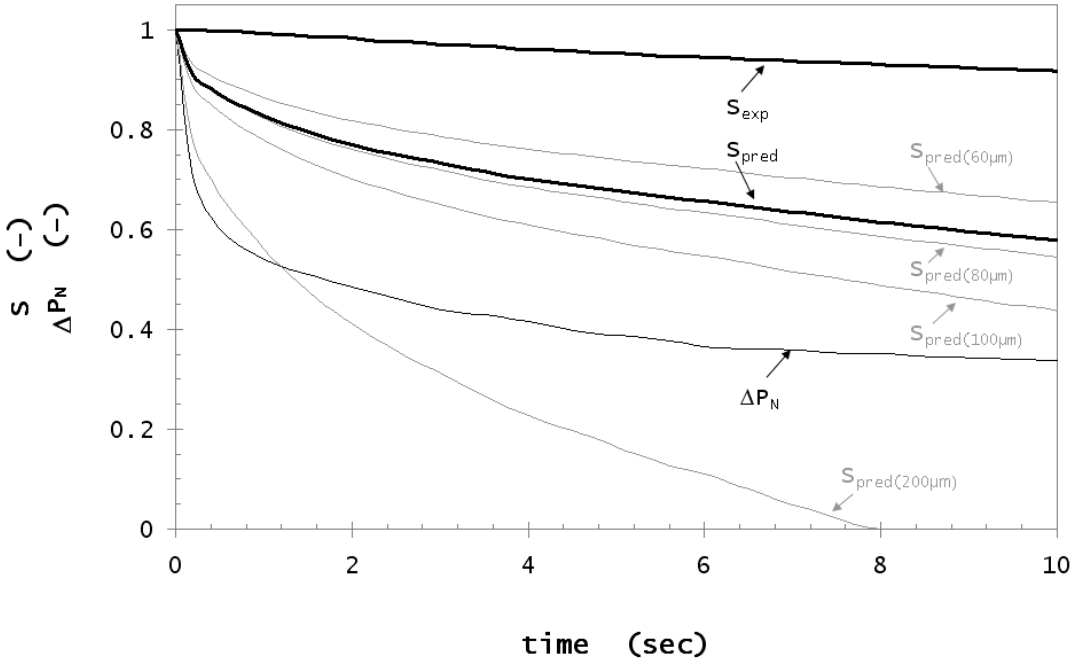

Figure 5.11.: Calculated (S_{pred}) and experimental (S_{exp}) saturation during filter cleaning. The saturation for three specific capillary diameters d_{mean} (80 µm), d_{mean}-σ (60 µm), d_{mean}+σ (100 µm) and a comparatively large capillary of 200 µm was modelled.

Figure 5.11 shows the experimental (S_{exp}) and theoretical capillary model saturation (S_{pred}) values for the first 10 seconds of filter cleaning/drainage for a fully saturated *Type A* filter.

As can be seen, the pressure drop decreased to approximately 30% of the initial value during this time, which corresponds to approximately 21 mbar. Although earlier experiments have shown that the pressure drop decreased further to approximately 15 mbar (as was described earlier in this work) during the remaining hour of the experiment, 90% of the total pressure drop decrease took place within the first 10 seconds, thus this time frame was selected as being sufficiently representative for the evaluation of the phenomenological model.

Figure 5.11 also shows the normalised pressure drop (ΔP_N). The four additional S_{pred} curves show the theoretical drainage of the mean and ±20 µm standard deviation (from the mean) capillary diameter and for comparison a relatively large (200 µm) capillary respectively. The experimental data shown is representative of the results found over multiple experiments. It can be seen that the saturation for all capillaries decreased most rapidly during the initial seconds when the air flow commenced. This corresponds well with findings published in other works [62, 88] which showed that an "acceleration phase" occurs during initial capillary rise or fall, which decreases over time to a slower rate. The capillary with the largest diameters shows the fastest decrease in saturation and is completely cleaned after approximately 8 seconds, whereas the smallest capillary has only been cleaned down to approximately 75% at the same time. This suggests that the liquid can move more easily in capillaries of a large diameter than in capillaries of small diameter. This corresponds to observations in other works, where it was shown that the capillary rise height increased faster in larger capillaries [55, 62]. This finding also supports the findings discussed in Figure 8.2. Larger capillaries are cleaned first, causing a quick initial pressure drop decrease, whereas it takes increasingly more effort to clean capillaries of decreasing diameters.

The difference between the theoretical and experimental saturation curve can be explained by the fact that the actual drained oil is only measured by the balance once it has completely drained to the bottom of the filter and then dripped into the collection canister on the balance which is suspected to lead to a time lag in the mass measured. Furthermore, it is possible that in the experimental case, the ends of cleaned capillaries may be clogged by oil draining from capillaries above (and flowing down the rear of the filter). This is assumed to affect the lower parts of the filter more, for obvious reasons.

It can be said that the phenomenological filter model is able to describe initial drainage during filter cleaning and show a relationship between saturation and pressure drop. However the model does not appear to capture all the processes occurring in the filter, so at this stage must be regarded as a descriptive, rather than predictive, model. It is likely that over the longer term, as S_{exp} decreases, the magnitude of forces may change such that capillarity becomes less significant.

5.7. Conclusion

This chapter has shown that both types of filters tested undergo a second loading stage beyond the first equilibrium state if they are not operated continuously, eventually reaching a second equilibrium state. An increase in pressure drop of 24% and 38% respectively and a saturation increase of 8% and 12% respectively, between the two equilibrium states was observed. This was attributed to a rearrangement of liquid in the filter during the breaks, clogging previously free passages, a process which was mainly driven by capillary forces. The ratio of shear and capillary forces was found to define whether these passages were able to be cleaned once aerosol flow was recommenced [89].

A simple phenomenological model based on the Lucas–Washburn equation was developed to describe drainage of supersaturated filter media. It was shown that capillary theory appears to describe the process which occurs as liquid is drained from supersaturated filters, at least during the initial phases [89].

The experiments conducted in this chapter represent a more realistic test for oil–mist (or coalescing) filters than typical laboratory testing [89].

This chapter has:

- developed a suitable test apparatus for CCV filters
- developed a realistic test procedure (discontinuous filtration)
- established a baseline dataset for filter performance with clean oil
- examined capillary effects in mist filters, including the approximate time–scales needed for liquid re–arrangement

The following chapters will therefore examine the influence of soot contamination and further explore the cleaning of mist filters.

6 Filtration of Degraded Oil

6.1. Introduction

Chapter 4 developed an accurate method for soot–in–oil analysis, while Chapter 5 developed a mist filter testing apparatus and examined the filtration of clean engine oil aerosol. This chapter will expand on the work of the previous two chapters, to examine the filtration of soot–in–oil aerosols.

As was discussed in Chapter 2, little attention has been given in literature to the filtration of colloidal (soot–in–oil) aerosols. In many processes however (particularly the cleaning of oil–mist filters in automotive, welding and machining applications), the oil is contaminated with solid particles such as wear particles, dust or soot. It was shown, that two oil ageing mechanisms (thermooxidative degradation and solid particle contamination) can significantly influence the oil properties and its ability to perform lubrication [3, 63, 74].

Solid contaminants
Investigations of diesel engine oil showed [2], that solid contaminants, such as wear particles, dust and soot, pass the pistons with blow-by gases and are carried into the crankcase, where they are collected by the oil–mist, accumulate and lead to a thickening of the oil.

Thermooxidative oil breakdown
A broad range of different thermal and thermooxidative oil degradation mechanisms were described in literature and their influence on oil viscosity was investigated. Thermal degradation processes such as oxidative breakdown and polymerisation of oil molecules [66, 90] are reported to possibly increase or decrease the oil viscosity. Evaporation of the lighter fractions in the oil leaves larger molecules (and thus a thicker oil) behind. During evaporation, additives such as viscosity index improvers and antioxidants can also evaporate, leading to a decreased oil viscosity and an increasing

oxidation rate [67, 91]. Larger oil molecules can be broken up by shear forces in contact with sliding parts of the engine [66] resulting in a decreasing oil viscosity (however, the smaller fractions eventually evaporate and thus this process technically increases oil viscosity).

Whereas the impacts of thermooxidative effects and contamination on oil viscosity has received substantial research, little attention has been given to the impact of viscosity changes on the performance of oil–mist filters.

This chapter investigates the filtration of soot–in–oil aerosol mist using fibrous filters. The influence of different oil degradation mechanisms on the performance of such filters will be investigated. Laboratory methods will be developed to reproduce oil deterioration and to study its effect on oil properties. An extensive study of the influence of oil viscosity on filter performance during discontinuous filter operation will be conducted, representing filter operation in a "real" engine crankcase ventilation system. A field test using 15 diesel vehicles will also be conducted over six months and the filters will be tested under laboratory conditions and thermogravimetrically analysed using a novel large-scale method adapted from the improved ASTM 5967 method explained in Section 4.5. The results obtained from the field test will then be compared to the results from laboratory oil ageing and filter testing.

6.2. Materials and Methods

6.2.1. Laboratory Filter Testing Apparatus and Materials

The filtration experiments were conducted using the filter testing apparatus shown in Figure 5.1. Castrol RX Super (as per Table 4.1) was used as test aerosol for the laboratory experiments. The filters used in the experiments were commercial CCV filters identical to those used in Section 5.2.3. The laboratory test soot was Printex U as per Table 4.1.

Based on the findings in Chapter 5, discontinuous filtration experiments were conducted in order to better approximate real-world conditions. The filters were preloaded using the "DAD" method and then challenged with aerosol according to the conditions described in Chapter 5.

6.2.2. Field Test Specifications

15 four wheel drive (light commercial vehicles) were chosen for the field test. Three different diesel engine types were fitted to the test vehicles as follows

Type 1: 2.5 litre 4 cylinder direct injection turbo Diesel meeting Euro-2 specification

Type 2: 2.5 litre 5 cylinder commonrail direct injection turbo diesel meeting Euro-3 specification

Type 3: 3.9 litre 4 cylinder direct injection turbo diesel meeting Euro-1 specification

Additionally, *Type* 2 engines were fitted with a bypass centrifuge for lubricant oil (MANN+HUMMEL (UK) LTD., Wolverhampton, United Kingdom). All other vehicles were fitted with full–flow lubricant oil filters only. The vehicles used SAE 15W-40 or SAE 5W-40 graded oil and were split into three groups as follows:

Group I: All vehicles that used 15W-40 (most *Type* 1 and all *Type* 3)

Group II: All vehicles that used 5W-40 and were not equipped with a bypass centrifuge (remaining *Type* 1)

Group III: All vehicles that used 5W-40 and were equipped with a bypass centrifuge (all *Type* 2)

The oil viscosities at 40 °C (as given by the manufacturers) ranged from 71 cSt to 107 cSt for the 5W-40 graded oils and from 95 cSt to 132 cSt for the 15W-40 graded oils. Due

to the fact that the field test vehicles were distributed all over Australia, an analysis of the engine oils after the 6 month test period was not possible.

The test filters were installed into the vehicles coinciding with an engine oil change and were in use for approximately 6 months. The initial weight of each filter was measured on a balance (AS120, OHAUS, New Jersey, USA) before the filter was installed. During the test, the oil was not changed and the vehicles were driven as usual, the distance travelled during the test period ranged from 600 km to nearly 20,000 km, with an average of approximately 8500 km. The total mileage of the engines prior to commencement of the test ranged from approximately 60,000 km to over 350,000 km. All vehicles used commercially available diesel fuel conforming to the Australian diesel fuel quality specifications [92].

6.3. Oil and Filter Analysis

The filters used in the current work consisted of stainless steel fibres and were found to be non-reactive in the TGA (no detectable mass loss up to 750 °C in N_2 atmosphere). Therefore, it was considered possible to adapt the modified ASTM 5967 method (Section 4.5) to conduct soot–in–oil analysis of the used filters.

After testing in the laboratory filtration apparatus, the field test filters were cut open and the filter media was carefully removed. The filter media was cut from top to bottom into 20 mm wide strips which then were separated into their single media layers and weighed on a high-precision balance (AW220, Shimadzu, Kyoto, Japan) before being analysed thermogravimetrically. Three sample strips were taken from each filter.

As conventional TGA instruments were not able to cope with the weight and the size of the 20 mm x 90 mm sample strips, a “scaled–up” version of the TGA process was developed. A quartz glass tube (500 mm length) was inserted into a Carbolite MTF 12/38/250 horizontal tube furnace (Carbolite, London, UK) and was purged with either dry air or high purity nitrogen (BOC, Australia) during the analysis.

The sample strip was placed in a ceramic boat in the quartz tube. Glass wool on both ends of the tube helped to create pressure slightly over ambient in the tube, thus preventing room air being imbibed during the analysis. A schematic of the apparatus is shown in Figure 6.1.

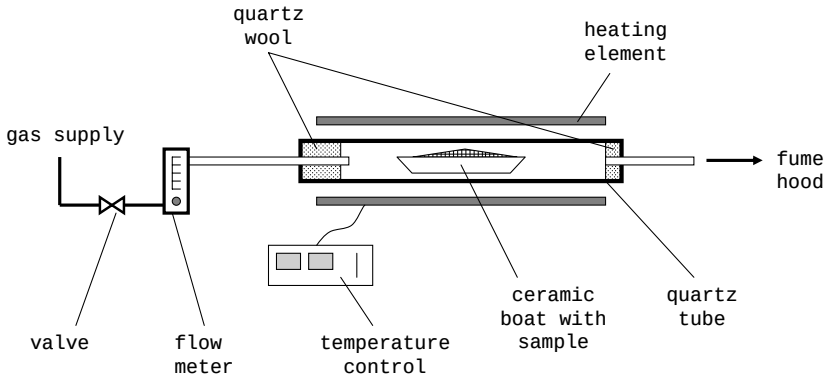

Figure 6.1.: Schematic of the tube furnace used for the large–scale determination of the soot and oil content in the test filters.

The temperature profile for the analysis was adapted from the improved ASTM 5967 method, however, to prevent the furnace tube from being damaged due to thermal stress in the quartz glass, a slower heating rate of 20 °C/min was used, as suggested by the manufacturer. After two minutes of nitrogen purge at a flow rate of 10 LPM, the sample was heated to 420 °C in a nitrogen atmosphere (2 LPM) and held isothermal for 15 min. The flow volume was regulated by a flow meter (Cole Palmer, Illinois, USA). Once the oil was completely evaporated, the sample was cooled down to room temperature by further nitrogen purging and its mass was measured on the high-precision balance. This additional step was necessary to prevent the soot from spontaneously combusting once the sample came in contact with room air. After the purge gas was changed to dry air (5 LPM) the sample was placed back in the furnace and heated to 700 °C, where it was held isothermal for 15 min to allow all soot to combust. After cooling, the sample was weighed again.

A high flow (5 LPM) of nitrogen was used to purge the furnace tube and expel remaining

oxygen prior to the analysis. The oxygen level in the tube was monitored by an ENERAC 3000 emission analyser (ENERAC, Westbury, NY, USA) where the ceramic boat was placed during the analysis. A heating test (see Section 4.3.1) was conducted using copper-II-oxalate hemihydrate (STREM Chemicals, Newburyport, USA) after purging to detect for oxygen traces. No oxygen could be detected by this method.

Although this thermoanalysis method did not provide in-situ monitoring of the sample weight (as is the case in conventional TGA instruments), it nevertheless delivered the necessary information to calculate the soot content of the oil captured in the filter.

The initial mass of the saturated filter decreased significantly during the first heating step under nitrogen atmosphere. The evaporation of the oil captured in the filter is responsible for this mass loss [81] and therefore the oil mass m_{Oil} can be calculated as

$$m_{Oil} = m_{Sample} - m_{Solid} \tag{6.1}$$

with m_{Sample} being the initial mass of the sample strip and m_{Solid} the mass remaining after the evaporation of the oil. The following combustion of the soot in dry air reveals the mass of soot m_{Soot} in the filter [81] as

$$m_{Soot} = m_{Solid} - m_{Inert} \tag{6.2}$$

with m_{Inert} being the inert mass remaining at the end of the analysis consisting of the filter fibres and traces of inert material in the filter referred to as ash [81]. Therefore the percentage soot content c_{Soot} in the oil captured in the filter can be calculated as

$$c_{Soot} = \frac{m_{Soot}}{m_{Oil} + m_{Soot}} = \frac{m_{Soot}}{m_{Sample} - m_{Inert}} \tag{6.3}$$

The saturation S of the sample strip (assumed to be representative for the whole filter) can be calculated as

$$S = \frac{m_{Oil} + m_{Soot}}{m_{Oil,max}} \frac{m_{Fibres}}{m_{Inert}} \tag{6.4}$$

with $m_{Oil,max}$ being the maximum oil holding capacity of the whole filter and the factor m_{Fibres}/m_{Inert} the ratio between the mass of the whole (clean) filter media and the inert mass of the sample strip. In both cases, it is assumed that it is only fibres that contribute to the mass and therefore this ratio describes which fraction of the whole filter the sample strip is. $m_{Filter,0}$ is the mass of the clean filter. All filters were weighed on the same balance (AS120, OHAUS, New Jersey, USA) before operation.

6.4. Oil Contamination and Filter Testing

Two different oil ageing methods were used in the laboratory to individually investigate the influence of each mechanism of oil degradation on the filtration performance of fibrous filters. The oil ageing method used in this work was based on the ASTM 7528 [93] method using a temperature of 170 °C and a heating period of 40 hours (as per the method), however the oil was heated in an open vessel. The ASTM method was chosen in preference to other oil ageing methods (such as IP 48 and DIN 51352) mainly for safety reasons, since the temperature was far below the flash point of the oil (230 °C).

2000 ml of new, unused Castrol RX Super 15W-40 diesel engine oil (as provided by the manufacturer) was heated in a glass vessel, inside an oven. A stainless steel tube was used to inject air (1 LPM) into the oil, finely dispersed through a porous ceramic cylinder to provide fine bubbles, uniform mixing and therefore even oxidation. Volatilised material was not collected.

To distinguish between the influence of thermooxidative breakdown and contamination on filter performance, oil samples were also prepared according to Table 6.1. Three different soot–in–oil standard samples (Castrol RX Super with 1.5%, 2.5% and 5% Printex U, see Section 4.4) were used to investigate the effect of soot contamination in oil

on the filter performance. The soot content of the oil was verified using a TA SDT 600 thermogravimetric analyser (TA Instruments, Delaware, USA) accordingly to Section 4.5. Additionally, one sample of "new" oil treated by thermooxidation and an oil sample gathered from one of the test vehicles (used in the field test) were investigated. As a reference, new (clean) oil as provided by the manufacturer was used. All oils were Castrol RX Super 15W-40 diesel oil.

Table 6.1.: Properties of oil samples used for laboratory filter testing and thermogravimetry.

#	**Oil (-)**	$\mathbf{c_{Soot}}$ **(-)**	ν_{40C} **(cSt)**
A	untreated	0%	107.5 ±0.21
B	oxidised	0%	99.7 ±0.16
C	untreated	1.5%	118.3 ±0.19
D	untreated	2.5%	124.1 ±0.15
E	untreated	5%	188.6 ±0.42
F	used	1.8%	149.7 ±0.28

The test filters were preloaded using the "DAD" method (see Section 5.4) and were then challenged with (aerosolised) oil continuously. Once equilibrium saturation and pressure drop were reached at the first equilibrium state EQ_1, the filters were subjected to discontinuous operation until the second equilibrium state EQ_2 was attained. Air and aerosol flow were stopped for 120 minute intervals and recommenced for 120 minute intervals during discontinuous operation. All filter tests were repeated at least three times.

The field test filters were tested in the filter test apparatus prior to the thermogravimetric analyses. Clean oil was used as aerosol and the filter were operated for approximately 10 minutes until a stable pressure drop and efficiency was attained. Flow velocity and concentration of the aerosol was identical to the conditions in Chapter 5. Due to the short filtration time, it was expected that the soot concentration and oil properties in the field test filters did not change significantly during laboratory testing. The collected oil during laboratory testing represented $< 1\%$ of the oil already in the filter.

6.4.1. Oil Viscosity Analysis

The soot–in–oil standard samples were analysed in a Brookfield LVDV II+ Pro viscometer (Brookfield Viscometers Ltd, Essex, UK) equipped with a small sample adapter and a #18 spindle. The temperature of the sample was maintained at 40 ±0.1 °C, by pumping heated water from a water bath to the sample cell adapter. Each oil sample was tested three times and the average value was calculated. The standard deviation was less than 0.25% for each oil mixture.

6.5. Statistical Analysis

The effects of the range of engine and oil specification on the final pressure drop of the field test filters were examined using linear regression. Due to limited data, Bayesian regression was used to determine the relationship between ΔP_{EQ2} and the oil and engine related data. The observed ΔP_{EQ2} was modelled as $y_i \sim Normal\ (\mu_i,\ \sigma^2)$, where y_i is the ΔP_{EQ2} for $i = 1...N$ observations. Bayesian regression was performed using Markov Chain Monte Carlo (MCMC) using WinBUGS 1.4.3 [94]. Convergence of the model was assessed using all convergence diagnostics in the CODA package [95]. From these diagnostics, the burn-in selection of the model was 10,000 iterations and a further 1,000,000 iterations were used to estimate the parameters α_i. The deviance information criterion (DIC) and model predictions were used to compare between the models [96]. The coefficients were modelled as Normal distributions, $\alpha \sim Normal\ (0,\ \sigma^2)$, where σ^2 was set to a large constant, thus all coefficients were treated as non–informative priors.

6.6. Preliminary Experiments

Although the TGA method was thoroughly validated in Section 4.5, preliminary experiments were conducted to validate the "scaled-up" tube furnace method used in this work. Calibration tests with soot–in–oil mixtures of known soot content were conducted to validate the tube furnace analysis method. Three different mixtures (Castrol RX Super with 1.5%, 2.5% and 5% Printex U) were used and the method was repeated three times for each sample. A 20 mm wide strip of new filter media was submerged into the oil sample for 1 hour and drained overnight before being analysed in the tube furnace using the same method as was later used to analyse the sample strips taken from the field test filters.

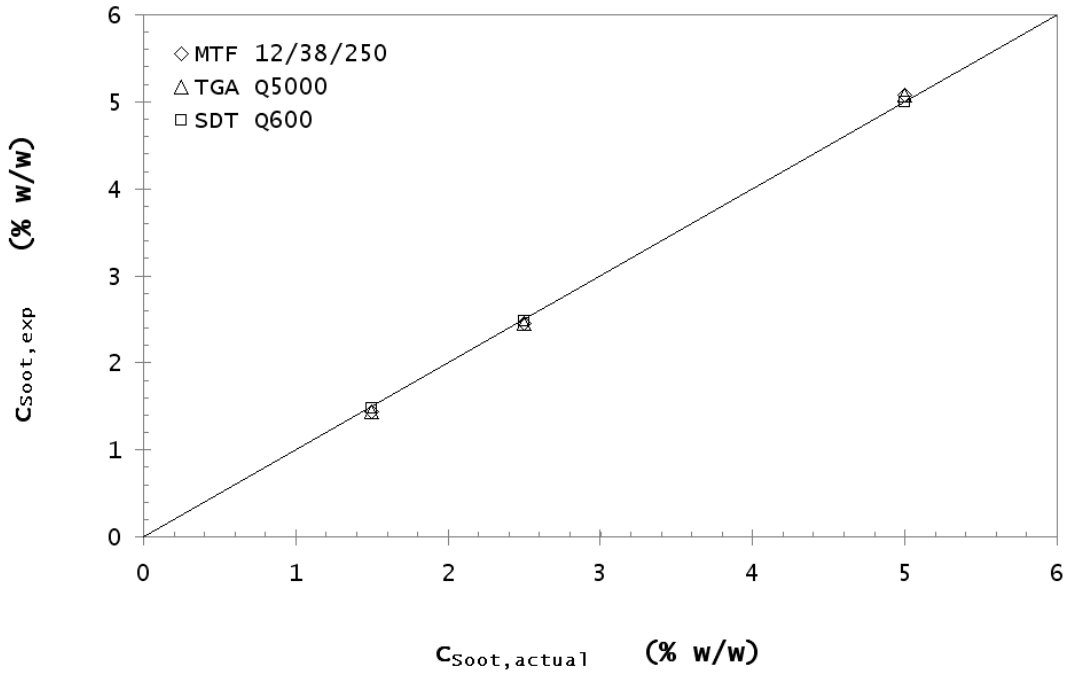

Figure 6.2.: Validation of the large-scale TGA method in the tube furnace. Filter samples with a known soot content ($c_{Soot,actual}$ = 1.5%, 2.5%, 5%) were used to validate the test method against a TA TGA Q5000 and a TA SDT Q600 thermoanalyser. A line showing the ideal relationship ($y = x$) has been added.

The sample strips and the oil samples were analysed in commercial thermoanalysers. 7 mm x 7 mm samples of the used filters were analysed in a TA TGA Q5000 instrument (TA Instruments, Delaware, USA) and the liquid oil samples were analysed in a TA SDT Q600 thermoanalyser (TA Instruments, Delaware, USA) to ensure the different methods for soot content determination were in agreement. The results are shown in Figure 6.2.

As can be seen, the soot content ($c_{Soot,exp}$) in the filter samples obtained from both the MTF tube furnace and the TA TGA Q5000 instrument showed an outstanding agreement with the actual soot content ($c_{Soot,actual}$) and the measured soot content in the oil by the TA SDT Q600 instrument. The reproducibility was found to be excellent, with deviations of less than 0.15% for all replicates.

6.7. Filtration Test Results

The pressure drop behaviour during discontinuous operation is shown in Figure 6.3. All pressure drop values were averaged during the air flow step for each cycle and normalised (ΔP_N) by dividing all values by the pressure drop present at the first equilibrium stage ΔP_{EQ1} of the untreated (i.e. as provided by the manufacturer) Castrol RX Super oil (15.5 mbar). Therefore the curves do not always commence at 1 on the y-axis. Cycle #0 shows the normalised pressure (see Section 5.5) drop at EQ_1 before discontinuous operation commenced.

It can be seen that all filters showed an increase in pressure drop during the initial cycles and reached a constant value, ΔP_{EQ2}, greater than ΔP_{EQ1}, for each curve. This higher pressure drop, once reached, was found to be stable (i.e. the filter would remain at ΔP_{EQ2}). Furthermore, the drainage rate (not shown) decreased during this stage from its equilibrium value to nearly zero and - after the second equilibrium state EQ_2 was reached - returned to a similar rate as before. The increase in pressure drop and the cessation of drainage were attributed to a second loading stage beyond EQ_1 as discussed in Chapter 5.

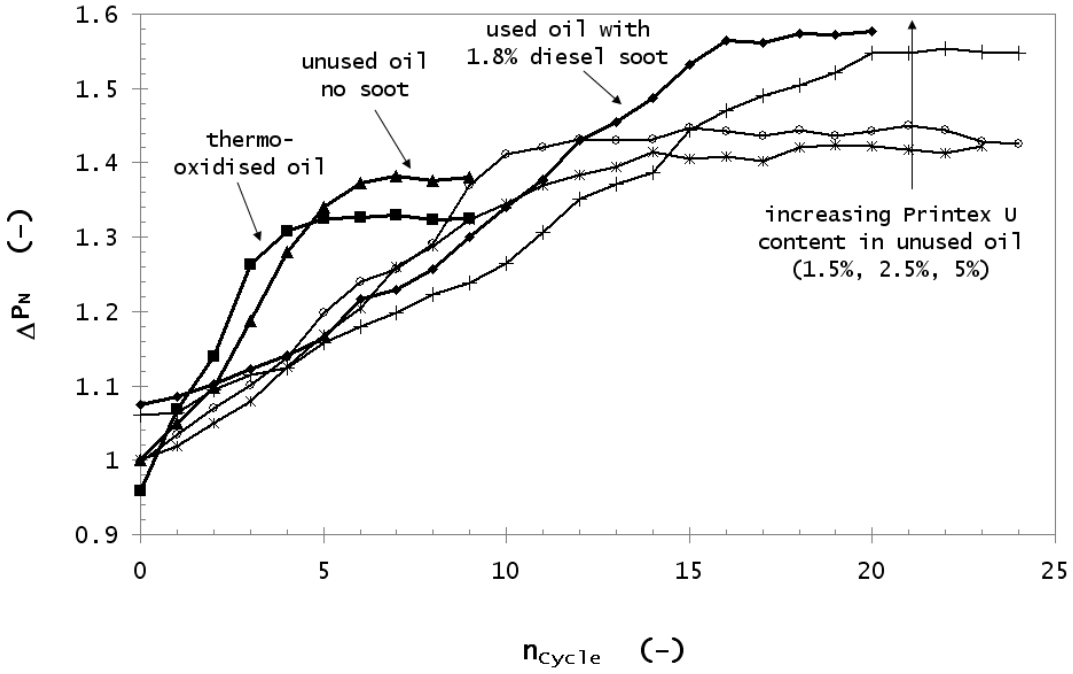

Figure 6.3.: Normalised pressure drop behaviour ΔP_N during initial cycles of discontinuous filtration. The oil samples consisted of untreated oil, artificially aged oil and three different mixtures (1.5%, 2.5% and 5%) of Printex U in unused oil. Additionally one "real" diesel oil sample (1.8% diesel soot) was examined.

It can be seen in Table 6.2 that most filters attained a similar ΔP_{EQ1} of approximately 15.5 mbar. However, the sample containing the artificially thermooxidated oil (B) showed an 0.7 mbar lower pressure drop (ΔP_{EQ1}), whereas the sample containing the highest soot content (E) and the sample obtained from the field test engine (F) showed a pressure drop that was slightly greater than the average.

The pressure drop increase between EQ_1 and EQ_2 was 5 – 10% higher for all samples containing soot (C–F) in comparison to the untreated oil (A) whereas the artificially oxidised oil (B) showed a slightly lower pressure drop increase. For the standard samples (C-–E), which contained untreated oil dosed with soot, an increasing tendency of 42% to 47% could be observed for increasing soot content (ΔP_{EQ2} = 22.01 ±0.21 mbar, 22.18 ±0.38 mbar and 24.11 ±0.23 mbar, respectively). The oil sample taken from a test vehicle

Table 6.2.: Results of discontinuous operation: pressure drop ΔP_{EQ1} and ΔP_{EQ2}, the number of cycles in the second loading stage, and the filter saturation S_{EQ2}. Oil properties (A-F) as per Table 6.1.

#	Δ $\mathbf{P_{EQ1}}$ (mbar)	Δ $\mathbf{P_{EQ2}}$ (mbar)	Cycles (-)	$\mathbf{S_{EQ2}}$ (-)
A	15.5 ±0.24	21.39 ±0.33	6 ±1	0.72 ±0.02
B	14.8 ±0.13	20.27 ±0.18	5 ±1	0.69 ±0.02
C	15.5 ±0.15	22.01 ±0.21	14 ±1	0.72 ±0.01
D	15.4 ±0.20	22.17 ±0.38	11 ±2	0.72 ±0.04
E	16.4 ±0.12	24.10 ±0.23	19 ±2	0.76 ±0.04
F	16.6 ±0.11	24.47 ±0.16	16 ±1	0.73 ±0.02

(F) showed an increase of 47% (ΔP_{EQ2} = 24.48 ±0.16 mbar) which is in the same range as for the other samples containing soot, however the increase was relatively high for a soot content of only 1.8%, compared to the increase that sample (C) and (D) showed. It should be noted that oil (F) possessed significantly higher viscosity. This suggests that the ageing processes which occur in real cases are not the same as those which occur during laboratory ageing (B).

The number of cycles required to reach EQ_2 during discontinuous operation reflects the same tendencies as were observed for the pressure drop increase. The artificially oxidised oil sample (B) required fewer cycles to reach EQ_2 than the untreated oil sample (A). The standard samples containing soot (C-E) required between 11 and 19 cycles, which is between 2 – 3 times the number of cycles required by the untreated sample (A). The test vehicle engine oil sample (F) showed a value which was in a similar range (16 cycles).

The artificially aged oil sample (B) showed a lower pressure drop ΔP_{EQ1}, a lower pressure drop increase and required fewer cycles to attain EQ_2 compared to the untreated oil sample (A). The samples containing soot (C–F) on the other hand, showed a higher pressure drop increase and the second loading stage requiring 2 – 3 times the number of cycles to attain EQ_2.

As can be seen in Table 6.2, the viscosity of the untreated oil (A) was measured as 107.5 cSt, which is very similar to the viscosity given by the oil manufacturer (114 cSt).

For the artificially aged oil (B), a slightly lower viscosity of 99.7 cSt was measured, whereas viscosity of the standard samples dosed with 1.5% and 2.5% (C-D) soot was only approximately 10 cSt and 15 cSt respectively higher than the viscosity of the untreated oil (A). The sample with 5% soot (E) however showed a greatly increased viscosity of 188.6 cSt which corresponds to a viscosity increase of approximately 75%. The viscosity of the oil sample taken from the test car (F) was measured as 149.7 cSt and thus was relatively high compared to the oil samples with corresponding soot content (C and D) which may be caused by additional factors in "real" engines that were not considered during laboratory oil ageing. These factors might be additional contamination with inert material (dust, dirt) or the fact that wear metal components in the oil act as catalysts and therefore change the oil ageing behaviour. Alternately, evaporation of lighter fractions may be more significant in the "real-world" case.

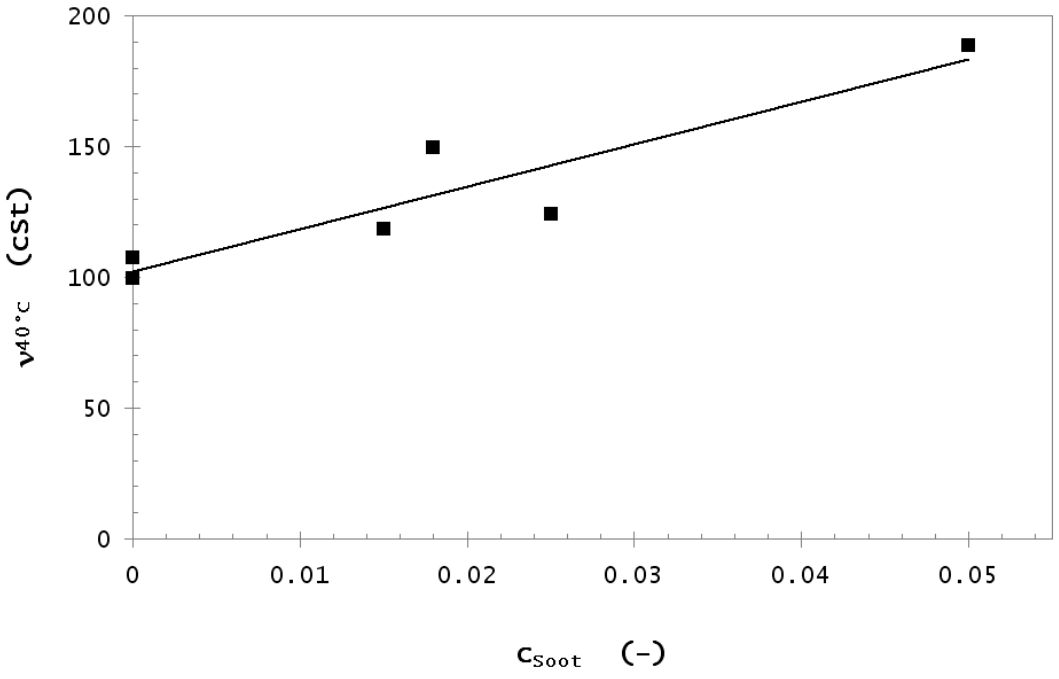

Figure 6.4.: Influence of the soot content c_{soot} on the (kinematic) oil viscosity ν_{40C} ($R^2 = 0.850$ with a slope of 1629.7 mm^2/s).

If the viscosity of the oil is plotted against the soot content of the oil, a linear correlation could be observed as can be seen in Figure 6.4. This agrees with findings by other authors [3], who found a near linear relationship between viscosity and soot up to levels of 5%. However, a more rapid increase was found when the oil viscosity at 100 °C or the base stock only was measured. Since both the viscosity and the soot concentration were determined with a high degree of accuracy (see Table 6.2 and 6.4.1), error bars were omitted for this figure.

The influence of the oil viscosity on the final pressure drop $\Delta P_{EQ2,N}$ of the filters, after the second loading stage, is displayed in Figure 6.5. The pressure drop values are normalised by dividing all values by the lowest $\Delta P_{EQ2,N}$ of the data points. It can be seen that the final pressure drop increases linearly with the viscosity of the oil sample used. Samples with a higher viscosity increased the pressure drop ΔP_{EQ2} and lead to a greater number of cycles to EQ_2.

The saturation S_{EQ2} of the filters was indeed different and seemed to follow the same trend as was observed for the pressure drop. Samples dosed with soot (C–E) had a slightly higher saturation, whereas the sample containing thermally oxidated oil (B) showed a slightly lower saturation than the reference sample with untreated oil (A). This result was also attributed to the different viscosities of the samples which affected liquid movement in the filter - the same effect that was found to be the reason for different pressure drop behaviour discussed in the previous section.

Thermogravimetric analysis of the drained oil captured during the laboratory filtration tests, revealed a slight decreased (0.1% to 0.3%) soot content in comparison to the soot content in the sample standards. This decrease however is marginal and is well within the range of the standard deviations. Therefore, it is believed that some soot accumulates in the filter over time during filtration, however, significantly longer filtration tests would be needed to investigate this issue, since the accumulation rate appears very low (see Chapter 7).

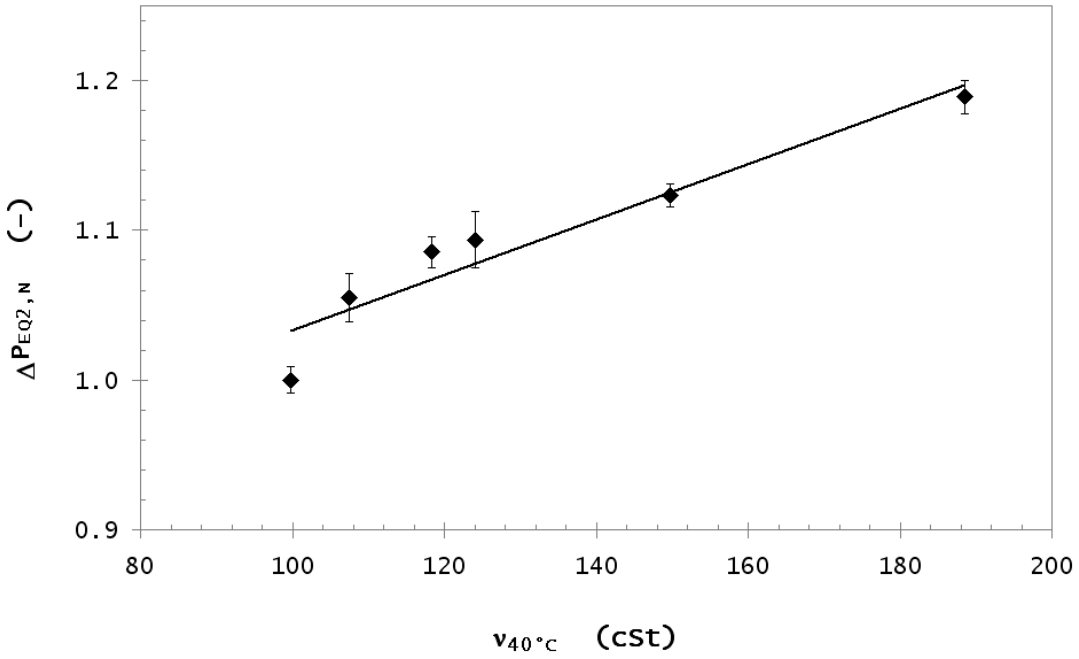

Figure 6.5.: Influence of the oil viscosity ν_{40C} on the final pressure drop $\Delta P_{EQ2,N}$ of the filters after the second loading stage (normalised).

From these results, we can conclude that contamination in the oil (such as the presence of soot) leads to an increased viscosity and therefore a corresponding increase in pressure drop. This increase appears to be linear. A viscosity increase was also observed by other authors [2] for oils of the same grade, however it was found not to be linear on the whole, though linear for blend oils with $< 5\%$ soot. Although the soot level in the engine oil sample (F) was similar to the soot content in the standards (C and D) the pressure drop and viscosity was elevated. Likely reasons for this were discussed earlier.

Thermooxidation on the other hand was found to lead to a decrease in oil viscosity in the laboratory case. This was also reflected in the filter performance. It was assumed that the evaporation of viscosity index improvers is responsible for the decrease and FTIR analysis of thermooxidated engine oil published by other authors [14] showed a decrease in the concentration of viscosity index improvers in the oil during oxidation. Other works indeed observed an increase in viscosity which was attributed to the evaporation of the lighter

fractions and subsequent polymerisation of the larger (remaining) molecules, however the increase was strongly dependant on oil quality and oil blending. These results therefore show that the thermal stability of oil varies due to a broad range of additives and various blends used to satisfy different lubricant requirements and to optimise lubrication abilities under different conditions, and also to the conditions to which the oil is subjected.

The findings from the filtration and thermoanalytical tests in this work suggested that two different mechanisms occur during oil deterioration which influence oil viscosity. Oil viscosity changes due to contaminants were found to have the strongest effect on mist filter performance, whereas thermooxidation had a less significant effect.

6.8. Field Test Results

Coincident with the laboratory tests, a field test was conducted using identical filters. Upon removal, these filters were analysed in the laboratory to determine ΔP_{EQ2}, S and soot content c_{Soot}.

The results of the thermoanalytical tests are shown in Figure 6.6. The measured soot content in the filters is plotted against the mileage the vehicle travelled during the six month testing period. It can be seen that the soot content in the filters increased near to linearity for all engines that were not equipped with a bypass centrifuge. The soot content for the filters ranged between 1% and 2.7% with one outliner with a soot concentration greater than 4%. This particular engine had user-modifications to increase engine output and the engine was nearing the end of its service life. Both these issues combined could be expected to increase the quantity of blow-by gases (and soot content of blow-by) and thus soot contamination of the oil. Therefore the data obtained from this engine were omitted for the calculation of the fit. Additionally, oil analysis conducted by a commercial company (Wear Check Oil Analysis, Hamilton, Australia) revealed high wear metal (lead, iron, aluminium) levels in the oil of this particular engine, up to 65 times higher than normal. The engines fitted with a bypass centrifuge ($Type$ 3) showed a lower rate of soot

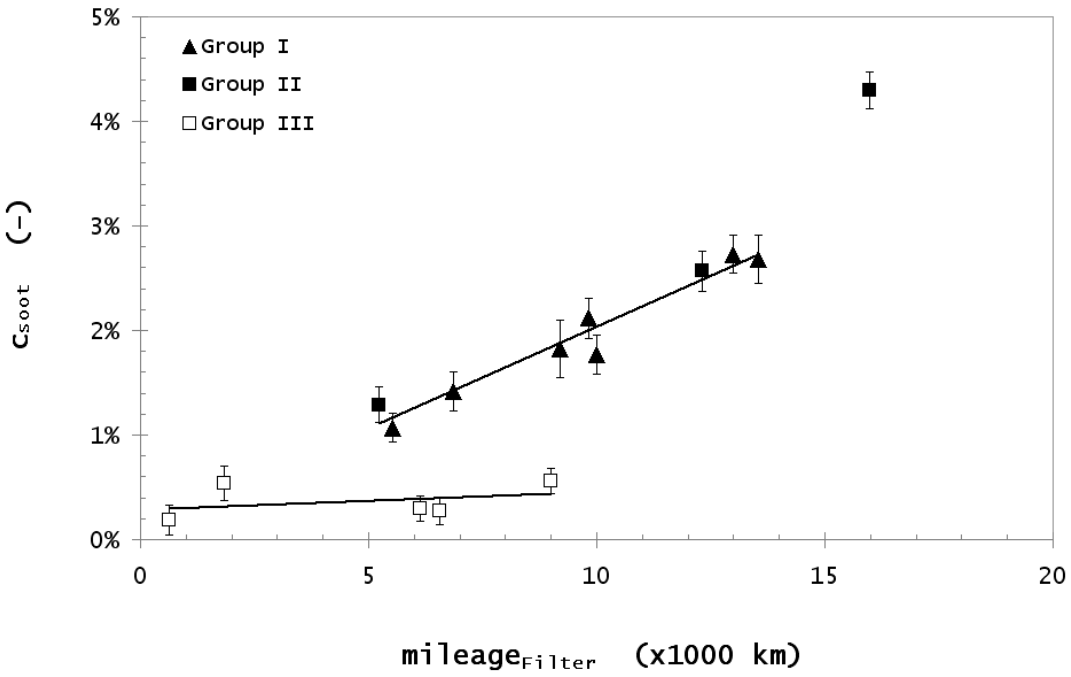

Figure 6.6.: Soot content c_{Soot} of the oil in the test filters after the distance travelled during 6 months field test.

increase, as could be expected if the bypass centrifuge is able to capture soot.

The pressure drops of the test filters are shown in Figure 6.7. The filters operated in vehicles that were not equipped with bypass centrifuges showed a higher pressure drop between 23.5 mbar and 71.9 mbar. There was no significant difference found between the oils of different SAE grades. Engines with bypass centrifuges showed a lower pressure drop of only 12.1 mbar to 16.3 mbar, with the lowest pressure drop originating from a filter which was only in use for 600 km and therefore had not yet reached full saturation yet ($S = 0.25$) and ΔP_{EQ2}. The other filters (for all engines) showed a saturation of $S = 0.64 \pm 0.07$. This suggests that S_{EQ2} was reached between 600 km and 1800 km. The engine with the mechanical fault stood out with a pressure drop of 71.9 mbar (not shown in Figure 6.7). For the linear fits both the filter obtained from the faulty engine and the filter that had not yet reached S_{EQ2} were omitted since they were found to not being representative The filter collection efficiency was measured for all filters as

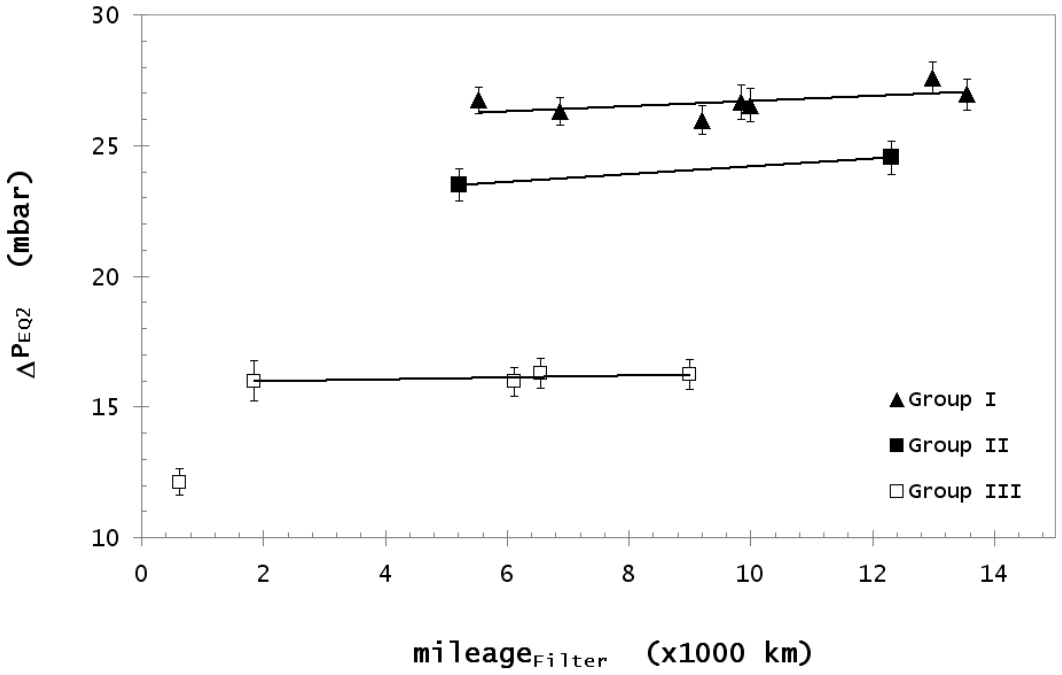

Figure 6.7.: Pressure drop ΔP_{EQ2} of the test filters as measured under laboratory conditions.

$E = 76.8\% \pm 3.3\%$, with no significant trends observed.

As was discussed earlier, the laboratory test filters (Figure 6.5) showed a markedly linear correlation between viscosity and pressure drop of the filter. However, since the field test was conducted with oils of two different oil grades and no viscosity data for the (used) oil were available, an alternative means of determining an equivalent viscosity of the used oil was found by multiplying the viscosity of the clean (unused) oil with the soot content after the field test.

This allowed a comparison between the results obtained from the field test and the laboratory results, which is shown in Figure 6.8. As before, the filter that was found to be not fully saturated and the filter obtained from the faulty engine were omitted in this graph.

It can be seen that all four datasets follow a linear trend, all with similar slopes, which

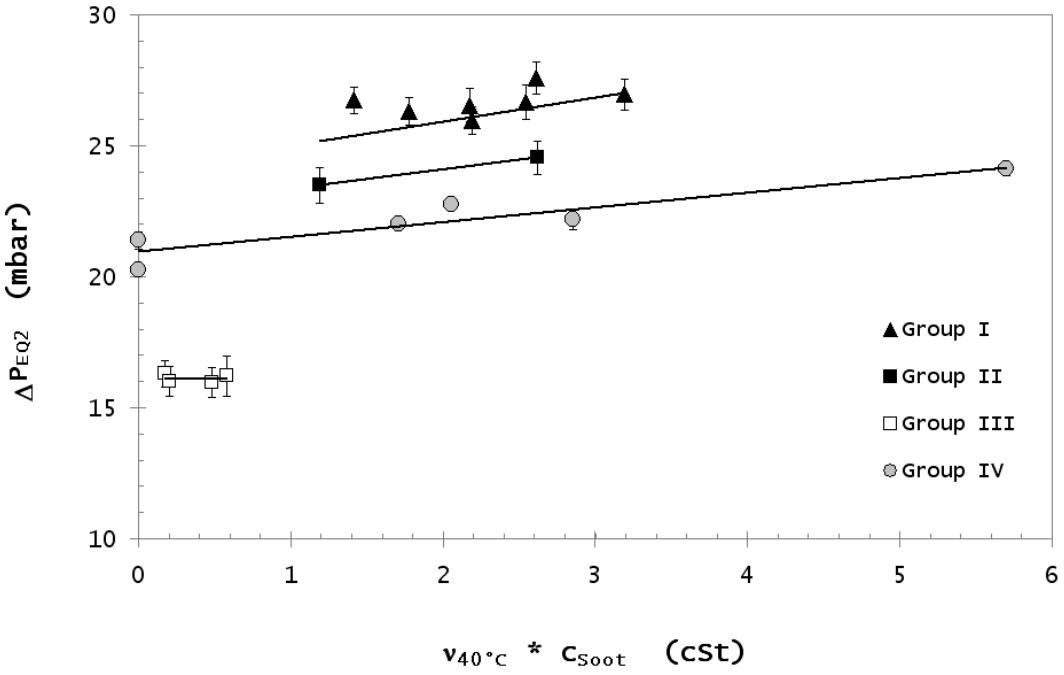

Figure 6.8.: Correlation between the "viscosity x soot"–term ($\nu_{40C} * c_{Soot}$) and pressure drop ΔP_{EQ2} of the test filters as measured under laboratory conditions. Group IV filters were the laboratory-loaded filters.

permits the pressure drop increase of a filter during use to be described by a linear function of the form

$$\Delta P_{EQ2} = b_1(\nu_{40C}\, c_{Soot}) + b_2 \tag{6.5}$$

with b_1 and b_2 being constants that describe the rate of increase (b_1) and the offset (b_2) of the pressure drop. By applying a least squares fit to each data set, the following values were obtained for b_1 and b_2 (Table 6.3).

Both the 15W-40 and the 5W-40 graded oils obtained from the engines with no bypass centrifuge installed showed a similar slope of 0.92 mbar/cSt and 0.73 mbar/cSt, respectively. The laboratory experiments (15W-40 graded oil), showed a linear increase of 0.56 mbar/cSt, which is lower than the rate found for most test engines. The oils

Table 6.3.: Parameters b_1 and b_2 to describe the linear pressure drop increase of the filters.

Group	**Oil**	$\mathbf{b_1}$ **(mbar/cSt)**	$\mathbf{b_2}$ **(mbar)**
I	field test	0.923	24.07
II	no bypass centrifuge	0.725	22.65
III	bypass centrifuge	∼0	16.15
IV	laboratory	0.561	20.97

obtained from engines with a bypass filter installed showed no significant increase in pressure drop. It is believed that solid particles (wear, soot, dust), which promote an increase in oil viscosity are removed by the centrifuge. Such an effect is likely apparent for the laboratory test filters, as no contaminants other than soot are added. It is also likely that a bypass filter would remove the largest soot agglomerates. A final consideration is that the engine of *Type* 3, the only Euro-3 engine, may influence the soot morphology or rate of soot deposition in the oil.

These findings suggest that the rate of the pressure drop increase is not significantly affected by the oil grade, but by oil ageing (thermooxidation and contamination) mechanisms which change the oil viscosity.

A Bayesian regression model was fitted to the whole data set to predict ΔP_{EQ2} for the field test data, based on known oil, contaminant and engine parameters. The resultant model (Equation 6.6) includes the saturation S, the filter efficiency E, the soot concentration c_{Soot}, the SAE SAE_u and W-SAE SAE_i oil grades, the engine capacity V_{Engine}, the odometer reading before and after he field test Odo_0 and Odo_E, respectively and the engine horsepower P_{Engine}. $Bypass$ is a dummy (boolean) variable denoting whether a bypass centrifuge was used or if the engine was fitted with a full–flow filter.

$$\Delta P_{EQ2} = \alpha_0 + \alpha_1\, S + \alpha_2\, E + \alpha_3\, c_{Soot} + \alpha_4\, SAE_u + \alpha_5\, SAE_i + \alpha_6\, V_{Engine}$$
$$+\alpha_7\, Bypass + \alpha_8\, Odo_0 + \alpha_9\, Odo_E + \alpha_{10}\, P_{Engine} \quad (6.6)$$

The coefficients α_0 - α_{10} are shown in Table 6.4.

Table 6.4.: Coefficients α_0 - α_{10} for the Bayesian regression model (Equation 6.6).

α_0	5.544991
α_1	18.135615
α_2	228.226020
α_3	732.945872
α_4	0.238692
α_5	-0.007854
α_6	27.002820
α_7	36.792138
α_8	-18.211766
α_9	18.889031
α_{10}	-2.2125831

A comparison between the pressure drop values obtained from the Bayesian regression model and the pressure drop values from the field test filter analysis in the laboratory showed a good agreement, as can be seen in Figure 6.9. It should be noted that none of the filters were excluded from this analysis.

To identify the parameters which had the greatest impact on the pressure drop, the mean value of each parameter ($\bar{S}$, $\bar{E}$, ..., $\bar{P}_{Engine}$) was multiplied against the corresponding coefficient. It was found, that, the engine configuration (P_{Engine} and V_{Engine}) had the greatest impact on the pressure drop, followed by the filtration efficiency E. Little to no influence can be attributed to the oil grade (SAE_u and SAE_{ui}) as was found previously. Soot content c_{Soot} and saturation S were found to be of minor importance.

These findings agree quite well with the conclusions drawn from the previous (laboratory) study, which showed that the pressure drop increase rate of both the field test and

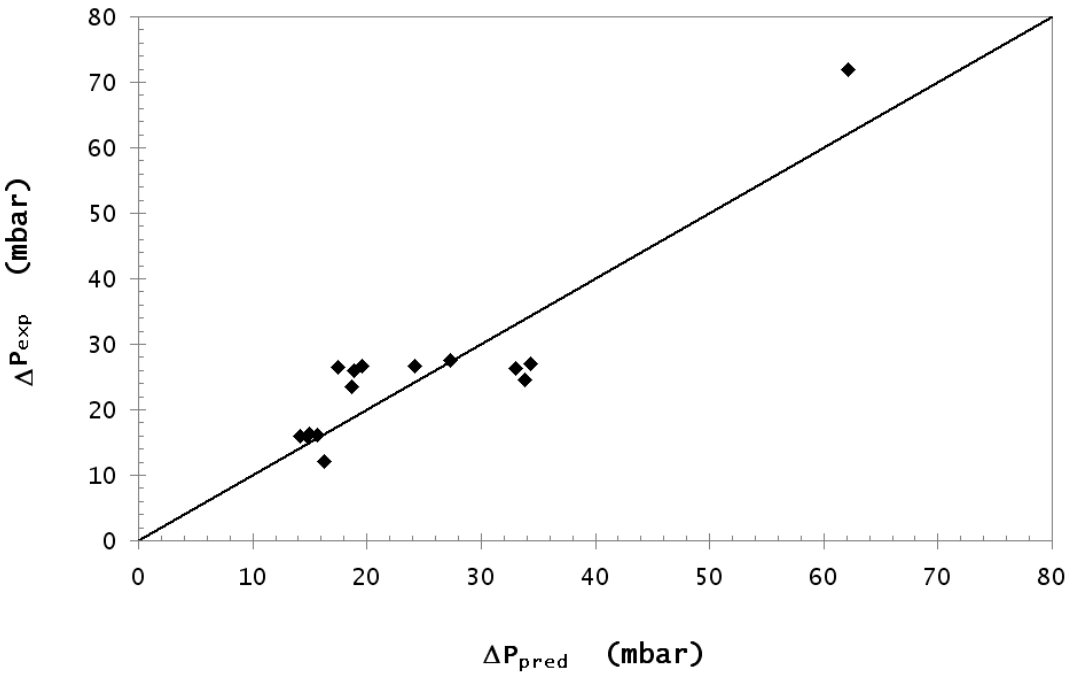

Figure 6.9.: Comparison between the pressure drop predicted by the Bayesian regression model ($\Delta P_{EQ2,pred}$) and the pressure drop measured ($\Delta P_{EQ2,exp}$) in the laboratory.

the laboratory test filters was not dependant on the oil grades of the different oils but on changes in the oil viscosity, which is predominantly affected by oil ageing. It is evident that the engine configuration (P_{Engine} and V_{Engine}) has a significant impact on the ageing process of the lubricant, since it strongly affects the amount of blow-by gases, contaminants, mechanical stress on the oil and operating temperature of the engine. The finding that the soot concentration c_{Soot} has a minor impact on the pressure drop evolution suggests that oil ageing and the corresponding increase in oil viscosity is dominated by other factors such as mechanical stress, catalytic activity of wear metal etc.

Special attention should be paid to the oil sample obtained from one of the *Type* 1 engines (F). This oil was used in both the field test (for the engine in question) and in the laboratory filtration test. The soot content of the sample was determined as 1.8% which was considered representative for the soot content of the (field test) oil samples

examined in this work. The field test filter from this engine revealed a pressure drop of 25.9 ±0.25 mbar (in laboratory testing), whereas the pressure drop (ΔP_{EQ2}) after discontinuous operation in the laboratory filtration test with the oil sample obtained from this engine was measured as 24.4 ±0.16 mbar. The saturation S was calculated as 0.72 ±0.16 for the field test filters using the same oil and 0.73 ±0.12 for the laboratory filter with an efficiency of 78.4 ±1.7% for the field test and 80.1 ±1.1% for the laboratory filter respectively.

Based on these findings it seems reasonable to suggest that the laboratory test methods are able to reproduce conditions similar to those experienced in a real diesel engine. However, additional factors which impact the viscosity change of the oil, such as mechanical stress or non–soot contaminants also need to be taken in account when artificially ageing engine oil for laboratory experiments.

6.9. Conclusion

In this chapter, laboratory filtration tests have shown that the oil viscosity has a major impact on the pressure drop behaviour of oil–mist filters. A higher soot content in the oil resulted in a higher oil viscosity and an increased final pressure drop ΔP_{EQ2} of the filter. Lower oil viscosity again (as for thermooxidated oil samples) resulted in a more rapid stabilisation of pressure drop but a lower final overall pressure drop ΔP_{EQ2}. It was found, that ΔP_{EQ2} increased linearly with viscosity [97].

A field test was also conducted using 15 vehicles equipped with three different diesel engine types. The filters were analysed in the laboratory after the test. A "scaled–up" version of the modified ASTM 5967 method presented in Chapter 4 allowed the determination of the soot content in the filters. It was found that the filters from engines with a bypass centrifuge installed showed no noticeable pressure drop increase during the field test period. The other filters showed a linear correlation between oil viscosity and ΔP_{EQ2}, which agreed well with the findings obtained from the laboratory filter

tests. However, the rate of increase was slightly higher for the field test filters which was attributed to additional oil ageing effects in the engine that were not taken into account during oil ageing in the laboratory. Furthermore, it was found that the oil grade is relatively unimportant for pressure drop development, whereas engine configuration has a major influence. These findings could be confirmed by a statistical analysis using Bayesian regression [97].

The work conducted in Chapter 6 has therefore provided important insight into the role of soot (and oil ageing) in CCV filters. Some evidence of soot accumulation was found, however the results were inconclusive. Chapter 7 will explore this issue further, by applying an "accelerated" ageing method.

7 Soot accumulation in fibrous oil–mist filters

7.1. Introduction

It was shown in Chapter 6, that soot contamination of engine oil can significantly influence oil–mist filtration by affecting viscosity, the question remains if soot particles can accumulate in the filter over time, or if they remain encapsulated by oil during collection and eventually drain with the collected oil. It was shown [49] that particles that are deposited on fibres can be "washed away" by subsequent liquid. However, drainage accumulation of soot in the filter may lead to high local viscosity or clogging of free passages through the filter. Both of which would likely result in higher pressure drop and higher interstitial velocities, which would likely be detrimental for the collection of ultrafine particles. However, recent research measuring droplet–fibre forces on filter fibres, could find no significant difference between droplets of sooty oil and clean oil [98]. However, viscosity would not be expected to influence droplet–fibre forces.

In order to simulate long–term CCV filter loading (and therefore soot accumulation), an "accelerated loading method" was devised, which passes the equivalent volume of liquid through the filter that would be supplied during approximately 380 hours of aerosol filtration in a typical application. The filters were then thermoanalytically investigated and filter soot content after 1 and 10 "passes" (equivalent to approximately 380 - 3100 hours of filtration) through the filter was determined.

7.2. Materials and Methods

A 2.5% soot-in-oil standard was prepared by adding artificial soot (Printex U) into engine oil (Castrol RX Super) as per Section 4.4. The mixture was stirred vigorously until the soot was evenly dispersed and the mixture was of homogeneous appearance. Samples of the mixture were analysed in a TA SDT Q600 thermal analyser using the modified soot–in–oil analysis method (see Section 4.5) and the soot content was determined as $c_{Soot,0}$ = 2.5% ±0.2% (w/w). Filters of both *Type A* and *Type B* were tested with three repetitions each.

To accelerate soot loading of the filter, 180 g (approximately 157 ml) of soot-in-oil mixture was poured into the cylindrically-shaped hollow space inside the saturated filter. This corresponds to approximately 3.6 times the maximal oil holding capacity $m_{Oil,max}$ of the filter and simulates a filter operation (using aerosol under the conditions specified earlier) of approximately 380 hours.

The soot–in–oil mixture was stirred immediately before being poured into the filter to assure even soot distribution in the oil. Compressed air was supplied to the filter inlet to assist filtration of the oil. The drained oil from the filter was collected in a vessel from which samples were taken for soot determination by TGA. The collected oil was then poured into the filter once again and passed through the media as described before, the drained oil was again collected and a sample was extracted. This procedure was repeated up to 10 times. At the conclusion of this "accelerated loading", the filters were then cut open and sample strips from the filter media were thermogravimetrically analysed as described in Section 6.3. All filters were preloaded with the 2.5% soot-in-oil standard using the "DAD" method (see Section 5.4).

Soot accumulation in these filters (I) and (J) (Table 7.1) was then compared to the soot accumulation in the filters used in previous laboratory filtration tests (C–F) in Chapter 6. All experiments conducted are shown in Table 7.1. The time t describes the equivalent time which would have been necessary for the filter to collect the same volume of liquid oil in aerosol form.

Table 7.1.: Filter and oil parameters for soot accumulation analysis (Pre = Preloading method, Filt = Filtration method, c_{Soot} = soot concentration in the "feed" oil (w/w)).

#	**Type**	**Pre**	**Filt**	m_{Oil} **(g)**	t **(hr)**	c_{Soot} **(-)**
C	Type A	DAD	Aerosol	73.01 ±0.57	121 ±0.95	1.5%
D	Type A	DAD	Aerosol	69.42 ±0.57	115 ±0.95	2.5%
E	Type A	DAD	Aerosol	79.04 ±1.13	131 ±1.89	5%
F	Type A	DAD	Aerosol	73.01 ±0.57	121 ±0.95	1.8%
G	Type A	DAD	Liquid	235.89 ±4.30	392.5 ±6.9	2.5%
H	Type A	DAD	Liquid	1855.89 ±31.46	3088 ±52.1	2.5%
I	Type B	DAD	Liquid	229.9 ±4.30	382 ±7.1	2.5%
J	Type B	DAD	Liquid	1848.9 ±31.46	3078 ±52.3	2.5%

The mass of soot $m_{Soot,in}$ passed through the filter can be calculated as

$$m_{Soot,in} = m_{Oil}\, c_{Soot} \tag{7.1}$$

with m_{Oil} being the amount of oil passed through the filter and c_{Soot} the soot content of the oil (w/w).

7.3. Soot accumulation

The results of the "accelerated loading" procedure can be seen in Figure 7.1. Additionally, results from previous aerosol filtration tests (Chapter 6) are included.

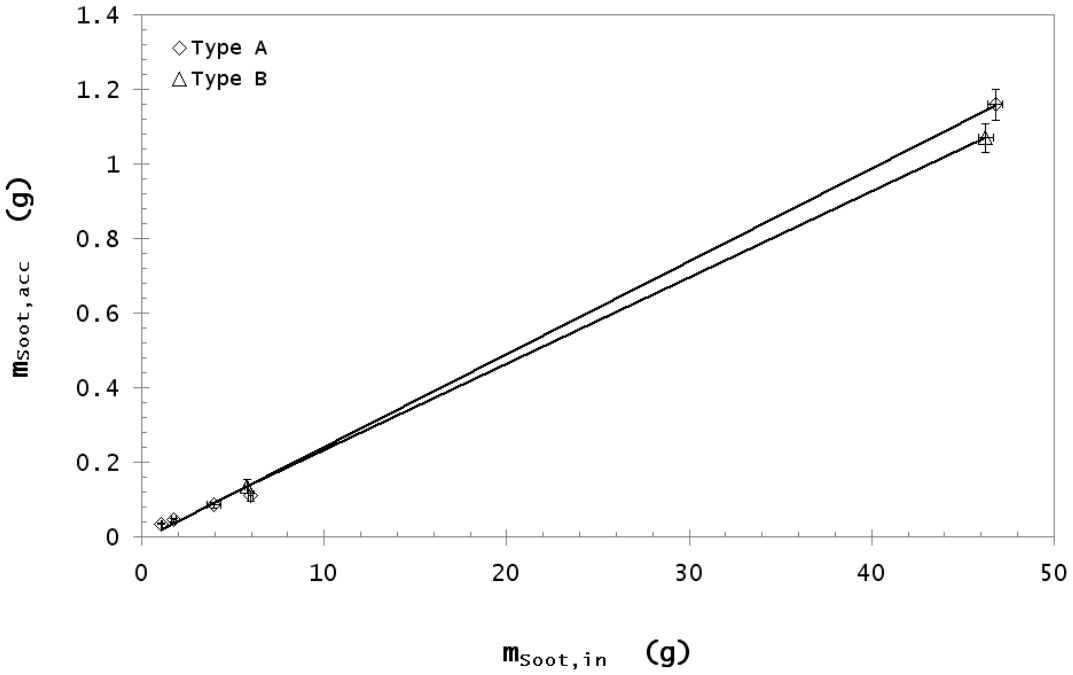

Figure 7.1.: Soot accumulation in *Type A* and *Type B* filters plotted against the loaded oil mass.

It can be seen, that soot content in the filter increased linearly with soot loading, regardless of the loading method. A linear fit through the dataset ($R^2 = 0.9998$) revealed a relationship of the form

$$m_{Soot,acc} = 0.0249\, m_{Soot,in} \tag{7.2}$$

for filters of Type A, where as for filters of Type B ($R^2 = 1$) the linear increase was of

the form

$$m_{Soot,acc} = 0.0231\ m_{Soot,in} \tag{7.3}$$

This finding shows that the method of "accelerated loading" appears to reproduce the results long–term aerosol loading experiments and thus allows an investigation of long–term CCV filter behaviour.

The slope of the linear fits in Figure 7.1 (0.0249 and 0.0231) can be interpreted as the soot accumulation rate of the filters or in other terms the filtration efficiency for soot of the filter. It is reasonable, that *Type A* filters showed a higher efficiency since their packing density was slightly higher - the difference however was marginal.

Although the single fibre efficiency theory (see Section 2.4.4) is commonly used to predict capture efficiency in filters removing solid particles from aerosols, it is nevertheless applicable for liquid filtration if electrostatic forces (ζ –potential) are neglected. Indeed, it has been found to be applicable to liquid–oil filters in engine filtration application [99]. Therefore, the single fibre collection efficiency was calculated to compare with the experimental soot deposition results. For the purpose of the calculation 350 nm [70, 100] was assumed to be the mass–mean agglomerate size, with a density of 1000 kg/m^3 [101]. The filtration velocity for these calculations was the flow rate of liquid through the filter over the filter area (the diameter was the average of the inner and outer filter diameter). An overall single fibre collection efficiency for soot agglomerates in a liquid filter of *Type A* (Filters G - H) was calculated as 0.0178 and 0.0142 for *Type B* (Filters I and J). This efficiency is in good agreement with the efficiency determined experimentally.

7.4. Conclusion

To investigate the accumulation of soot in oil–mist filters an "accelerated loading method" was used to simulate an equivalent of between approximately 380 and 3800 hours of filter operation with soot–in–oil aerosol. These data were then combined with data from Chapter 6 for soot deposition in aerosol loaded filters. It could be shown, that soot accumulates in the filter at a rate of approximately 0.0249 g per gram of soot loaded for *Type A* filters and 0.0231 g per gram for *Type B* filters. Comparison with the fibre efficiency theory revealed very similar efficiency rates of 0.0178 g and 0.0142 g, respectively.

These findings are important for the filtration of "colloidal" aerosol particles, as accumulated solid particles captured in the liquid would be likely to accelerate filter clogging or interfere with liquid transport which could potentially reduce drainage rate and increase saturation. It was shown in Chapter 6, that soot contamination plays a major role in oil viscosity increase and thus would likely also influence drainage behaviour. It is therefore desirable, to remove both soot and oil from the filter if possible. A mechanism for soot removal from mist filters is beyond the scope of this thesis, however overall liquid/aerosol saturation has been found to have the most pronounced effect on pressure drop. Chapter 8 will explore the regeneration of oil–mist filters by reducing liquid saturation, initially investigated in Chapter 5.

8 Filter Regeneration

8.1. Introduction

From Chapters 5 and 6 it should be clear that filter pressure drop is strongly dependant on saturation. Therefore, if saturation can be reduced, pressure drop also will be reduced. Furthermore, Chapter 7 showed, that soot which accumulates in the filter is likely to increase (local) viscosity and therefore also increases pressure drop. As a mist filter typically increases only slowly in saturation, a significant reduction in S would give a long–term reduction in ΔP. This would be advantageous, since a reduced pressure drop (flow resistance) would increase both capture and energy efficiency. It was shown in Section 5.6, that a saturated filter drains significant amounts of oil during the first seconds of filtration, driven by drag forces that were able to (partially) clean clogged passages through the filter. Drainage, however was limited due to counteracting capillary forces which resist the air flow forces. However, the question remains whether filters could be "artificially" cleaned or regenerated by removing oil from the filter using high air flow rates or other means.

In dust filtration applications [102, 103] a surface filter can be cleaned or regenerated using a jet of compressed air to remove the "cake" of particles clogging the filter. Once the filter cake is (partially) removed, the permeability of the filter increases significantly, which lowers the flow resistance and thus the pressure drop across the filter. It is a logical extension therefore, that a modified form of "pulse–jet" cleaning could be applied to oil–mist filters in order to clean the clogged passages, thus returning the filter to its initial unsaturated condition (or close to). Cylindrical filters could also conceivably be cleaned by high velocity rotation. Such a method would induce centrifugal forces which would force the liquid captured in the filter to the outside, where it can drain or detach in droplets. Filter cleaning by rotation can be conducted in-situ (during filtration with aerosol flow continuing) or externally where the filter is dismounted from the chamber and cleaned separately.

The regeneration ability of oil–mist filters will be examined in this chapter using three different methods to apply additional force on the liquid to assist drainage. Furthermore, filters cleaned with a "pulse–jet" were tested for their ability to be re–used and the efficiency of "pulse–jet" cleaning on filters preloaded using different methods ("RAS" or "DAD") was investigated.

The three cleaning methods investigated in this chapter are

C1: cleaning by high velocity air flow

C2: cleaning by rotation without air flow

C3: cleaning by rotation during filtration (air and aerosol flow)

8.2. Material and Methods

The cleaning methods were applied on both *Type A* and *Type B* filters. The filters were preloaded using Castrol RX Super lubricant oil using the "DAD" method (unless specified otherwise in Section 8.7).

After both preloading and cleaning, all filters were tested in the filter testing apparatus shown in Figure 5.1 at conditions specified in Chapter 5 (55 LPM air flow with a loading rate of 175 $\pm$4.3 mg/m^3). Filters were challenged with clean oil aerosol in the filter testing apparatus for approximately 30 seconds, in order to determine their "initial" pressure drop. The filter mass was measured on a high–precision balance beforehand.

Filters used in Section 8.4 and 8.5 were either in–situ (during filtration) or externally cleaned by rotation immediately after preloading with oil (and determination of pressure drop and weight). Filters used in Section 8.3 were filtered for longer after preloading and weighing until the first equilibrium state was reached and then cleaned before they were once again preloaded, weighed and filtered (continuously) until they reached an

equilibrium state (EQ_1) again. The process was conducted for a number of increasing "pulse-jet" velocities (u_{Jet}).

To calculate the normalised pressure drop ΔP_N, the pressure drop over the last 15 seconds of each filtration step (after cleaning or at EQ_1) was averaged and divided by the average pressure drop over the first 15 seconds after preloading.

Cleaning Method C1

Filters of *Type A* were regenerated by removing oil from the filter using a higher than normal flow rate of air through the filter. Regeneration was conducted externally using a specially constructed apparatus which injected compressed air into the top of the filter (in the flow direction, unlike common "reverse-pulse" cleaning of dust filters). Air flow was continued until no further oil was observed to drain. Three filters were tested for each regeneration flow rate used.

Cleaning Method C2

An apparatus was developed to clean the test filters at different rotational speeds (n = 370, 580, 1160, 1600 and 2470 rpm). The filters were held fixed at top and bottom. The bottom of the filter was supported by a small platform that was was able to spin freely on ball bearings. A motor and controller were able to supply a constant (known) speed. After t = 15, 30, 45 and 600 seconds, rotation was discontinued and the filters were carefully removed and their weight was determined. After 600 seconds of rotation, the filters were tested in the filter testing apparatus. Each test was repeated for three filter replicates. Filters of both *Type A* and *Type B* were tested.

Cleaning Method C3

In order for the filter to be permitted to rotate during filtration, the filter chamber of the laboratory filter testing apparatus shown in Figure 5.1 was replaced with a modified chamber (Figure 8.1) which was equipped with sealed bearings and a motor drive.

The filter was located in a sealed bearing with a specially machined locating groove and driven by a shaft connected to a motor. The shaft was mounted into the lid of the filter housing through a further sealed bearing. By adjusting the supply voltage, the speed of

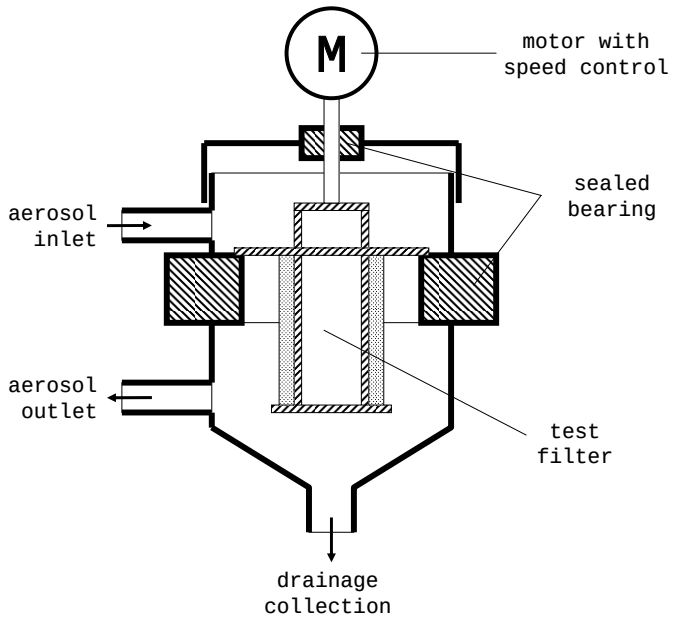

Figure 8.1.: Schematic of the modified filter chamber for filter rotation experiments (Cleaning method C3).

the motor could be controlled. The filters were rotated at $n = 450$, 900, 1500, 2000, 2300 and 2500 rpm after preloaded off–line. During rotation, the filters were challenged with aerosol. The filters were removed and weighed when no significant drainage and changes in pressure drop were observed. In this test, only filters of *Type A* were tested. Each test was repeated at least three times.

Re–use of filters after regeneration using the C1 cleaning method

Two *Type A* filters were compared using different combinations of preloading methods as shown in Table 8.1. The filters underwent a preloading and an aerosol saturation stage as per normal. Once the first equilibrium state EQ_1 was reached, they were subjected to discontinuous operation until the second equilibrium state EQ_2 was reached (as described in Chapter 5). The filters were then cleaned by a flow of high velocity air (compressed air "pulse–jet") before the next round of preloading commenced. The preloading method

alternated between the "DAD" and the "RAS" method, with one filter starting with the "DAD" method and the other with the "RAS" method.

Table 8.1.: Preloading configuration for two filters (*Type A*) that were cleaned and reused.

	Filter 1	**Filter 2**
1st test	DAD	RAS
2nd test	RAS	DAD
3rd test	DAD	RAS

8.3. Filter Regeneration Using the C1 Cleaning Method

Pressure Drop (normalised) ΔP_N and saturation S at the first equilibrium state EQ_1 and after Regeneration R are shown in Figure 8.2. Each test was repeated at least three times.

It can be seen that both saturation and pressure drop could be significantly reduced after using the "pulse–jet" cleaning method (Method C1). The relationship between saturation and "pulse–jet" velocity u_{Jet} appears to be linear (see linear fit through the dataset) of the form

$$S = -0.0479\, u_{Jet} + 0.6548 \tag{8.1}$$

However, it is known from other work [34] that during filtration a "static" amount of oil remains in the filter that cannot be removed by airflow forces. This means that the relationship shown above appears linear in the range between $u_{Jet} = 0.2$ to 3.9 m/s, however would likely follow a curve and eventually attain a constant, non–zero value – the "static" saturation. The pressure drop after cleaning follows the "pulse–jet" velocity in a curve of the form

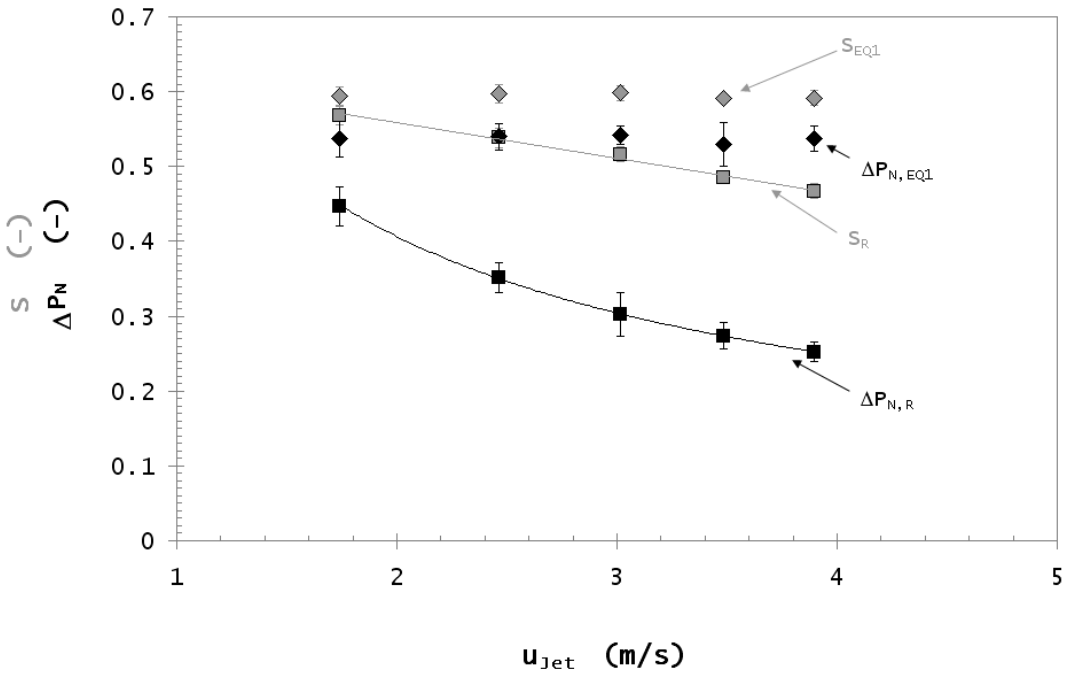

Figure 8.2.: Normalised pressure drop ΔP_N and saturation S immediately after the cleaning and after reaching EQ_1. The filters (*Type A*) were cleaned using different velocities u_{Jet} with a reverse "pulse–jet".

$$\Delta P_N = 0.666 u_{Jet}^{-1/\sqrt{2}} \tag{8.2}$$

as was indicated by the logarithmic fit through the dataset. Therefore the current results agree with the "static" saturation theory and suggest that ΔP_N will eventually plateau.

Furthermore, it could be shown that the filter was able to attain very similar equilibrium conditions ($\Delta P_{N,EQ1}$ and S_{EQ1}) after each cleaning process which allows possible re–usage of the filter.

8.4. Filter Regeneration Using the C2 Cleaning Method

Normalised pressure drop ΔP_N, efficiency E and saturation S values after cleaning at different rotational rates is shown in Figure 8.3. Filters of *Type A* are assigned black symbols and *Type B* grey symbols. Lines between the data points are for ease of viewing only and are not suggesting relationship in data. All values were determined after 600 seconds cleaning. Each data point was calculated from at least three repetitions.

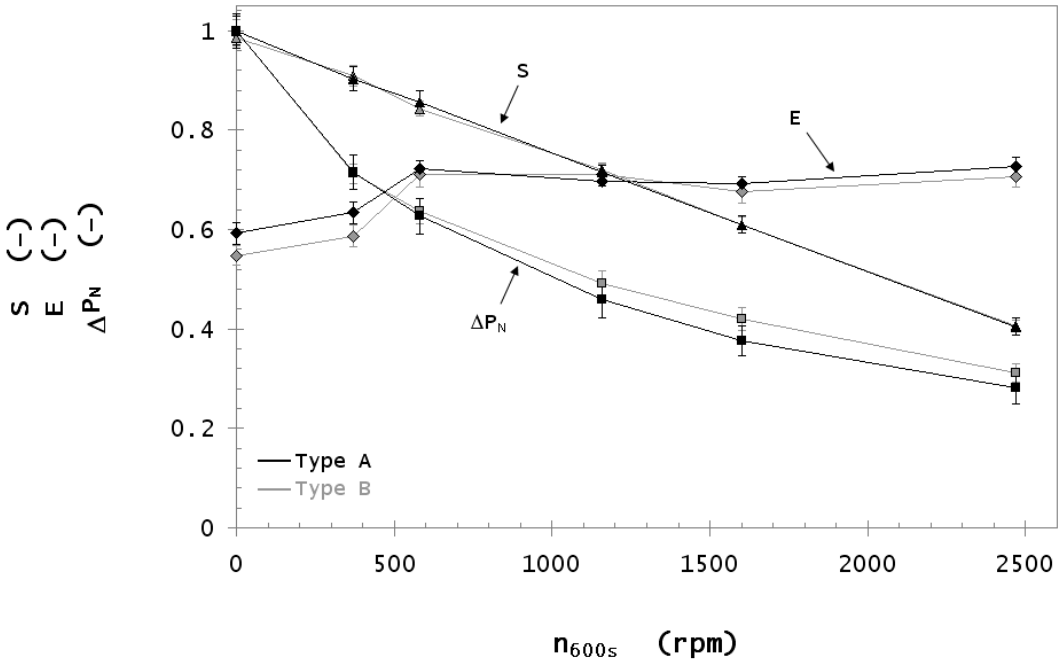

Figure 8.3.: Filter saturation S, normalised pressure drop ΔP_n and filter efficiency E for test filters of *Type A* and *Type B* after 600 seconds cleaning by rotation at rates of n = 370, 580, 1160, 1600 and 2470 rpm.

Both filter types showed a very similar behaviour, with ΔP_n and S decreasing with increasing rotational speed. In both cases, little drainage was observed in the filter testing apparatus for $n < 1160$ and no drainage for $n \geq 1160$ after filter cleaning.

The decrease in ΔP_n could be described by a logarithmic relationship (as a function of n, with $n > 0$) which was of the form

$$\Delta P_n = -a_1 ln(n) + a_2 \tag{8.3}$$

with a_1 and a_2 being empirically determined constants. Although *Type B* Filters showed a slightly higher ΔP_n, which might be due to the higher packing density of this type, the difference is within the range of the error bars and therefore can be deemed negligible. The constants a_1 and a_2 were each found to be very similar for both filter types with $a_1 = 0.2219 \pm 0.015$ and $a_2 = 2.0348 \pm 0.0879$, respectively. The saturation S decreased linearly with increased rotational speed and no significant difference was observed between the two filter types. The filters cleaned at the maximum speed ($n = 2470$) showed a pressure drop approximately 70% below the initial pressure drop and a 60% lower saturation. Filtration efficiency was found to slightly increase with increasing n, which was attributed to a "resetting" of the filter back into an earlier loading stage by removing oil from the filter. This effect provided more effective collection area (see Section 2.6.1) and thus a higher collection efficiency. The lower efficiency for $n = 0$ and $n = 370$ is likely from re–entrainment of particles from the rear of the filter.

It is obvious from these findings that rotating the filters (particularly at higher speed) is able to drive liquid out of the filter and is beneficial for pressure drop and efficiency of the filter. It is believed, that pressure drop and saturation eventually level off and it is not possible to clean the filter completely due to strong capillary forces that hold a "static" amount of oil in the filter.

To describe the saturation during cleaning, the weight of the test filters was determined after $t = 5$, 30, 45 and 600 second for each rotational speed. The saturation was calculated using Equation 2.30 and is shown in Figure 8.4 for both *Type A* and *Type B* filters. For reasons of clarity, error bars were omitted in this graph since the error bars shown in Figure 8.3 were deemed to be representative for all rotational speeds. It can be seen, that both filter types showed near–identical saturation curves for each rotational velocity and that a higher rotational rate leads to a lower saturation for each time set. This finding is not surprising and the reasons were discussed earlier. The decrease in saturation is

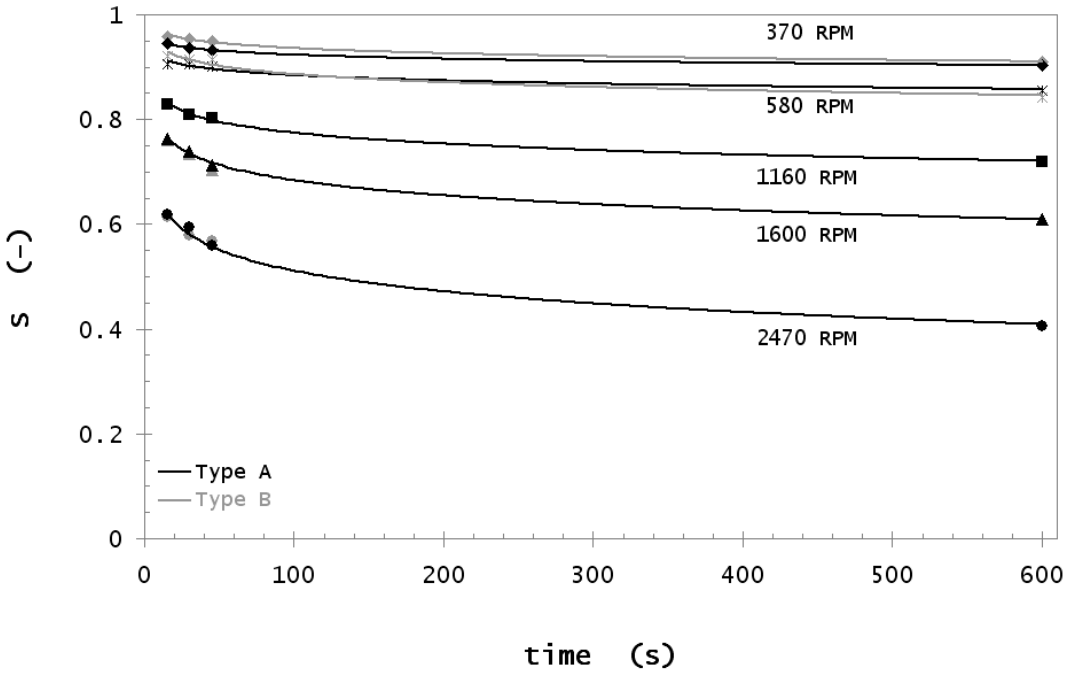

Figure 8.4.: Saturation S of *Type A* and *Type B* filters after 15, 30, 45 and 600 seconds of cleaning at different rotational speed (using the C2 cleaning method). Logarithmic trendlines have been fitted to the dataset.

most rapid in the early cleaning stages and decreases over time. As is suggested by the trendlines, the saturation behaviour follows a logarithmic relationship in the form of

$$S = \frac{c_1 ln(t) + c_2}{\frac{2\alpha}{d_f}} \tag{8.4}$$

with c_1 and c_2 being parameters and t is the cleaning time. The term $2\alpha/d_f$ is the relationship between filter packing density and fibre diameter and is a surrogate for capillary diameter [62]. The parameters c_1 and c_2 account for rotational rate, i.e. $c_i = f(n)$, and were empirically derived as

$$c_1 = -1.8287\ 10^{-7}\ n - 7.9102\ 10^{-5} \tag{8.5}$$

and

$$c_2 = -1.0048\ 10^{-6}\ n + 9.6198\ 10^{-3} \tag{8.6}$$

If Equation 8.4 is valid, the saturation must reach a constant value for $t \to \infty$. Or in more realistic terms must significantly decrease in slope as t increases. Figure 8.5 shows $\Delta S = dS/dt$ of a filter rotated at 2470 rpm for one hour. It can be seen, that after only 10 minutes, the saturation changes at a rate of only 0.6% per minute, which in the most cases can be considered negligible compared to the effort required to rotate the filter. Therefore, it would be optimal to rotate the filter only for 10 - 20 minutes and no longer. However, an increase from 2470 to 3500 rpm would require only 8 minutes time to reach a saturation decline of less than 0.2% per minute compared to approximately 30 minutes if cleaned at a speed of 2470 rpm. These results show, that filter cleaning by rotation is an efficient way to significantly reduce filter saturation (and thus pressure drop) and the filters eventually attain a near–constant saturation.

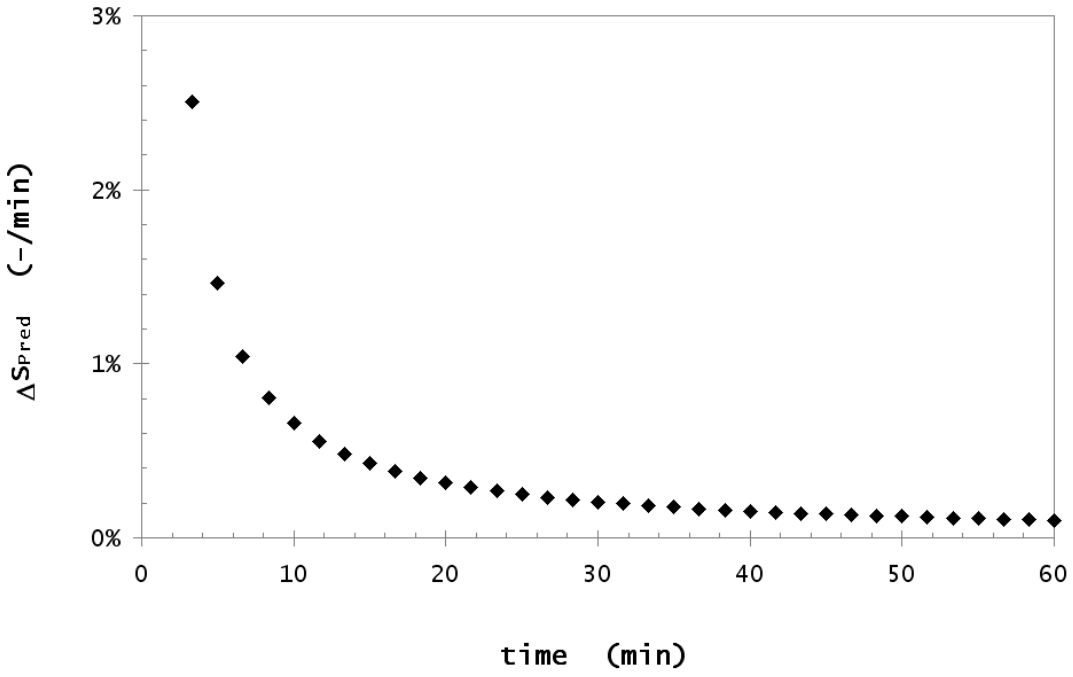

Figure 8.5.: Theoretical $\Delta S = dS/dt$ (Equation 8.4)decrease over time for a *Type A* filter rotated at 2470 rpm using the C2 cleaning method.

To verify the cleaning model, the saturation $S = f(n, t)$ was predicted using Equations 8.4 - 8.6 for combinations of n and t used in previous cleaning tests. A comparison between the saturation obtained during the filter cleaning tests S_{exp} and the predicted saturation S_{pred} is shown in Figure 8.6 for *Type A* and Figure 8.7 for *Type B* filters.

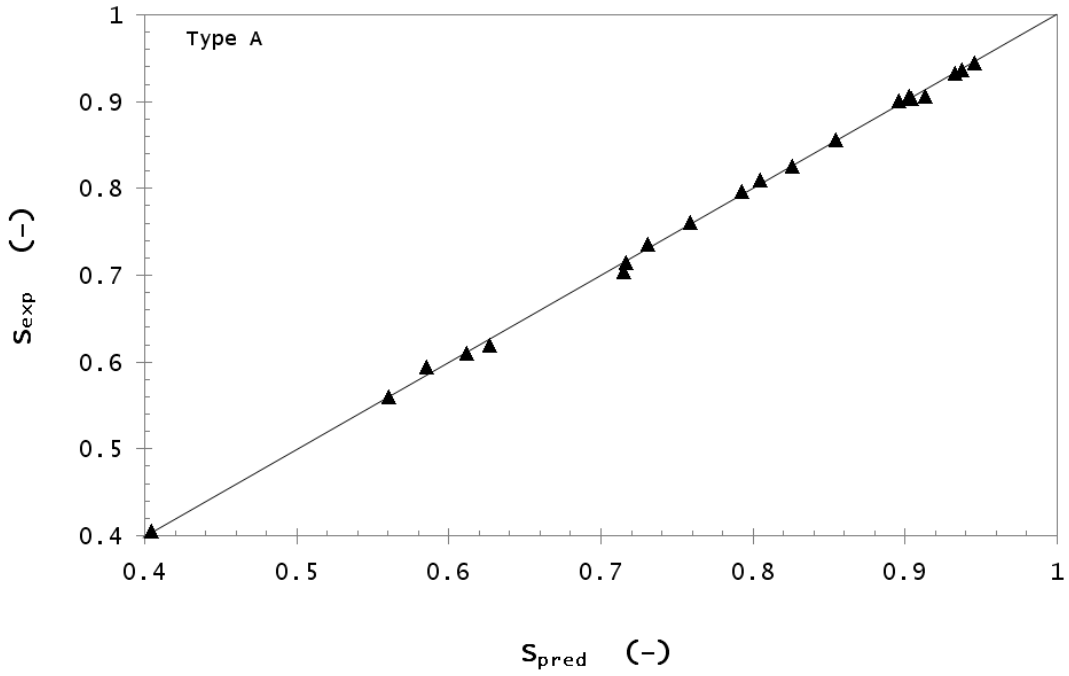

Figure 8.6.: Experimentally obtained saturation S_{exp} and predicted saturation S_{pred} for a *Type A* filter. S_{pred} was calculated using Equation 8.4.

As can be seen, the measured and predicted values show an outstanding agreement for both filters with linear fits through each dataset showing $R^2 = 0.9991$ for *Type A* and $R^2 = 0.9988$ for *Type B* filters.

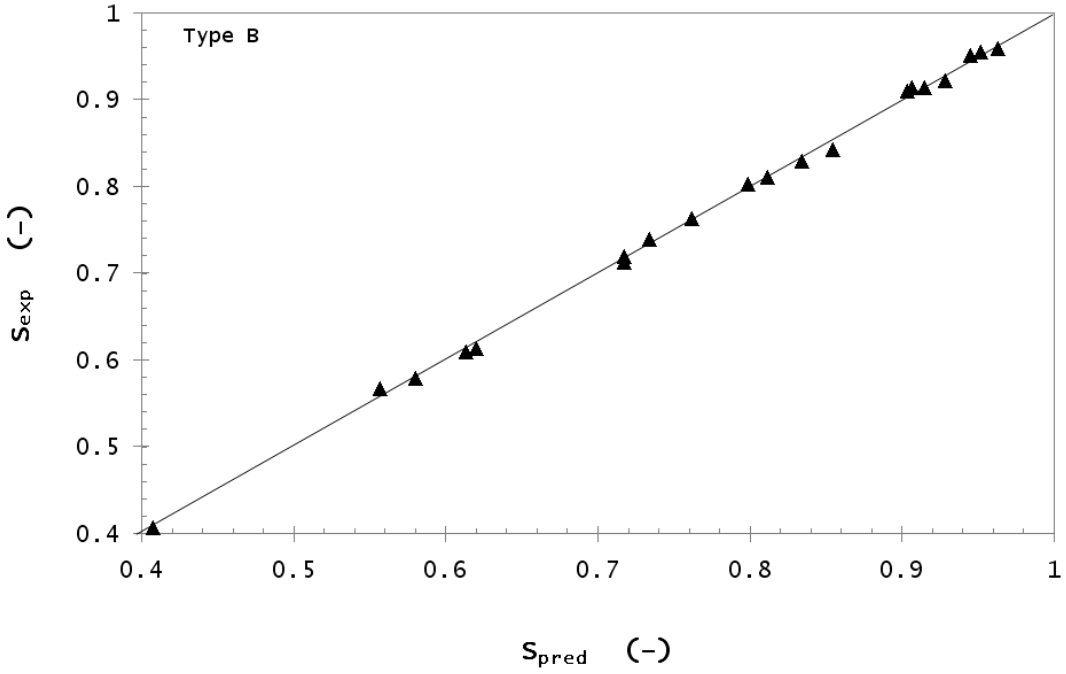

Figure 8.7.: Measured (S_{exp}) and predicted (S_{pred}) saturation for a *Type B* filter. S_{pred} was calculated using Equation 8.4.

8.5. Filter Regeneration Using the C3 Cleaning Method

The C3 cleaning method involved passing air (or aerosol) through the filters while they were rotating. The normalised pressure drop ΔP_n and the saturation S after filter cleaning at different revolution rates is shown in Figure 8.8. As no oil droplets were found (during preliminary experiments) in the downstream safety filter and the hoses, a mist eliminator was not required in this apparatus.

As was observed in the previous case (Figure 8.3) where no aerosol flow was applied, a significant decrease in both ΔP_n and S was achieved during rotation. Likewise, the relationship between ΔP_n and n could be expressed by a logarithmic fit through the dataset of the form

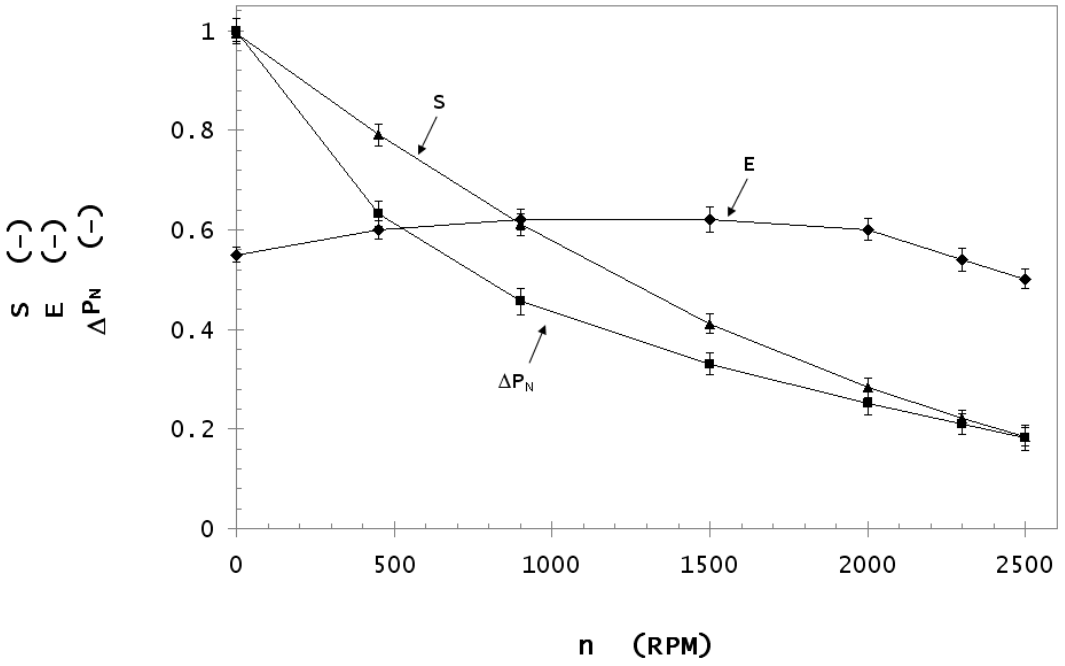

Figure 8.8.: Filter saturation S and normalised pressure drop ΔP_n of the test filters after cleaning at rotational rates of n = 450, 900, 1500, 2000, 2300 and 2500 rpm during aerosol flow. It should be noted that a different motor and controller were used for the C2 and C3 experiments, which accounts for the different rotational rates.

$$\Delta P_n = -a_3 \, ln(n) + a_4 \tag{8.7}$$

with $a_3 = 0.2601 \pm 0.018$ and $a_4 = 2.2249 \pm 0.0429$ and $n > 0$ The saturation decreased linearly with the rotational speed. For the maximum speed of $n = 2500$ a saturation of $S = 0.18$ and a normalised pressure drop of $\Delta P_n = 0.18$ were measured. Drainage could be observed during all tests. The decreased efficiency for $n \leq 450$ and $n \geq 2300$ is likely to result from re-entrainment of expelled liquid accumulated at the rear of the filter as discussed in the previous section. This finding is of great importance since the previous section showed that high rotational speeds were beneficial for the filter saturation and thus the resulting pressure drop, since the time required to clean the filter (which would represent downtime or time off–line) could be significantly decreased by increasing the

speed. However, in 8.4 cleaning was conducted externally, which means that expelled oil could be completely removed prior to reinstalling the filter and continuation filtration. Figure 8.8 in contrast shows that a compromise has to be made when applying the in–situ cleaning method in which the benefit of a lower saturation and pressure drop is countered a reduction in the overall filtration efficiency during the cleaning process.

The saturation model developed in the previous section was used to predict the saturation values for filters cleaned in–situ with aerosol flow (at the different n) as used in this test. The comparison between the predicted and measured saturation can be seen in Figure 8.9. Error bars for S_{exp} were omitted, however can be seen in Figure 8.8.

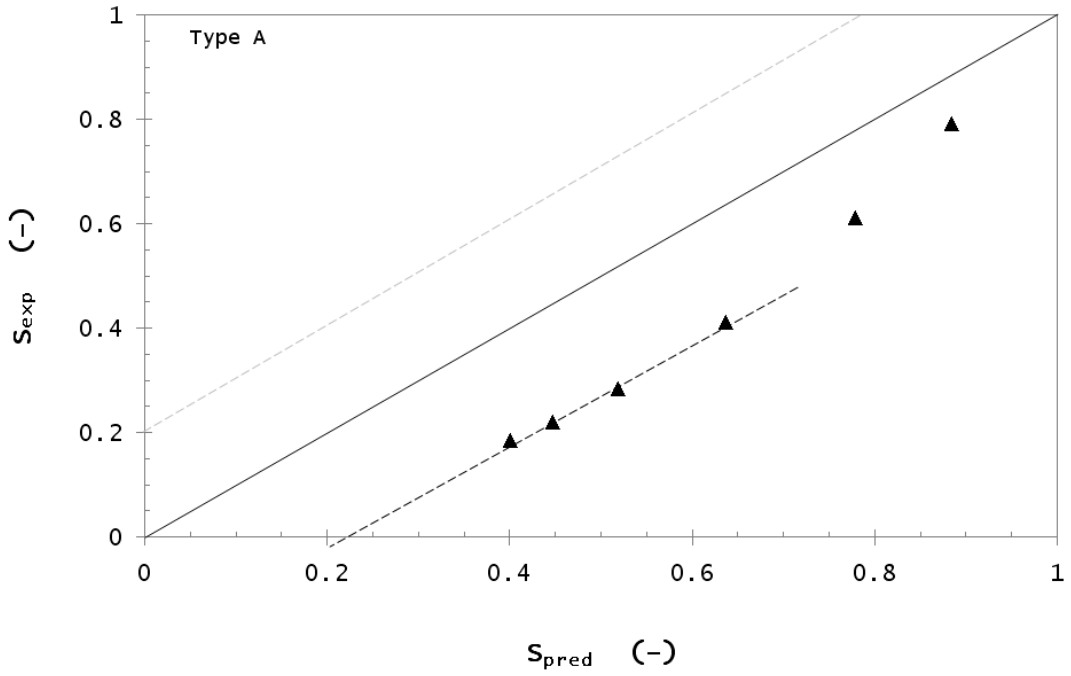

Figure 8.9.: Experimentally obtained saturation S_{exp} and predicted saturation S_{pred} for a *Type A* filter. S_{pred} was calculated using Equation 8.4. A dashed (black) line was included that shows a linear fit through the S_{exp} for $S_{pred} < 0.7$. The dashed grey line suggests the ratio between S_{pred} and S_{exp} if aerosol flow against the flow direction was applied.

It is obvious that S_{exp} is much lower than S_{pred}. The linear fit through the data set for

$S_{pred} < 0.7$ showed a relatively constant underestimation of the measured saturation by 0.225. This difference likely derives from the additional drag forces applied to the liquid by aerosol flow, thus the saturation decrease can be attributed to a combination of the influence of drag forces and centrifugal forces. The influence of the drag forces on the drainage behaviour of a saturated filter was described in Section 5.6, where it could be shown that for filters of *Type A* a measured reduction in saturation of 10% within the first 10 seconds of cleaning by an aerosol flow of 55 LPM (the usual aerosol flow rate in this work) was achieved. It could also be expected therefore, that if the air flow direction through the filter was reversed, from outside to inside the filter, that the rotational and air flow forces would serve to counteract each other, and produce results along the grey dotted line in Figure 8.9.

It is possible that the relatively simple model has not captured all of the physics. However, the trends in both model and experimental data are nearly parallel so it is considered most likely that the constant underestimation of the predicted saturation derives from additional drag forces that were not accounted for.

8.6. Comparison of the Cleaning Methods

Comparing the three cleaning methods with each other, it is obvious that filters cleaned by either method show a similar logarithmic decrease in ΔP_n and a linear decrease in S. However, by combining drag forces and centrifugal forces (C3 cleaning method), the greatest amount of liquid could be driven out of the filter. The highest rotational speed used in the C2 and C3 method was almost the same ($n = 2470$ and $n = 2500$). The resulting (normalised) pressure drop ΔP_N at highest speed was 0.28 ± 0.021 for the C2 experiments and 0.18 ± 0.025 for the C3 experiments, which equates to a 15% decrease. The saturation could be decreased to 0.40 ± 0.016 and 0.18 ± 0.019, respectively, a difference of approximately 35% in oil removal.

The impact of additional drag forces becomes more significant with higher rotational

speed. It is believed, that liquid, which has already been removed from its "original" location in the filter is now pushed towards the rear of the filter rather than draining within the filter. Once it has reached the rear, the liquid can overcome surface tension due to additional drag forces and detach from the filter media. Thus, there is less liquid on the rear or draining within the filter, which can potentially be imbibed back into the filter media upon cessation of flow and rotation. The influence of the additional drag forces is also reflected in the constants a_1 and a_3 in Equation 8.3 and 8.7, respectively - a_3 is larger than a_1 and thus responsible for more rapid decrease in ΔP_N.

However, the increased possibility that particles may detach from the rear of the filter and thus re–entrain is not to be ignored. It is likely, that detached droplets would be carried off by the air flow instead of being collected on the filter chamber and allowed to drain. This additional re–entrainment explains the decreasing efficiency in Figure 8.8 for higher rotational rates.

To compare the three methods, the $\Delta P_N/S$ ratios for all data points were calculated and are shown in Figure 8.10.

All three methods clearly showed an exponential relationship between ΔP_N and S (i.e. $\Delta P_N \sim e^S$). Method C1 however, showed a much steeper increase, which implies that ΔP is greater for a similar saturation (to C2 and C2) making this method less efficient. The two methods using rotation (C2 and C3) showed a similar, lower increase. As was already discussed earlier in this section, the method using rotation and aerosol flow was capable of removing more oil and reducing the pressure drop to a lower level. This reasons from the fact that due to a combination of aerosol flow and rotation the highest force onto the liquid was applied.

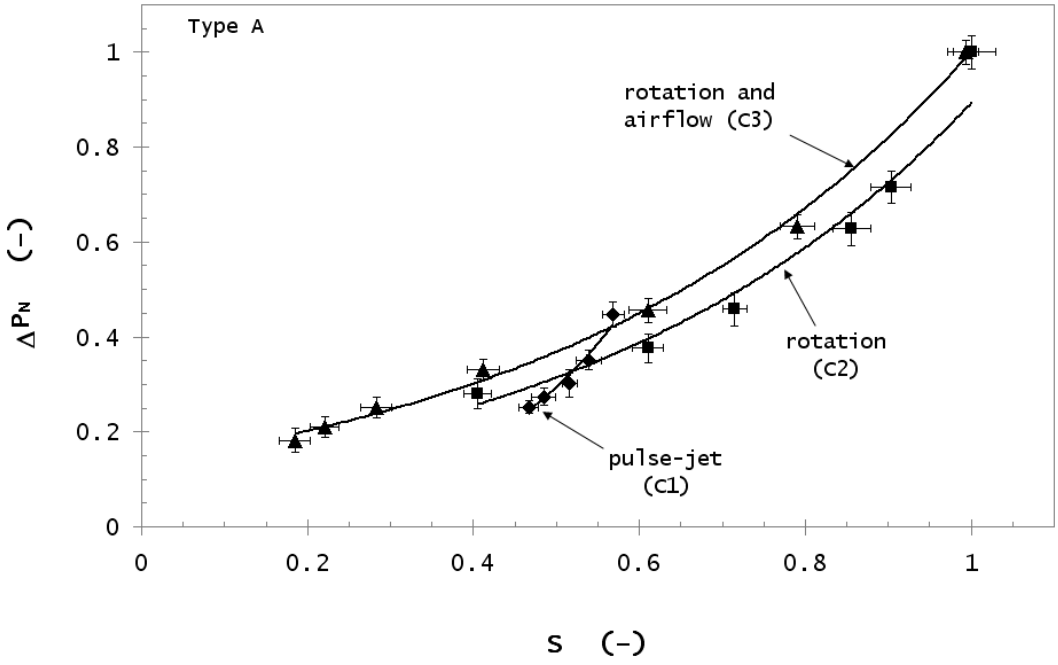

Figure 8.10.: $\Delta P_N/S$ ratio for *Type A* filters cleaned using the three suggested cleaning methods C1, C2 and C3.

8.7. Re–using Regenerated Oil–Mist Filters

The logical next step of this work is to examine repeated re–use of cleaned or regenerated filters, to ensure their performance does not alter significantly. Therefore, two *Type A* filters were tested in consecutive repetitions of "preloading, discontinuous operating and cleaning" sequences with the preloading method being varied according to Table 8.1.

The pressure drop of the first 15 filtration steps during discontinuous operation is shown in Figure 8.11 for both filters. All pressure drop values are normalised to the first equilibrium state pressure drop ΔP_{EQ1} of the initial test and therefore the curves do not necessarily commence at 1 on the y axis for the second and third test. It can be seen that, regardless of the preloading method, both filters show a similar behaviour for each test. As was also observed in earlier experiments, the pressure increased during the initial

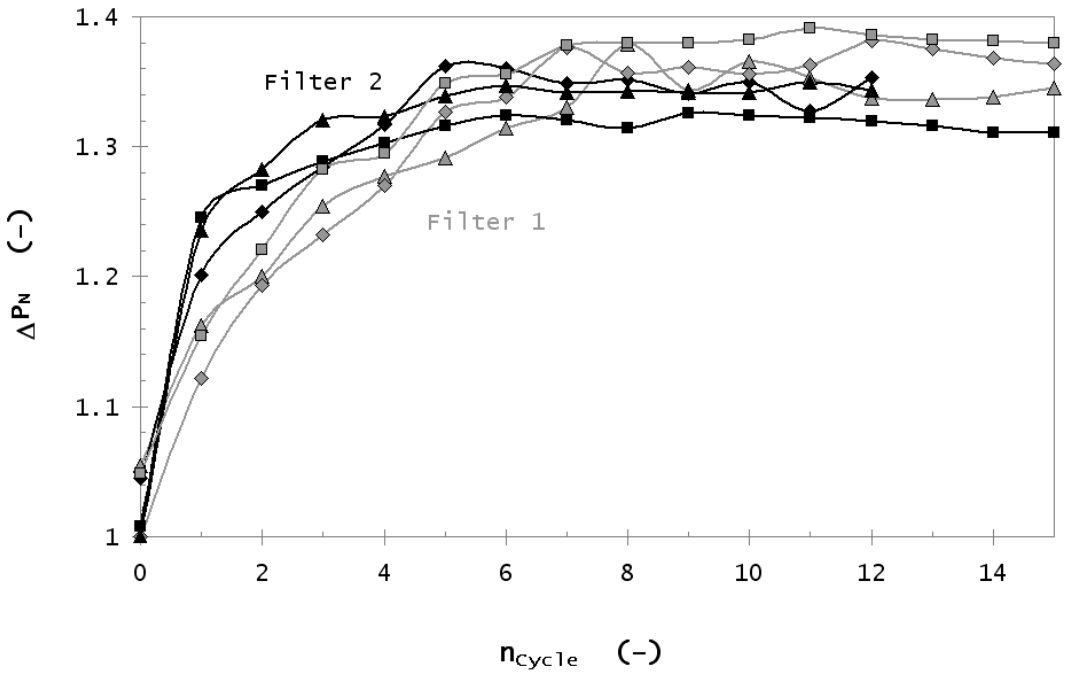

Figure 8.11.: Pressure drop behaviour of two *Type A* filters with three repetitions of discontinuous operation. The filters were "pulse–jet" (Method C1) cleaned once they reached EQ_2 and subsequently preloaded with a different method before undergoing continuous and discontinuous operation again (see Table 8.1). The three test stages are pictured by different markers (diamonds: first test, triangles: after 1st regeneration, squares: after 2nd regeneration)

cycles and then reached a constant value ΔP_{EQ2} approximately 35% (±4%) greater than ΔP_{EQ1} for each curve. This value agrees well with the results of earlier experiments. The first equilibrium state pressure drop ΔP_{EQ1} of the following tests was 2 - 5% higher than the pressure drop for the initial tests, which corresponds to a pressure drop difference of less than 0.75 mbar. This finding was also observed in earlier experiments (Figure 8.2).

The cleaning process using a compressed air jet (Method C1) was shown to be an efficient method to remove oil from the filter and the filter saturation could be decreased from an average of 0.71 ±0.01 to 0.52 ±0.01 as can be seen in Table 8.2. The results were very similar for both preloading methods.

Table 8.2.: Filter saturation at the second equilibrium state S_{EQ1} and immediately after regeneration S_{Reg} (u_{Jet} = 3 m/s, Method C1) for different preloading methods.

	"DAD"	**"RAS"**
S_{EQ2}	0.70 ±0.01	0.72 ±0.01
S_{Reg}	0.51 ±0.01	0.54 ±0.01

These findings lead to the conclusion that filters can be cleaned by additional force on the liquid to assist drainage (or the removal of oil from the filter) and be re–used regardless of their previous "history". The filters were shown to return to the same states (i.e. EQ_1 and EQ_2) at similar pressure drops and saturation for both continuous and discontinuous operation.

To estimate the average interval a *Type A* filter can be operated between two regenerations, a maximal filter saturation in discontinuous operation was assumed to be $S_{EQ2} = 0.72$ (based on Figure 5.9 and Table 6.2), which was reached after 6 cycles of discontinuous operation (Table 6.2) after a filtration period of 12 hours. The filter will be cleaned once it reached EQ_2 and cleaning will continue until a remaining saturation of $S_{Reg} = 0.3$ was attained, a value that seemed reasonable and could be achieved by applying either of the three cleaning methods (Figure 8.10). However, no information was available how long the filter could be operated discontinuosly until it attained the first equilibrium state EQ_1 once again. Since it was shown [52] that flow interruptions during the loading stage (before the filter attained EQ_1 had no influence on the loading behaviour of the filter, it seemed reasonable to calculate the time it would take the filter to collect particles during continuous operation until the saturation at the first equilibrium state $S_{EQ1} = 0.61$ (Figure 5.9) was reached if a constant collection efficiency of $E = 0.71$ (Figure 5.6) was assumed and no drainage occured (which is the case for the loading stage). With a known loading rate of 0.601 g/hr the loading time could be calculated to be approximately 20 hours until S_{EQ1} was reached (starting after cleaning when the filter saturation was $S_{Reg} = 0.3$). Therefore, the interval between the cleaning steps amounts to 32 (20 hours continuous and 12 hours discontinuous operation) hours

with the assumptions made.

The influence of soot loading on ΔP during successive regeneration and re–use cycles was not explored experimentally. However, based on the results of Chapter 7, it would be logical to assume that the soot is not removed from the filter during regeneration, and therefore soot accumulation in the filter would occur at a rate proportional to soot concentration and filtration time. Therefore, regeneration would not to be expected to increase filter life span if soot clogging was the primary issue.

8.8. Conclusion

In this chapter, different filter cleaning methods were developed and assessed. Filters were cleaned using either rotation or a pulse of compressed air ("pulse jet"), at different rotational speeds or "pulse-jet" velocities, respectively. Filters cleaned by methods C1 and C2 were cleaned off–line, i.e. they were removed from the filter chamber. A combined cleaning method using both techniques was able to be applied during filtration, which did not require the filter to be removed.

It was found, that all methods were able to remove a significant amount of oil from the filter resulting in reduced saturation and pressure drop. In all three cases, pressure drop was found to decrease logarithmically with rotational speed or jet velocity, whereas saturation decreased linearly (or close to).

An empirical model was developed to predict filter saturation as a function of rotational speed n and cleaning time t for a filter that was solely cleaned by rotation. The model was verified for both filter types *Type A* and *Type B* and excellent agreement with experimentally determined values was shown. It was found that applying this model to a filter cleaned by both rotation and air flow resulted in an underestimation of the saturation reduction, which was attributed to the additional cleaning effect induced by air flow. An estimation based on the drainage model presented in Chapter 5 found that the difference of 0.2 between measured and predicted saturation is likely to result from

the additional drag forces.

Repeated filter cleaning and loading cycles were also performed, which showed that the filters exhibited a very similar behaviour before and after regenerations. Pressure drop and saturation at both equilibrium states EQ_1 and EQ_2 were found to be nearly identical regardless of the previous preloading technique. These findings lead to the conclusion that filters can be cleaned by applying additional force on the liquid to assist drainage (or the removal of oil from the filter) and furthermore be re–used regardless of their previous "history". This important finding opens the door to novel filtration systems which would allow much higher filter life spans and thus less downtime. By optimising cleaning processes, filter collection efficiency and operational efficiency (power consumption) could be significantly improved, which would be a benefit for the filter life cycle and impacts on environment. Indeed, while Chapter 7 has shown that CCV filters would likely have a life span limited by soot deposition, mist filters receiving clean oil could have an almost unlimited life span. Furthermore, even for a filter collecting sooty oil, its life span could likely be significantly prolonged by reducing saturation, which may in turn ensure pressure drop stays below the required filter (change) threshold for longer.

9 Conclusions

This thesis has conducted a detailed investigation into the influence of soot contaminants and discontinuous operation on the performance of fibrous oil–mist filters. The work was split into five major chapters which focused on soot–in–oil analysis, discontinuous filtration, degradation/contamination of engine oil and its influence on filter performance, accumulation of soot particles in the filter and regeneration of saturated oil–mist filters.

In **Chapter 4**, it was shown that significant combustion and pyrolysis occur at temperatures above 450 °C and that the lower end of this temperature range conflicted with the temperature specified by the ASTM 5967 engine oil analysis standard. It was shown that a constant relative quantity of soot was lost during thermogravimetric analysis which led to an underestimation of the soot content by approximately 30 - 40% (for samples with more than 5% (w/w) soot) for the soot–in–oil mixtures examined. For samples containing significantly less than 5% soot (initially), the soot remaining was close to the detection limit of this technique. An investigation of four different thermogravimetric analysers was conducted, which proved that even well-maintained equipment was prone to imbibe oxygen during analysis and that disadvantageous furnace chamber design could prevent air from being expelled, allowing traces of oxygen to remain, distorting results.

An improved oil analysis method was developed, which was able to provide increased accuracy of soot determination compared to the ASTM 5967 method. The method has been proven to be significantly more robust and therefore far less sensitive to mass loss induced by combustion (with oxygen traces in the instrument) and pyrolysis effects. Additionally it was found advantageous to include a pre–purging time of 60 minutes prior to analysis.

In **Chapter 5**, the influence of air flow breaks during filter operation was investigated. It was shown that both types of filters tested underwent a second loading stage beyond

the first equilibrium state if they were not operated continuously and that they reached a second equilibrium state. An increase in pressure drop of 24% and 38% respectively and a saturation increase of 8% and 12% between the two equilibrium states was observed. This was attributed to a rearrangement of liquid in the filter during the breaks, clogging previously free passages, a process which was mainly driven by capillary forces. The ratio of shear and capillary forces was found to determine whether these passages were able to be cleaned once aerosol flow was recommenced.

A simple phenomenological model based on the Lucas–Washburn equation was developed to describe drainage of supersaturated filter media. It was shown that capillary theory appeared to describe the process which occurs as liquid is drained from supersaturated filters, at least during the initial phases.

The experiments conducted in this chapter represent a more realistic test for oil–mist (or coalescing) filters than typical laboratory testing.

In **Chapter 6**, the influence of oil ageing processes and contamination on the performance of fibrous oil–mist filters was examined.

Laboratory filtration tests have shown that oil viscosity has a significant impact on the pressure drop behaviour of oil-mist filters. A higher soot content in the oil resulted in a higher oil viscosity and in an increased final pressure drop ΔP_{EQ2} of the filter. Lower oil viscosity again (as for thermooxidated oil samples) resulted in a more rapid stabilisation of pressure drop but in a lower final overall pressure drop ΔP_{EQ2}. It was found, that ΔP_{EQ2} increased linearly with viscosity.

A field test was conducted, using 15 vehicles equipped with three different diesel engine types. The filters from the test vehicles were analysed in the laboratory after completion of the test. A “scaled–up” version of the modified ASTM 5967 method presented earlier was developed, and used to analyse the soot content of the filter. In general, the filters showed a linear correlation between oil viscosity and ΔP_{EQ2}, which agreed well with the findings obtained from the laboratory filter tests. However, the rate of increase was

slightly higher for the field test filters, which was attributed to additional oil ageing effects in the engine that were not taken into account during oil ageing in the laboratory. It was furthermore found that oil grade was relatively unimportant with respect to pressure drop evolution, whereas engine configuration had a major influence. These findings were confirmed by statistical analysis using Bayesian linear regression.

In **Chapter 7**, the accumulation of soot particles in the filter was investigated. An "accelerated loading method" was used to simulate up to 3000 hours of filter operation with soot–in–oil aerosol. Oil with a defined soot content was passed through *Type B* filters by a "pulse-jet". The drained liquid was collected and analysed and in some experiments passed multiple times through the filters. After loading, filters were thermoanalytically investigated and the soot content in the filter determined. It was found, that the soot filters accumulate soot at a near–constant rate, depending on the soot concentration and oil velocity through the filter. This finding was supported by the single fibre efficiency theory.

In **Chapter 8**, three different filter cleaning methods were developed and assessed. Filters were cleaned using rotation and/or a pulse of compressed air ("pulse jet") at different rotation speeds or "pulse-jet" velocities, respectively. Filter regeneration was conducted externally (i.e. filtration was stopped during cleaning) or in–situ, during filtration.

It was found, that all methods were able to remove a significant amount of oil from the filter, resulting in a lower saturation and pressure drop. In all three cases, pressure drop was found to decrease logarithmically with the the rotational speed or the jet velocity, respectively whereas the saturation decreased close to linearity.

An empirical model was developed to predict filter saturation as a function of the rotational speed n and the cleaning time t for a filter that was solely cleaned by rotation. The model was verified for both filter types, *Type A* and *Type B* showing excellent

agreement with experimentally determined values. It was found that applying this model to a filter cleaned by both rotation and air flow resulted in an underestimation of the saturation decrease which was attributed to additional cleaning effects induced by air flow. An estimation based on the drainage model presented in Chapter 5 found that the difference of 0.2 between measured and predicted saturation was likely to result from the additional drag forces.

Consecutive repetitions of "preloading, operation, cleaning" sequences showed that the filters showed a very similar behaviour after regeneration. Pressure drop and saturation at both equilibrium states (i.e. EQ_1 and EQ_2) were similar. This behaviour was found to be nearly identical, regardless of the previous preloading technique. These findings lead to the conclusion that mist filters are able to be cleaned by additional force on the liquid to assist drainage (or the removal of oil from the filter) and be re–used regardless of their previous "history". The cleaning process is however, not expected to remove accumulated soot.

In conclusion, this work has provided both a significant and novel contribution to the field of oil–mist filtration (amongst other fields) by:

1. developing a new/improved soot–in–oil analysis method

2. developing a large–scale expansion of the above method for soot–in–oil–in–filter analysis

3. developing a new (discontinuous) filter testing method, and thoroughly evaluating oil–mist filtering performance with this method

4. comparing field and laboratory tested CCV filters

5. evaluating the influence of soot contamination and oil ageing effects on mist filters in both a laboratory and field (on–engine) scenario

6. examining soot accumulation in oil–mist filters

7. examining regeneration and cleaning of oil–mist filters

8. developing of a novel rotating filter apparatus

It is hoped, that this work will lead to a new generation of regenerable or cleanable oil–mist filters with a longer operational life span (minimising waste and saving precious resources) and lower operational costs (the filter elements used in this work cost approximately AU$ 70), thereby providing the more sustainable filtration technology, which is beneficial for both the user and the environment.

A Appendix

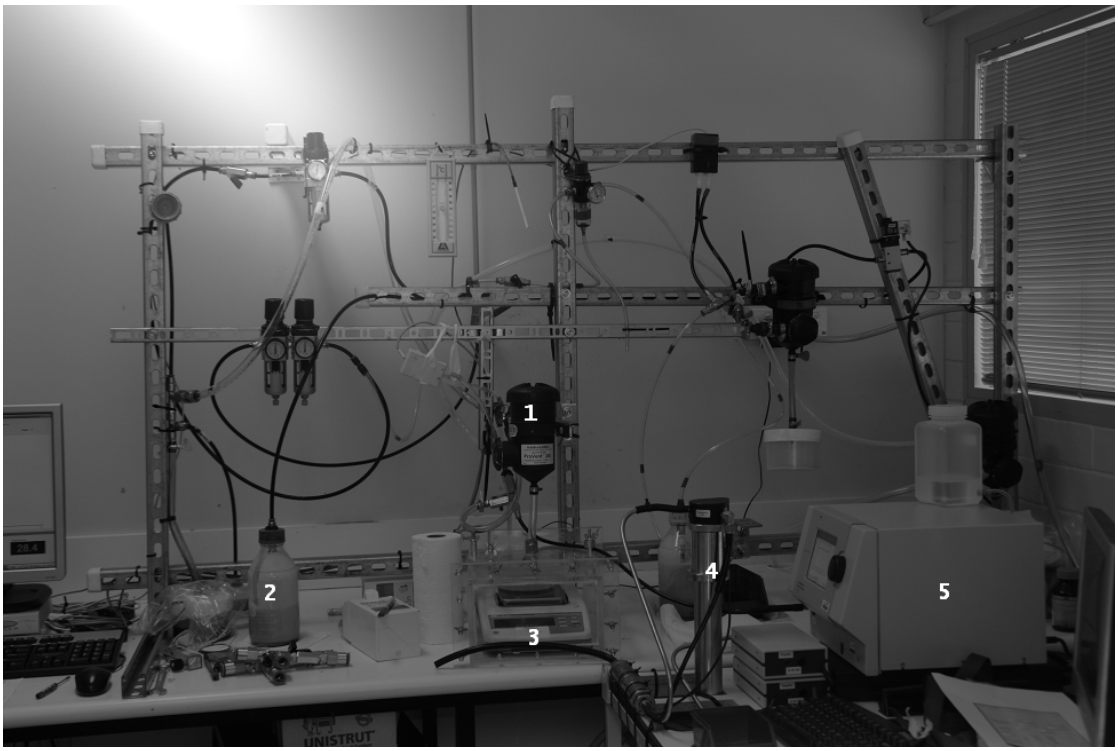

Figure A.1.: Image of the filter testing apparatus.

A picture of the filter testing apparatus is shown in Figure A.1. The major components of the test rig are numbered as follows:

1. Filter testing chamber
2. Aerosol generator (collison nebuliser)
3. Drainage measurement chamber
4. TSI 3081: Differential Mobility Analyser (DMA)
5. TSI 3775: Particle counter (CPC)

References

[1] European Union. Directive 2005/55/ec of the european parliament and of the council, 2005.

[2] M. Diaby, M. Sablier, A. Le Negrate, M. El Fassi, and J. Bocquet. Understanding carbonaceous deposit formation resulting from engine oil degradation. *Carbon*, 47(2), 2009.

[3] S. George, S. Balla, V. Gautam, and M. Gautam. Effect of diesel soot on lubricant oil viscosity. *Tribology International*, 40(5):809–818, 2007.

[4] S. Aldajah, O. O. Ajayi, G. R. Fenske, and I. L. Goldblatt. Effect of exhaust gas recirculation contamination of diesel engine oil on wear. *Wear*, 263(1):93 – 98, 2007.

[5] K. Trenbath, M. P. Hannigan, and J. B. Milford. Evaluation of retrofit crankcase ventilation controls and diesel oxidation catalysts for reducing air pollution in school buses. *Atmospheric Environment*, 43(37):5916 – 5922, 2009.

[6] Timothy K. M. Beatty and J. P. Shimshack. School buses, diesel emissions and respiratory health. *Journal of Health Economics*, 30(5):987 – 999, 2011.

[7] R. Pohanish. *Sittig's Handbook of Toxic and Hazardous Substances and Carcinogens. Volume 2.* Wlliam Andrew Publishing, Norwich, New York, USA, 2002.

[8] G. Polichetti, S. Cocco, A. Spinali, V. Trimarco, and A. Nunziata. Effects of particulate matter (pm10, pm2.5 and pm1) on the cardiovascular system. *Toxicology*, 261(1):1 – 8, 2009.

[9] R. V. Dáz and E. R. Dominguez. Health risk by inhalation of pm2.5 in the metropolitan zone of the city of mexico. *Ecotoxicology and Environmental Safety*, 72(3):866 – 871, 2009.

[10] Castrol. Material safety data sheet for castrol rx super 15w-40, 2007.

[11] F. Löffler. *Staubabscheiden.* Georg Thieme Verlag, Stuttgart, Germany, 1988.

[12] R. C. Brown. *Air Filtration: An Integrated Approach to the Theory and Applications of Fibrous Filters.* Pergamon Press, 1993.

[13] D. C. Walsh. Recent advances in the understanding of fibrous filter behaviour under solid particle load. *Filtration and Separation*, 33(6):501–506, 1996.

[14] J. Cerny, Z. Strnad, and G. Sebor. Composition and oxidation stability of sae 15w-40 engine oils. *Tribology International*, 34(2):127–134, 2001.

[15] F.Owrang, H. Mattsson, J. Olsson, and J. Pedersen. Investigation of oxidation of a mineral and a synthetic engine oil. *Thermochimica Acta*, 413(1):241 – 248, 2004.

[16] W. C. Hinds. *Aerosol Technology*. J.Wiley & Sons, New York, 1999.

[17] J. W. Gentry and K. R. Spurny. Measurements of collection efficiency of nuclepore filters for asbestos fibers. *Journal of Colloid and Interface Science*, 65(1):174–180, 1978.

[18] M. J. Manton. The impaction of aerosols on a nuclepore filter. *Atmospheric Environment (1967)*, 12(8):1669–1675, 1978.

[19] C. Tien. *Granular Filtration of Aerosols and Hydrosols*. Butterworth, Boston, 1989.

[20] W. Peukert. High temperature filtration in the process industry. *Filtration and Separation*, 35(5):461–464, 1998.

[21] J. C. Ruiz, P. Blanc, E. Prouzet, P. Coryn, P. Laffont, and A. Larbot. Solid aerosol removal using ceramic filters. *Separation and Purification Technology*, 19(3):221–227, 2000.

[22] D. J. Acheson. *Elementary Fluid Dynamics*. Oxford University Press, 1990.

[23] H. K. Versteeg and W. Malalasekera. *An Introduction to Computational Fluid Dynamics: The finite volume method*. Prentice Hall, 2007.

[24] H. Schlichting. *Boundary-Layer Theory*. Springer, Berlin, 1979.

[25] P. A. Davidson. *Turbulence: An Introduction for Scientists and Engineers*. OUP Oxford, London, 2004.

[26] V. A. Gushchin, A. V. Kostomarov, P. V. Matyushin, and E. R. Pavlyukova. Direct numerical simulation of the transitional separated fluid flows around a sphere and a circular cylinder. *Journal of Wind Engineering and Industrial Aerodynamics*, 90(4):341 – 358, 2002.

[27] M. D. Allen and O. G. Raabe. Re-evaluation of millikan's oil drop data for the motion of small particles in air. *Journal of Aerosol Science*, 6:537–547, 1982.

[28] K. Sutherland. *Filters And Filtration Handbook*, volume 0005. Elsevier Books, 2007.

[29] C. N. Davies. *Air Filtration.* Academic Press, U.S., 1973.

[30] S. Kuwabara. The forces experienced by randomly distributed parallel circular cylinders or spheres in a viscous flow at small reynolds numbers. *Journal of the Physical Society of Japan*, 14(4):527–532, 1959.

[31] P. Contal, J. Simao, D. Thomas, T. Frising, S. Callé, J.C. Appert-Collin, and D. Bémer. Clogging of fibre filters by submicron droplets. phenomena and influence of operating conditions. *Journal of Aerosol Science*, 35(2):263 – 278, 2004.

[32] T. Frising, D. Thomas, D. Bémer, and P. Contal. Clogging of fibrous filters by liquid aerosol particles: Experimental and phenomenological modelling study. *Chemical Engineering Science*, 60(10):2751 – 2762, 2005.

[33] P. C. Raynor and D. Leith. The influence of accumulated liquid on fibrous filter performance. *Journal of Aerosol Science*, 31(1):19 – 34, 2000.

[34] D. Kampa. A model for steady-state oil transport and saturation in a mist filter. In *8th World IMACS / MODSIM Congress Cairns*, 2009.

[35] H. Mohrmann. Loading of fiber filters with aerosols consisting of liquid particles. *Staub - Reinhaltung der Luft*, 30(8), 1970.

[36] T. P. Liew and J. R. Conder. Fine mist filtration by wet filters - 1. liquid saturation and flow resistance of fibrous filters. *Journal of Aerosol Science*, 16(6):497–509, 1985.

[37] G. L. Fairs. High efficiency fibre filters for the treatment of fine mists. *Transactions of the Institution of Chemical Engineers*, 36, 1958.

[38] B. J. Mullins and G. Kasper. Comment on: "clogging of fibrous filters by liquid aerosol particles: Experimental and phenomenological modelling study" by frising et al. *Chemical Engineering Science*, 61(18):6223–6227, 2006.

[39] F. W. Minor, A. M. Schwarty, E. A. Wulkow, and L. C. Buckles. Behaviour of liquids on single textile fibers. *Textile Research Journal*, 129, 1959.

[40] I. Agranovski. *Filtration of ultra small particles on fibrous filters.* PhD thesis, 1995.

[41] B. J. Mullins, I. E. Agranovski, R. D. Braddock, and C. M. Ho. Effect of fiber

orientation on fiber wetting processes. *Journal of Colloid and Interface Science*, 269(2):449–458, 2004.

[42] D. C. Walsh, J. I. T. Stenhouse, K. L. Scurrah, and A. Graef. The effect of solid and liquid aerosol particle loading on fibrous filter material performance. *Journal of Aerosol Science*, 27(Supplement 1):617–618, 1996.

[43] R.-J. Roe. Wetting of fine wires and fibers by a liquid film. *Journal of Colloid and Interface Science*, 50(1):70–79, 1975.

[44] S. Payet. *Filtration stationnaire et dynamique des aersosols liquides submicroniques*. PhD thesis, 1991.

[45] K. W. Lee and B. Y. H. Liu. Theoretical study of aerosol filtration by fibrous filters. *Aerosol Science and Technology*, 1:147–161, 1982.

[46] S. Payet, D. Boulaud, G. Madelaine, and A. Renoux. Penetration and pressure drop of a hepa filter during loading with submicron liquid particles. *Journal of Aerosol Science*, 23(7):723–735, 1992.

[47] R. Gougeon, D. Boulaud, and A. Renoux. Theoretical and experimental study of fibrous filters loading with liquid aerosols in the inertial regime. *Journal of Aerosol Science*, 25(Supplement 1):189–190, 1994.

[48] W. Sun and D.-R. Chen. Filer loading characteristics of liquid-coated particles, 2002.

[49] B.J. Mullins, R. D. Braddock, and I. E. Agranovski. Particle capture processes and evaporation on a microscopic scale in wet filters. *Journal of Colloid and Interface Science*, 279(1):213–227, 2004.

[50] I. E. Agranovski and M. Shapiro. Clogging of wet filters by dust particles. *Journal of Aerosol Science*, 32(8):1009 – 1020, 2001.

[51] T. Frising, V. Gujisaite, D. Thomas, S. Callé, D. Bémer, P. Contal, and D. Leclerc. Filtration of solid and liquid aerosol mixtures: Pressure drop evolution and influence of solid/liquid ratio. *Filtration and Separation*, 41(2):37–39, 2004.

[52] T. Frising, D. Thomas, J.-C. Appert-Collin, S. Callé-Chazelet, and P. Contal. Influence of liquid aerosol stop-and-go on the performance of fibrous filters. *Filtration*, 5(4):9, 2005.

[53] M. Denesuk, G. L. Smith, B. J. J. Zelinski, N. J. Kreidl, and D. R. Uhlmann.

Capillary penetration of liquid droplets into porous materials. *Journal of Colloid and Interface Science*, 158(1):114 – 120, 1993.

[54] M. Hilpert and A. Ben-David. Infiltration of liquid droplets into porous media: Effects of dynamic contact angle and contact angle hysteresis. *International Journal of Multiphase Flow*, 35(3):205–218, 2009.

[55] A. Marmur and R. D. Cohen. Characterization of porous media by the kinetics of liquid penetration: The vertical capillaries model. *Journal of Colloid and Interface Science*, 189(2):299–304, 1997.

[56] T. Gillespie. The capillary rise of a liquid in a vertical strip of filter paper. *Journal of Colloid Science*, 14(2):123–130, 1959.

[57] C. M. Reed and N. Wilson. The fundamentals of absorbency of fibres, textile structures and polymers. i. the rate of rise of a liquid in glass capillaries. *Journal of Physics D: Applied Physics*, 26(9):1378, 1993.

[58] F. A. L. Dulien. *Porous Media: Fluid Transport and Pore Structure*. San Diego, Academic Press, 1992.

[59] R. J. Gummerson, C. Hall, W. D. Hoff, R. Hawkes, G. N. Holland, and W. S. Moore. Unsaturated water flow within porous materials observed by nmr imaging. *Nature*, 281(5726):56 – 57, 1979.

[60] E. W. Washburn. The dynamics of capillary flow. *Physical Review*, 17(3):273, 1921.

[61] D. A. Lockington and J.-Y. Parlange. A new equation for macroscopic description of capillary rise in porous media. *Journal of Colloid and Interface Science*, 278(2):404 – 409, 2004.

[62] B. J. Mullins, R. D. Braddock, and G. Kasper. Capillarity in fibrous filter media: Relationship to filter properties. *Chemical Engineering Science*, 62(22):6191 – 6198, 2007.

[63] A. D. H. Clague, J. B. Donnet, T. K. Wang, and J. C. M. Peng. A comparison of diesel engine soot with carbon black. *Carbon*, 37(10):1553 – 1565, 1999.

[64] M. Kawamura, T. Ishiguro, K. Fujita, and H. Morimoto. Deterioration of antiwear properties of diesel engine oils during use. *Wear*, 123(3):269 – 280, 1988.

[65] C. I. Chen and S. M. Hsu. A chemical kinetics model to predict lubricant performance in a diesel engine. part i: simulation methodology. *Tribology Letters*, 14(2):83 – 90, 2003.

[66] AMSOIL. *Why Does Motor Oil Deteriorate?* Technology and News, Charlton, Texas, USA, 2011.

[67] M. Kaufman. *The Motor Oil Bible: Exposing the 3,000 Mile Oil Change Myth.* CreateSpace, Charleston, USA, 2010.

[68] H. Sauter and P. Trautmann. Messung und abscheidung von ölnebelaerosolen aus der kurbelgehäuseentlüftung von verbrennungsmotoren. *MTZ Motortechnische Zeitschrift*, 61(12):874 – 878, 2000.

[69] H. A. K. Shahad. An experimental investigation of soot particle size inside the combustion chamber of a diesel engine. *Energy Conversion and Management*, 22(2):141 – 149, 1989.

[70] U. Leidenberger, W. Mühlbauer, S. Lorenz, S. Lehmann, and D. Brüggemann. Experimental studies on the influence of diesel engine operating parameters on properties of emitted soot particles. *Combustion Science and Technology*, 183(1):1 – 15, 2012.

[71] G. A. Stratakis and A. M. Stamatelos. Thermogravimetric analysis of soot emitted by a modern diesel engine run on catalyst-doped fuel. *Combustion and Flame*, 132(1-2):157 – 169, 2003.

[72] J. Song and P. Peng. Characterisation of black carbon materials by pyrolysis-gas chromatography-mass spectrometry. *Journal of Analytical and Applied Pyrolysis*, 87(1):129 – 137, 2010.

[73] ASTM. Standard test method for diesel engine oils in t-8 diesel engine d5967-08, 2008.

[74] S. George, S. Balla, and M. Gautam. Effect of diesel soot contaminated oil on engine wear. *Wear*, 262(9-10):1113 – 1122, 2007.

[75] G. Mullins and J. Truhan. Measurement of semi-volatiles in used natural gas engine oil using thermogravimetric analysis. *International Journal of Engine Research*, 8(5):439–448, 2007.

[76] D.C. Walsh. Oil analysis 101. *Orbit*, 25(2):50–55, 2005.

[77] M. Seipenbusch, J. van Erven, T. Schalow, A. P. Weber, A. D. van Langeveld, J. C. M. Marijnissen, and S. K. Friedlander. Catalytic soot oxidation in microscale experiments. *Applied Catalysis B: Environmental*, 55(1):31 – 37, 2005.

[78] N. Nejar, M. Makkee, and M. J. Illán-Gómez. Catalytic removal of nox and soot

from diesel exhaust: Oxidation behaviour of carbon materials used as model soot. *Applied Catalysis B: Environmental*, 75(1-2):11 – 16, 2007.

[79] J. Mullens, A. Vos, R. Carleer, J. Yperman, and L. C. Van Poucke. The decomposition of copper oxalate to metallic copper is well suited for checking the inert working conditions of thermal analysis equipment. *Thermochimica Acta*, 207:337–339, 1992.

[80] E. Jakab and M. Omastová. Thermal decomposition of polyolefin/carbon black composites. *Journal of Analytical and Applied Pyrolysis*, 74(1-2):204 – 214, 2005.

[81] D. E. Larkin. Compositional analysis by thermogravimetry: The development of a standard method, 1988.

[82] ASTM. Standard practice for proximate analysis of coal and coke d3172 - 07a, 2007.

[83] ASTM. Standard test method for carbon black content in olefin plastics d1603 - 06, 2006.

[84] D. Uner, M. K. Demirkol, and B. Dernaika. A novel catalyst for diesel soot oxidation. *Applied Catalysis B: Environmental*, 61(3-4):334 – 345, 2005.

[85] A. Bredin, A. V. Larcher, and B. J. Mullins. Thermogravimetric analysis of carbon black and engine soot - towards a more robust oil analysis method. *Tribology International*, 44(12):1642 – 1650, 2011.

[86] M. Hilpert. Effects of dynamic contact angle on liquid infiltration into inclined capillary tubes: (semi)-analytical solutions. *Journal of Colloid and Interface Science*, 337(1):138 – 144, 2009.

[87] M. Hilpert. Effects of dynamic contact angle on liquid withdrawal from capillary tubes: (semi)-analytical solutions. *Journal of Colloid and Interface Science*, 347(2):315 – 323, 2010.

[88] S. Jaganathan, H. V. Tafreshi, and B. Pourdeyhimi. A realistic modeling of fluid infiltration in thin fibrous sheets. *Journal of Applied Physics*, 105(11):8, 2009.

[89] Arne Bredin and Benjamin J. Mullins. Influence of flow-interruption on filter performance during the filtration of liquid aerosols by fibrous filters. *Separation and Purification Technology*, 90(0):53 – 63, 2012.

[90] R. M. Mortier and S. T. Orszulik. *Chemistry and Technology of Lubricants*. Edmundsbury Press, Suffolk, 1997.

[91] G. C. Ofunne, A. U. Maduako, and C. M. Ojinnaka. High temperature oxidation stability of automotive crankcase oils and their base oils. *Tribology International*, 23(6):407 – 412, 1990.

[92] Australian Government. Diesel fuel quality standard, 2001.

[93] ASTM. Bench oxidation of engine oil by robo apparatus d7528-09, 2009.

[94] D. J. Lunn, A. Thomas, N. Best, and D. Spiegelhalter. Winbugs - a bayesian modelling framework: concepts, structure, and extensibility. *Statistics and Computing*, (10):12, 2002.

[95] N. G. Best, M. K. Cowles, and S. K. Vines. *CODA: Convergence diagnosis and output analysis software for Gibbs sampling output*, volume Version 0.3. 1995.

[96] A. Gelman, J. B. Carlin, H. S. Stern, and D. B. Rubin. *Bayesian Data Analisis*. Chapman & Hall/CRC, Florida, 2004.

[97] A. Bredin, R. A. O'Leary, and B. J. Mullins. Filtration of soot-in-oil aerosols: Why do field and laboratory experiments differ? *Separation and Purification Technology*, submitted and accepted, 2012.

[98] R. Mead-Hunter. *Modelling Micro-Scale Coalescence and Transport Processes in Liquid Aerosol Filtration*. PhD thesis, 2012.

[99] H. Banzhaf, M. Lehmann, and G.-M. Klein. The loading of liquid filter media. In *Filtech Wiesbaden*, 2007.

[100] M. M. Maricq and N. Xu. The effective density and fractal dimension of soot particles from premixed flames and motor vehicle exhaust. *Journal of Aerosol Science*, 35(6):1251 – 1274, 2004.

[101] J. Yoon, M. Kim, S. Song, and K. M. Chun. Calculation of mass-weighted distribution of diesel particulate matters using primary particle density. *Journal of Aerosol Science*, 42(6):419 – 427, 2011.

[102] A. Dittler and G. Kasper. Simulation of operational behaviour of patchily regenerated, rigid gas cleaning filter media. *Chemical Engineering and Processing: Process Intensification*, 38(4-6):321 – 327, 1999.

[103] J. Binnig, A. Bredin, J. Meyer, and G. Kasper. Dimensional analysis of the cleaning pulse intensity in a surface filter test rig. *Powder Technology*, 211(2):275 – 279, 2011.

Table of Figures

Table of Tables